The Creeping Motion of Immiscible Drops Through a Converging/Diverging Tube: I. Non-Newtonian Effects of Viscoelastic Drops. II. Effects of Constant Pressure Gradient Condition for the Flow. III. Motion of Drops Through a Parallel Channel.

Thesis by
Francisco E. Avila-Segura

in Partial Fulfillment of the Requirements
for the Degree of
Doctor of Philosophy

California Institute of Technology
Pasadena, California
1988
(Submitted September 29, 1987)

To my mother

To my brother Rafael

Acknowledgements

Every aspect of my life has been enriched by the people I met during these years at Caltech. I will always remember Professor R. H. Sabersky and Professor C. E. Brennen; I greatly appreciated their attitude toward students and their understanding. Adelaide D'Ambrosio, Luca d'Agostino and Enrique Geffroy occupy a very special place in my heart. Arturo Cifuentes has been also an excellent friend and has always given me unconditional support in the rough times. I want to thank the students in my group for their pleasant company. It was truly a pleasure to have Bo Kyung Chi and later on Ardith El-Kareh (*The Inspired*) as my office mates. Special thanks to Jim Stoos and Ed Ascoli (both great guys). I want to thank Kathy Lewis not only for all the work involved in typing the present version of my thesis, but also for the kindness and promptness with which she did it. Many thanks to George Griffith and his pals of the White Cadillac Band. George gave me high priority with respect to his multiple projects and always offered me his moral support whenever I needed it. I am very grateful to a group of very dear friends that contributed to expand my world from Caltech to far-away places and provided me with a very friendly environment. So, I thank Markus Meister (Germany-Italy), Salvador Parisi (Brasil), Hal Zarem (U.S.A.), Luciana Astiz (Mexico-Tenochtitlan), Hector Jensen (Chile), Eric Majani (France), Robert Beck (Costa Rica, chico!), Agnes Allard (France, oh la la!), Jaywant Arakeri (India), and Vigor Yang (Taiwan). I found a lot of love and fun within the Italian Community of Caltech and I want to thank them all for it. They are, however, too many to be listed, allora... Forza Italia!...

I am deeply grateful to Professor Baltasar Mena for his friendship of many years and because he has closely watched the developments of my professional career. My gratitude to Mr. Abel Ramirez and Mr. Roberto Hernandez of the Athenaeum for their fine acceptance.

I am much obliged to the following Institutions that provided financial support for my studies and research: CONACYT, Mexico, D.F. Mexico, Universidad Nacional Autonoma de Mexico, Mexico, D. F. Mexico, California Institute of Technology, Pasadena, CA U.S.A. In this regard, I am deeply grateful to Carol Mastin for her understanding and supportive help. I am also thankful to Professor A. L. Albee and Professor F. S. Buffington.

Finally I want to thank Professor L. G. Leal for having admitted me in his group, suggested my research topic and provided his useful criticisms and corrections.

Abstract

Experimental results are presented for the motion of neutrally buoyant drops of non-Newtonian fluid through a wavy wall tube within a Newtonian suspending fluid. The motion of these drops exhibits very different behavior with respect to both Newtonian drop-Newtonian suspending fluid system and Newtonian drop-viscoelastic suspending fluid system. In particular, drop breakup behavior is strongly modified. At small flow rates (small capillary numbers) viscoelastic drops undergo drop breakup. At large flow rates (large capillary numbers) breakup phenomena do not occur and axial drop elongation is inhibited. For the cases in which drop breakup occurs, it produces important effects on the time-dependent response of the extra pressure drop and on the drop mobility. For high polymer concentration (1%) in the viscoelastic drop, the resulting elastic effects are overshadowed by the increase in viscosity which accompanies the addition of polymer.

The effects of flow type on the dynamics of the drop motion in a wavy wall tube are investigated. According to the nature of the driving mechanism there are two types of flow, each one of them presenting different properties (though identical for non-drop conditions). One flow is susceptible to changes in flow resistance that may appear in the experimental setup, the other is such that the volumetric flow rate is constant. The former is generated by imposing a constant pressure gradient (CPG conditions), the latter is generated by a gear pump (CFR conditions). Drop deformation in a CPG experiment is less severe than it is in a CFR experiment. Also, under CPG conditions, the axial elongation and the mobility of a moving drop are

independent of the viscosity ratio, whereas under CFR conditions they depend on it. In addition, the magnitude of the extra pressure drop caused by the passage of the drop through the test section is smaller under CPG conditions than it is under CFR conditions.

Finally, a more realistic simulation of flow dynamics in porous media is considered. For this purpose, a parallel channel device was tested under constant pressure gradient conditions. Measurements were taken in both arms of this device for the extra pressure drop caused by the passage of drops through one of the channels (a wavy wall tube). The ratio of the mean value of such measurements is nearly constant regardless of the value of the total volumetric flow, drop size or viscosity ratio. Obviously, the pressure drop measured in the bypass tube is a tangible indication of the increase (or decrease) in the volumetric flow through it, due to the motion of the drop through the other arm of the experimental apparatus.

Table of Contents

Chapter 1

Non-Newtonian Effects of Viscoelastic Drops Moving Through a Converging/Diverging Channel

1. Introduction

There are many interesting problems related to the two-phase flow of liquid drops moving within another liquid fluid. Processes involved in the preparation of emulsions, the preparation of polymer blends, the mixing of additives to polymer materials, the motion of red blood cells in the capillaries, and the motion of a two-phase fluid in porous media are all related in one way or another to the deformation and sometimes dispersion of drops moving in a suspending fluid.

A number of researchers have studied these problems, both theoretically and experimentally. Usually, in order to make the particular two-phase flow problem tractable, special conditions have been adopted. Most commonly, the liquids studied have been Newtonian, and the flows studied have been simple "unbounded" flows, such as a simple shear flow or hyperbolic flow as obtained in a four-roll mill. For the sake of tractability, especially in theoretical works, most studies until recently have also considered only limited regions of parameter space, where drop deformation is small.

The present work continues a series of studies in our laboratory of the motion of drops through capillary tubes with periodically increasing and decreasing radius. These studies are aimed at a better understanding of the dynamics of two-phase flows in porous media at the scale of individual channels. The relationships between the independent flow variables in this relatively simple flow system, i.e. the physical properties of the fluids, the volumetric flow rate, and the channel geometry, and the dependent flow variables, such as the extra pressure drop caused by the drop, or the average velocity ("mobility") of the drop, are important in eventually understanding two-phase flows in a "real" porous matrix. An additional critical

additional critical factor is an understanding of the conditions for drop breakup in this type of flow system.

The earliest work in our laboratory was due to Ho and Leal (1975) who studied the creeping motion of neutrally buoyant, Newtonian drops through a straight circular tube of comparable diameter, for both Newtonian and viscoelastic suspending fluids (this paper will be referred to as I). Later, Olbricht and Leal (1981) studied the effects of buoyancy forces when the density of the drop is different from that of the suspending fluid, for the same flow system (this work will be referred to as II). Finally, the creeping motion of drops through a horizontal converging/diverging tube was also studied by Olbricht and Leal (1983) for Newtonian drops in both Newtonian and non-Newtonian suspending fluids, including both neutrally buoyant and non-neutrally buoyant drops (this study will be referred to as III).

In the following, we present the results of experiments on the motion of neutrally buoyant drops of a non-Newtonian fluid moving within a Newtonian suspending fluid through a wavy wall tube. Although this may seem to be a somewhat minor variation on the previous study of Olbricht and Leal (1983) for Newtonian drops in a viscoelastic liquid, we shall see that this is not at all the case. The preceding study demonstrated that the breakup of drops suspended in viscoelastic fluids was always strongly *inhibited* and modified in form compared to a similar system with a Newtonian suspending fluid. The tendency of Newtonian drops at moderate capillary numbers to undergo breakup is perhaps the most significant feature of their motion in the wavy-wall tube. In the present study, we will show that this and other aspects of their motion are strongly modified again, both with

respect to the Newtonian drop-Newtonian suspending fluid system and the Newtonian drop-viscoelastic suspending fluid system studied earlier. Interest in viscoelastic drops is motivated, in part, by the prevalence of "waxy crudes" in North American oil deposits where the petroleum phase can be highly non-Newtonian in behavior.

2. Experimental

2.1 Apparatus

Except for some slight modifications, the experimental setup used in our experiment is the same as that used by Olbricht and Leal (1983). Hence, it need not be described in any detail. As illustrated in Fig. 1, two video cameras are used. One moves along a rail parallel to the test section and thus tracks the droplet in its passage through the test section; drop deformation is seen through this camera. The second camera is focused at a strip chart recorder (Houston Omniscribe) which records the actual time dependent pressure loss along the test section, as obtained from a differential pressure transducer indicator. In addition, a timer was attached to the chart recorder in order to measure the duration of the drop passage through the test section so that an average velocity $\bar{u}$ can be calculated.

The images photographed by the two video cameras were combined in real time on a single screen TV monitor by means of a "screen splitter", and the composed image was recorded by a Panasonic II videorecorder. By means of the combined image, we were able to visually correlate the time variations of the pressure drop with the motion and shape of the droplet as it moves through the wavy wall tube. The test section contains 18 periodially repeating units forming the wavy wall

channel, and is 27 cm long. The detailed structure and exact measurements of this test section are reported in III.

Much of the previous and current data is presented in terms of a *single effective radius*, r_{HP} for the wavy-wall tube. The motivation for assigning a constant effective radius to the wavy wall channel was discussed in III, but the general idea is that it allows results from the wavy wall geometry to be compared with the previous results (for example, I) which were taken in a straight wall tube. The effective radius used in this and previous studies from our laboratory is defined as the radius of fictitious straight-wall tube which causes the same pressure drop per unit length for a single-phase Newtonian fluid as does the wavy-wall tube when the same volume flow rate is applied. This is known as the Haegen-Poiseuille radius. An estimate for r_{HP} was obtained theoretically in III on the *ad hoc* basis of applying the Haegen-Poiseuille law for a straight tube to a differential length dz of the wavy wall tube, and then integrating over one period of the channel to obtain an overall pressure drop for a periodic unit. Olbricht and Leal found that this procedure resulted in a theoretical value of 0.316 cm for r_{HP} for the particular wavy-wall tube used in the present study. Actual measurements of flow rate and pressure drop through the test section gave an *experimental* value for the equivalent hydraulic radius in excellent agreement with this theoretical value.

2.2 Condition of Experiments and Experimental Techniques

The temperature during the present experiments was kept constant at 25°C. Details of the experimental procedures may be found in previous works (I, II, III), and little will be said here regarding them. However, it is important, in order to avoid possible future confusion, to note that a numerical discrepancy was found

between the results given here for ΔP^+ and the corresponding result given in III. These discrepancies arose from the increased precision used in the present study for *calibration* of the pressure transducer system in the presence of extremely small differential pressures (see Appendix for calibration procedure). As a consequence, comparisons in this paper between results for Newtonian and viscoelastic fluids were all based upon our own results — when necessary, experiments with Newtonian drops were repeated to obtain directly comparable data. It should be emphasized, however, that the discrepancies found with past work were quantitative in nature — in no case were the qualitative trends reported earlier found to be incorrect.

2.3 Experimental Materials and Dimensionless Parameters Governing the Flow

As stated earlier, the two-phase system studied here consists of viscoelastic drops moving within a Newtonian medium. The Newtonian suspending fluid was a Ucon Oil 1715 LB series (Union Carbide) having a viscosity of 6.54 poises at 25°C and a density of 0.9980. Solutions of Separan AP-30 in distilled water were used as the drop liquid at two different concentrations, 0.5% and 1% by weight. The density of these liquids (0.9997 and 1.0008 respectively) at 25°C was nearly the same as that of the Ucon oil, and therefore no appreciable buoyancy effects were present in the experiments ($\Delta\rho \sim 0(10^{-3})$). Experimental results will be presented in terms of several independent dimensionless parameters, which are intended to take account not only of the properties of the Newtonian suspending liquid but also the viscoelastic nature of the suspended phase. We discuss these parameters below.

The most important is the capillary number, which provides a measure of the relative importance of viscous and surface tension forces. Of course, the importance of the capillary number for deformation of Newtonian droplets within a Newtonian suspending liquid has been well established since the early work by Taylor (1934) on the deformation of drops subjected to viscous shear flows. The capillary number Γ for the present experiments is defined as $\Gamma = \mu_0\bar{v}/\gamma$, where μ_0 is the suspending fluid viscosity, $\bar{v}$ is the average flow velocity defined as the ratio of the volumetric flow rate Q to the *effective* cross-sectional area of the test section (hence, $\bar{v} = \frac{Q}{\pi r_{HP}^2}$), and γ is the interfacial tension between the two phases. In the present experiments, variations in Γ were brought about primarily by changes in the flow rate (i.e. variations of $\bar{v}$).

Another important parameter for Newtonian fluid systems is the viscosity ratio $\sigma \equiv \mu_i/\mu_o$, where μ_i is the viscosity of the drop. It is convenient, for purposes of comparison, to retain this parameter in the present study. However, it is important to recognize that there are substantial ambiguities involved in assigning a single viscosity to a viscoelastic liquid drop moving through a wavy wall channel — not only because of the non-Newtonian characteristics of the drop and the complex kinematics of the flow field, but also because the different drop volumes used in our experiments lead to nontrivial modifications in the flow. Unlike Newtonian fluids, the effective viscosity ratio for viscoelastic drops in Newtonian fluids is not strictly a material parameter, but depends on the flow rate (i.e. on Γ) due to the shear-rate dependence of the viscoelastic fluid properties. In order to estimate a sensible value for the drop viscosity, we follow a number of earlier researchers [Han and Funatsu (1978), Chin and Han (1979,1980); Olbricht and Leal (1981,1983)] and estimate the

viscosity of the suspended drops from shear viscosity data at the "average" wall shear rate of the suspending fluid, β_ω (estimated as the wall shear rate within the "equivalent" straight-wall tube). For a Newtonian fluid, the wall shear rate is

$$\beta_\omega = \frac{4Q}{\pi r_{HP}^3} . \tag{1}$$

We believe this to provide a reasonable estimate of the characteristic shear rate for estimation of *drop* viscosity in the present system, especially for those larger drops which must deform according to the actual geometry of the channel. Values for Γ and σ used in this work, as well as values for other physical properties of the 0.5% and 1.0% solutions studied here, are given in Tables 1(a) and 1(b) respectively. The value of the viscosity ratio given there is based upon the value of the wall shear rate at the particular flow-rate corresponding to each value of Γ, and viscometric rheological data for 0.5% and 1% solutions of Separan AP30 in water (Leal et al., 1971).

Another independent variable in the present study is the drop size (or drop volume). In order to characterize the size of a drop, we follow Olbricht and Leal (1983) and introduce λ as the ratio of the radius of the undeformed drop to the effective radius of the tube r_{HP}. The drop volumes and the corresponding λ's used in our experiments are given in Table 2. Relatively large values of drop volume were used for the present study compared to previous work. Where it is necessary to compare results for viscoelastic and Newtonian drops, the Newtonian data of earlier studies was extended to larger values of λ.

In order to account for the viscoelastic character of the suspended drops, it is necessary to introduce at least one elastic parameter. Before discussing this,

however, we note that the *purely-viscous* non-Newtonian property of shear-thinning is already inherently included in the viscosity ratio — where the drop viscosity is taken as the shear viscosity at the effective wall shear rate. The relative importance of elasticity is characterized in this present study by the dimensionless Deborah number, which is the ratio of the primary relaxation time of the fluid, θ_f, to a characteristic timescale for changes in the rate of strain of the flow, θ_p. We have estimated the relaxation time θ_f from rheological data for the shear viscosity and the primary normal stress difference according to a formula which pertains to the convected Maxwell fluid, i.e.

$$\theta_f = \frac{\zeta_{11} - \zeta_{22}}{2\mu_i \dot{\gamma}^2} \tag{2}$$

where $\zeta_{11} - \zeta_{22}$ is the primary normal stress difference for a steady simple shear flow with shear rate $\dot{\gamma}$. Values for $\zeta_{11} - \zeta_{22}$, μ_i and $\dot{\gamma}$ were taken from available viscoemetric data (Leal et al., 1971) at the effective wall shear rate β_w. θ_p was estimated to be the inverse of the strain rate τ that a viscoelastic drop experiences as it moves from a bowed section to a constriction in a section of the wavy-wall tube. The strain rate τ is calculated following the analysis of Marshall and Metzner (1977) for flow in the frusta of right cylindrical cones, which was derived as an approximation for flows into and out of the constrictions in a porous medium. In their analysis, the characteristic time for the flow is given by

$$\theta_p = \left[\sqrt{D/Dt(|II_d|)^{1/2}}\right]^{-1} \tag{3}$$

where II_d represents the second invariant of the deformation rate tensor. Marshall and Metzner's analysis shows that the RHS of this expression can be approximated in the form

$$\frac{D}{Dt}\sqrt{|II_d|} = \frac{V}{L_1}\sqrt{\frac{3}{2}(V/L_1)^2 + \frac{1}{4}(V/(L_2)^2} \tag{4}$$

where V is the mean velocity of flow through a porous medium or conduits and L_1 and L_2 are two length scales related to the geometry of the particles which make up the porous medium. Combining (2)-(4), Marshall and Metzner obtained an approximate expression for the Deborah number,

$$De = \theta f\frac{V}{L_1}\sqrt{\frac{3}{2} + \frac{1}{4}(L_1/L_2)^2} \tag{5}$$

We used Eq. (5) in our work to calculate a value for De. In our case, we have taken V to be

$$V = V_s = \frac{\bar{u}}{\bar{v}}(\bar{v}_2 - \bar{v}_1) \tag{6}$$

where $\bar{v}_1$ and $\bar{v}_2$ are the average velocity of the suspending fluid, without the drop, calculated at the throat and bowed section of the wavy-wall tube, respectively, and $\bar{u}/\bar{v}$ is the drop mobility (defined below) which is expected to account for the actual rate at which the viscoelastic drops move; L_1 (0.75 cm) is the length scale characeristic of a half period in the tube geometry; L_2 (0.45 cm) is the radius of the maximum cross sectional area of the wavy-wall tube. Introducing Eq. (6) into Eq. (5), our expression for De becomes

$$De = \theta_f\frac{V_s}{L_1}\sqrt{\frac{3}{2} + \frac{1}{4}(L_1/L_2)^2} \tag{7}$$

In addition to the time-dependent drop shape which was recorded on videotape, the other important *dependent* variables are the dimensionless extra pressure drop, ΔP^{++}; the dimensionless magnitude of the periodic part of the signal pressure,

$\delta(\Delta P^{++})$, and the drop mobility, $\bar{u}/\bar{v}$. ΔP^{++} is the measured *change* in the pressure drop *caused by a droplet* in its passage through the test section, rendered dimensionless by the quantity $\mu\bar{v}/r_{HP}$. For practical purposes, our results are presented here in terms of ΔP^{+}, defined as an arithmetic average of the maximum and minimum value of the periodic pressure signal, i.e., $\Delta P^{+} = \frac{1}{2}(\Delta P^{++}_{max} + \Delta P^{++}_{min})$. Likewise, we define the nondimensionalized magnitude of the periodic part of the pressure signal as $\delta(\Delta P^{++}) = (\Delta P^{++}_{max} - \Delta P^{++}_{min})$, which can be important, as we will see, under certain flow conditions. The drop mobility is the mean velocity of the drop as it passes through the test section (the distance between fixed marks located at the ends of the test section, divided by the elapsed travel time) relative to the average flow velocity. ΔP^{+} is thought to provide one measure of the relative accessibility of individual pores of a porous matrix to two-phase flow relative to pores that do not contain drops. Likewise, the drop mobility ($\bar{u}/\bar{v}$) is thought to be related to the mobility of the suspended phase in an actual two-phase flow through a porous media. We will also make use of a drop deformation parameter d, defined here as the ratio of the maximum longitudinal drop length measured along the centerline of the flow to the wavelength of a single period of the wavy-wall tube.

Finally, we found it useful on a strictly empirical basis to introduce the dimensionless group ($De/\Gamma\sigma$) since drop shape and drop deformation seemed to correlate better with this ratio of parameters, than with any of the parameters taken individually.

3. Experimental Results

A drop moving within the wavy-wall tube causes a periodic variation in the pressure signal. There is one oscillation each time the drop passes through one period of the test section. In addition, small spurious transient disturbances appear at the beginning and at the end of each experiment corresponding to the passage of the drop over the pressure ports located at the entrance and the exit of the test section. The particular form of the pressure signal depends on the time-dependent drop shape, the latter depends on λ (drop size), on Γ (ratio of viscous forces to interfacial tension forces) and presumably on elastic forces as will be discussed in the following sections.

3.1 Small-Γ Systems (0.5% Polymer Concentration)

We first consider the two smallest flow rates within the range of our experiments which correspond to Systems 1 and 2 [see Table 1(a) for their properties]. We additionally limit our discussion to drops which are 0.5% polymer. Later, we shall consider similar results for a 1% polymer solution.

3.1.a System 1

System 1 corresponds to the slowest flow rate used in the present study, Q = 1.05 cc/min, which already gives Γ = 0.077 (and, consequently, σ = 1.68). The most surprising and potentially important fact is that the elasticity of the drops, at this very small flow rate and small Γ, actually appears to promote drop breakup (for λ => 1.442). This result is entirely opposite the behavior observed for viscoelastic suspending fluids, which always tended to stabilize drops against breakup. In fact, in the present case, Newtonian drops flowing under the same conditions would not undergo breakup at all! On the other hand, we find that large viscoelastic drops ($\lambda \geq 1.442$) in a Newtonian suspending fluid break up as they pass through the first

constriction of the test section! We shall discuss the details of this breakup process, as well as observations of the drop shape later in this subsection.

First, however, we highlight two additional differences between the present results for a viscoelastic drop at small flow rates ($\Gamma = 0.077$), and the behavior of a Newtonian drop in a Newtonian fluid. These are

(i) *Insensitivity of drop behavior to polymer concentration for 0.5% polymer and lower concentrations* — specifically, we tested two additional polymer concentrations for the drop fluid (0.01% and 0.1%) for the same $\Gamma = 0.077$. The results for drop mobility and for the time-dependent pressure signal are practically identical for all three polymer concentrations. This is particularly surprising in view of the fact that the viscosity is much different for the three fluids tested, and the viscosity ratio was found in earlier studies to be very important for both mobility and pressure for Newtonian drops in Newtonian fluids. The only difference in the drop mobility relative to the Newtonian case is that there appears to be a minimum in $\overline{u}/\overline{v}$ at an intermediate value of $\lambda \approx 1.04$, whereas Newtonian-Newtonian systems appear to approach the asymptotic value for $\overline{u}/\overline{v}$ in the limit $\lambda >> 1$ in a monotonic fashion. Figures 2(a) and 2(b) show, respectively, ΔP^+ vs. λ and $\overline{u}/\overline{v}$ vs. λ for the small-Γ systems. Data for a Newtonian-Newtonian system with large values of λ has also been included for comparison purposes. Note that for system 1, in those cases where drop breakup occurs, ($\lambda \geq 1.44$) the mobility of both the leading drop and the trailing drop (after breakup) has been plotted. Insofar as the time-dependent pressure is concerned, one can see in Fig. 3 that the actual

time-dependent pressure signals for drops made of 0.01%, 0.10% and 0.5% polymer are practically identical for a value of $\lambda = 1.15$, as is also the case for the other values of λ. The photographs in Fig. 4 show the three different viscoelastic drops in a highly deformed configuration at the moment of breakup and again the close resemblance among them can be seen.

(ii) *The phase relationship between* ΔP^+ *and drop position is different for viscoelastic drops as compared with Newtonian drops.* The maximum value of the time-dependent pressure signal for a viscoelastic drop in a Newtonian suspending fluid is attained as the drop *approaches* a constriction of the wavy-wall tube. In the case of a Newtonian-Newtonian system, on the other hand, maximum values of ΔP^+ were always attained when the drop was midway through a constriction. It is evident that elasticity of the viscoelastic drops plays a strong role, for this small Γ, in resisting drop deformation, hence requiring larger values of ΔP^+ to force the drop into a constriction.

It is evident that the differences cited above between Newtonian and viscoelastic drops at small Γ are due largely to pure elastic effects in the liquids. The strongest evidence that shear thinning or other "nonelastic" manifestations of non-Newtonian behavior is not a significant factor is that drop dynamics is basically invariant to changes in polymer concentration from 0.01% to 0.5% by weight. On the other hand, all elastic effects discussed above were found to occur at a relatively constant value of De of $O(10^{-1})$. The De number calculated on the basis of Eq. (7) for the smallest flow rate (Γ =

0.077) is De = 0.086 for 0.5% solutions De = 0.05 for the 0.1% solution and De = 0.02 for a 0.01% solution, respectively. Such a low estimate does not rule out the existence of at least moderate elastic effects. Of particular interest in this regard, is the work of Marshall and Metzner (1967) on the flow of viscoelastic fluids through porous media. They found that the critical value of De, at which appreciable influences of fluid elasticity were first observed, was between 0.05 and 0.06.

It is difficult to understand why drop elasticity promotes drop breakup at this low flow rate. Drop breakup was observed only for drop sizes such that $\lambda \geq 1.442$ ($\Gamma = 0.077$, $\sigma = 1.68$). The mode of drop breakup is illustrated in the photographic sequence shown in Fig. 5 for the 0.5% polymer solution. The viscoelastic drop moves very slowly into the first constriction in the wavy-wall tube and takes on the dog-bone shape shown in the first photograph in Fig. 5. This shape is not much different than would be observed for a Newtonian drop at the same value of λ and Γ. In the present case, however, the central waist becomes thinner and thinner until finally the drop splits into two daughter drops. The breakup process observed resembles closely the snap-off process that oil bubbles undergo when they are forced to move slowly through the throat of a capillary pore which initially contains only water. Quasi-static analyses of this snap-off process are described in detail by Pickell et al. (1966) and Roof (1970). Additionally, dynamic effects in the snap-off process for gas bubbles moving within constricted capillary have been studied recently in a series of papers by Radke et al. (1987). These studies, though, have been made for Newtonian-Newtonian systems and their results depend on

the particular characteristics of their experiments (for example, the unconstricted capillary radius, the geometry of the constriction, the length of the initial bubble, etc.). However, the mechanism for snap-off is common in all those systems. Snap-off occurs due to a difference in the interfacial curvature that allows suspending liquid (wetting phase) to be driven by surface tension into a growing collar at the pore constriction. In our particular case, a viscoelastic drop breaks up at the first constriction of the wavy-wall tube while an equivalent Newtonian drop does not. A comparison between the corresponding drop shapes may be made by looking at the photographic sequences in Figs. 5(a) and 5(b), which show, respectively, the changes in shape of both a viscoelastic drop and an equivalent Newtonian drop as they move through the first constriction of the wavy-wall tube. Such comparison shows clearly that even though both drops begin with similar shapes (first and second photographs in both sequences), their shapes become quite different as they advance through the constriction. We denote the radius of the waist of the viscoelastic drop as $W_1(t)$ and the radius of the waist of the Newtonian drop as $W_N(t)$. For the viscoelastic drop, $W_1(t)$, is independent of time for a short interval, roughly between the time of the first photograph and just before the second photograph, of Fig. 5(a). Afterward, however, $W_1(t)$ decreases rapidly for an interval of time between, t_o, at which a sharp curvature starts to form in the waist of the drop, and a time t_b, at which the drop breaks up. t_o corresponds to the second photograph and t_b corresponds to the fourth paragraph in Fig. 5(a). The time taken for drop breakup to occur is $t_b - t_o = 9$ sec. Note that the characteristic time for the flow process at $\Gamma = 0.077$ based on Eq. (3) (residence time

for the drop) is about the same magnitude (θ_p = 8.3 sec), therefore allowing the snap-off process to occur. We will see that this is not the case for the next larger flow rate in which it seems that the shorter time residence time for the drop in the constriction does not provide enough time for snap-off of the drop. In contrast, we can see from Fig. 5(b) that $W_N(t)$ is essentially constant function at all times. The photographic sequence shows that the Newtonian drop moves through the constriction without any sign of possible breakup. The fifth photograph in Fig. 5(a) shows the two daughter drops produced after drop breakup, its counterpart in Fig. 5(b) shows the intact Newtonian drop entering the second constriction of the test section while it has not yet entirely cleared of the first one.

In the remainder of this subsection, we give a detailed account of drop deformation, drop breakup and their influence on the dynamics of the drop for System 1. First of all, the time-dependent pressure signal depends strongly on λ, as was also true of the Newtonian and non-Newtonian systems studied earlier. Typical pressure signals from the pressure transducer chart recorder are shown in Fig. 6 for several values of λ. Corresponding photographs showing the drop shape are presented in Fig. 7. For these small Γ systems, the smallest drop, i.e. λ = 0.61, barely deforms (its undeformed radius is smaller than the radius of the "throats" in the wavy wall tube) and the extra pressure drop is essentially constant, independent of time. When λ increases to 0.77, the droplet undergoes much more deformation (its undeformed radius is larger than the radius of the throats in the wavy wall tube) and the pressure signal becomes clearly time dependent and periodic. As λ increases, the drop

undergoes a great deal of deformation, the drop shape in the throat resembling a peanut with a narrow waist and bulbous ends parts that occupy an entire period of the wavy wall test section. Such is the case for $\lambda = 1.04$ (drop volume 0.15 cc) and $\lambda = 1.15$ (drop volume 0.20 cc). It is interesting to note that we have a minimum value for the drop mobility at $\lambda = 1.04$, with larger values obtained for $\lambda = 1.15$ ($\overline{u}/\overline{v}$ vs. λ is shown in Fig. 2(b)). This fact was mentioned earlier in this section as an example of departure from purely Newtonian-Newtonian behavior, but remains basically unexplained. However, a smaller increase in mobility, $\overline{u}/\overline{v}$, with increase in λ was also found for $\lambda \approx 1.44$, which we do understand to be a consequence of drop breakup. Indeed, for $\lambda = 1.44$ (original drop volume 0.40 cc), drop breakup produced two daughter drops, the first slightly larger than the second; therefore, the first drop had a volume slightly larger than 0.20 cc (hence, $\lambda > 1.15$), and the second drop had a volume less than 0.20 cc (hence, $\lambda < 1.15$). Now, as these two drops travel along the test section, the first drop "advances" its relative position with respect to the second drop — so much so that, by the end of the run through the test section, there are about two periods of the wavy wall tube between them. Indeed, it can be seen in Fig. 2(b) that there is a reasonable quantitative agreement between the velocity of the smaller drop after breakup for $\lambda = 1.44$, and the velocity of a single drop for $\lambda = 1.04$.

The different mobilities for the two daughter drops give rise to a very complex dependence of the time-dependent pressure signal on the relative positions of the drops, i.e., while both drops move in phase with respect to the geometry of the wavy wall tube, their relative contributions to the extra

pressure drop are additive. On the other hand, when one drop moves within a bowed section, while the other drop moves within a narrow section, their relative contribution to ΔP^+ tends to counteract each other. The in-phase mode brings about relatively large values of $|\delta(\Delta P^{++})|$ about the "zero" differential pressure line, whereas the out-of-phase mode produces smaller values of $|\delta(\Delta P^{++})|$ at a slightly lower mean value. The actual form of the time-dependent pressure signal caused by the viscoelastic drop with an original volume of 0.40 cc may be seen in Fig. 8. The averaged effect of these oscillations is a small negative extra pressure drop as shown in Fig. 2(a).

For the next larger drop, $\lambda = 1.655$. The original drop (with a vol = 0.60 cc) breaks up at the first constriction, producing two daughter drops of approximately equal volumes ($\lambda \sim 1.31$) which travel at equal speeds through the test section. It may be noted that the velocity shown as $\overline{u}/\overline{v}$ in Fig. 2(b) is that of the lead drop of the pair after breakup. The nearly equal velocity of the trailing drop is also shown. Because the drops travel with the same velocity, the pressure signal does not depend on the relative position of the drops. The two large daughter drops have a drop mobility that behaves in the same way as the case described earlier, i.e., their drop mobility is larger than that corresponding to values of $\lambda \sim 1$. In this case, there is a second drop breakup — the trailing drop splits into two smaller drops at the last constriction before the exit of the test section, though the influence of this second breakup is not felt in either $(\overline{u}/\overline{v})$ or in ΔP^+ because immediately afterward the three drops exit the test section.

The largest drop size used in this experiment was $\lambda = 1.822$. In this case, breakup again occurred at the first constriction. The original drop produced two daughter drops of approximately equal size (~0.40 cc), which travel at the same velocity through the first half of the test section. At appropximately the middle of the wavy wall tube, however, breakup occurred again for the trailing drop, giving birth to two smaller droplets, the first of which was slightly larger than the second. Again (with the three drops now traveling along the wavy wall tube), the first two drops continue at the same velocity they had earlier. However, the mobility of the third drop, i.e., the smallest of the drop, is about 10% less than the mobility of the two leading drops.

3.1.b System 2

System 2 is generated from a flow rate Q = 1.63 cc/min ($\Gamma = 0.11$, $\sigma = 1.37$). Drop breakup was not observed in this system for any drop size, apparently because the increased flow rate was too large and the drop did not have time to build a sufficiently thick liquid collar around its waist to finally pinch off. The largest drops ($\lambda \geq 1.442$) do assume very deformed configurations, but never proceed to the extreme case of drop configuration that led to breakup for large drops in System 1. As in system 1, the waist radius of a large drop ($\lambda \geq 1.442$) in system 2, say $W_2(t)$, is also a *decreasing* function of time (and in this sense, the behavior is different from that experienced by a Newtonian drop),but it does not reach a configuration such that pinch-off is imminent. Rather, the minimum value $W_2(t)$ attains at time t_m is about 60% of the initial value $W_2(t)$, i.e., $W_2(t_m) = 0.60\ W_2(t_o)$. The time taken to thin from $W_2(t_o)$ down to $W_2(t_m)$ is $t_m - t_o = 5$ sec, which is the total

"residence time" for the flow process at Γ=0.011 (θ_p = 5.18 sec). The drop simply has no time to decrease its waist radius $W_2(t)$ below 60% of $W_2(t_o)$, i.e., to generate the sharper curvatures at its waist which characterize "pinch-off".

In some ways, System 2 seems to be an intermediate case between small and large Γ systems. For instance, drop-breakup was not observed for System 2 and this turned out to be a distinctive characteristic common to all large Γ systems. However, the dependence of drop mobility on λ was found to be very similar to that discussed for System 1. Figures 2(a) and 2(b) show respectively the average extra pressure drop ΔP^+ vs. λ and the drop mobility ($\bar{u}/\bar{v}$) vs. λ for system 2. One can see that all of the trends discussed earlier for Γ = 0.077, with respect to the average extra pressure drop and drop mobility, remain valid for Γ = 0.11. The only difference is that breakup was not observed for any λ in this case.

3.2 Large Γ-Systems (0.5% Polymer Concentration)

In the following, we consider experimental results for the 0.5% polymer solutions at higher flow rates which yield System 3 with Γ = 0.26, System 4 with Γ = 0.34, System 5 with Γ = 0.58, and System 6 with Γ = 1.12. Corresponding values for the viscosity ratio and other properties are given in Table 1(a). All of these relatively large-Γ systems show qualitatively similar behavior and hence they are discussed together. In addition, some of our results for a more concentrated polymer solution (1.0%) are also considered in this section in order to make the discussion on drop deformation more complete.

3.2.a Drop Shape and Drop Deformation

The main *common* feature of the large-Γ systems is that drop breakup was not observed, at least not in the definitive way described above for the smallest Γ system. Consequently, the average extra pressure drop was not affected at all by breakup phenomena. The largest drops moving at the largest flow rates did develop extremely thin, hair-like tails that sometimes were left behind the drop in the form of minute droplets, but this had no measurable influence on the volume of the drop, nor on ΔP^+ or $\bar{u}/\bar{v}$. For the largest flow rates (Γ=0.58 and Γ=1.12) and $\lambda \geq 1.04$ the pressure signal did not attain a constant mean value during the drop passage through the first periods of the wavy wall test section as it did for smaller Γ values. Rather, it first decreased monotonically and only achieved a constant mean value over the last third of the test section. The values of ΔP^+ were taken for such cases in the corresponding last third of the pressure signal curve. Fig. 9 shows the pressure signal for λ=1.04 and λ=1.15 at Γ=0.58 . For these large flow rates the parameter d as well as the drop shape depended very weakly on Γ . Table 4(a) shows (0.5% solution, all λ's) how small are the changes of d are, relative to changes in Γ which vary by more than a factor of four. Figure 10 shows photographs of three drops (0.5% solution) of equal size (λ=1.15) which are moving at three different flow rates. We can see that the changes undergone by both d and drop shape are very small with respect to Γ. In the same figure, the third photograph shows a somewhat sharper drop (Γ=0.58 , d = 1.20) relative to the shape shown in the second photograph. Likewise, the second photograph shows a somewhat sharper drop (Γ=0.34 , d = 1.10) relative to the shape shown in the first

photograph. The drop shown in the first photograph moves at Γ=0.26 with d = 1.00. A similar result is obtained for the other values of λ. The relevance of these results stands in the fact that the drop shape (and the parameter d) in a Newtonian-Newtonian system under similar flow conditions were found in (III) by Olbricht and Leal (1983) to be much more sensitive to changes in flow rate. However, their results only emcompass the range $0.62 \leq \lambda \leq 1.15$. The phenomena we have observed for viscoelastic drops occurs for $0.62 \leq \lambda \leq 1.65$. However, it seems reasonable to expect the same type of behavior for the Newtonian-Newtonian systems for the last two larger values of λ . Table 4(c) shows our experimental results with Newtonian-Newtonian systems. Parameter d is obtained for two different flow rates and two different viscosity ratios. There it is clear how sensitive d is with respect to Γ for Newtonian systems. It appears that the drop deformation behavior just described for viscoelastic drops is due to the effects on drop deformation of the time-dependent response of the viscoelastic drop liquid to the Lagrangian unsteadiness of the flow, and that the elastic forces act on the drop as an extra restoring mechanism against longitudinal elongation of the drop. Such a mechanism would exist in addition to the interfacial tension forces which are also present.

It is important to note that the lack of dependence of d on Γ cannot be attributed to the effects of the companion shear-thinning properties of the drop liquid. One may infer from previous works on Newtonian-Newtonian systems (III) that deformation is decreased *weakly* with decrease in the viscosity ratio, all else being equal, and it may at first seem that the decrease in viscosity ratio with increase of flow rate (due to shear thinning) may compensate for the

increase of Γ and thus account for the lack of change in d with Γ. However, in order for a lower viscosity ratio to start being noticeable in the reduction of drop deformation, a very large decrease in the viscosity ratio would be required. For instance, for an increase in flow rate of less than double, i.e. from 4.7 cc/min to 8.6 cc/min (Newtonian-Newtonian systems), a decrease from σ = 14.6 down to σ = 0.7 is required before the decrease in viscosity ratio would start to be noticeable in compensating for the increase of Γ in inhibiting drop deformation (of course, in dealing with Newtonian-Newtonian systems a change in viscosity ratio implies a change of the constituting materials).

The case of viscoelastic drops (0.5% concentration) is different because changes imposed in flow rate bring about only small changes in the viscosity ratio. Indeed, even when the flow rate increases by more than four times in magnitude, the associated decrease in viscosity ratio is only a factor of two relative to the viscosity ratio corresponding to the slowest flow, i.e. while the flow rate increases from 3.8 cc/min to 15.94 cc/min, the viscosity ratio decreases only from 0.92 to 0.46. This relatively weak dependence of σ on flow rate clearly rules out shear-thinning effects as a plausible explanation for the lack of sensitivity of drop deformation on Γ.

In order to further investigate the effects of elasticity on drop deformation, it is useful to briefly consider the effect of having a more concentrated Separan solution (1%) for the drop. The results seem at first contrary to expectations, i.e., these 1% drops deformed in a manner wich resembles resembling the deformation behavior in the Newtonian case (d significantly increases with Γ) more than that observed for the 0.5% viscoelastic solution,

despite the fact that, in absolute terms, the 1% solution is more elastic than the 0.5% solution, as shown in Tables 3(a) and 3(b) (De number has been calculated by means of Eq. 7). This surprising result seems due to the fact that, in addition to the stronger elastic properties of the 1% solution relative to the 0.5% solution, the viscosity is also much larger and consequently, the drop behavior may be dominated by stronger viscous effects which overwhelm any changes in the elastic effects. The viscosity ratio for both polymer concentrations may be seen in Tables 1(a) and 1(b). Table 4(b) provides information about d as a function of Γ (1% solution, all λ's). It shows a much larger drop elongation represented by d (hence, a much larger change in drop shape) relative to those values obtained for the 0.5% solution. Comparison between Table 4(a) and Table 4(b) shows the different scale at which the changes of d with respect to Γ take place in each solution. In addition, Fig. 11 shows the photographs of three drops (1% solution) of the same size (λ=1.15) which are moving at three different flow rates. We can clearly see the larger changes of both d and drop shape with respect to Γ relative to the much smaller changes undergone by these variables for 0.5% drops moving under the same flow conditions (compare Fig. 11 with Fig. 10).

Our results regarding drop deformation behavior for 0.5% and 1% solutions, and the comparison with Newtonian drop behavior, seems to offer no clear correlation with any of the governing parameters Γ, σ or De if they are considered independently. However, if we consider all of them acting simultaneously in a single group, then we may have a better insight on the mechanisms involved in drop deformation. Assuming that, for these large-Γ systems,

the elastic forces represented by De number are indeed an additional restoring mechanism (as seems to be the case from our experimental results), then the ratio $\Gamma\sigma/De$ would have the physical significance of a balance between deforming-restoring interactions. Hence, a larger value of $\Gamma\sigma/De$ should correspond to a larger value of d and vice-versa. There is, in fact, a parallelism between the observed behavior of the deformation parameter d for the 0.5% and 1% solutions, and the magnitude of the group $\Gamma\sigma/De$. For instance, for the 0.5% solution where d remains almost constant, the parameter $\Gamma\sigma/De$ also remains nearly constant, i.e. $1.4 < \Gamma\sigma/De < 1.6$, in spite of the fact that Γ, σ, and De vary individually. On the other hand, for 1% solutions where d varies significantly with respect to Γ, the parameter $\Gamma\sigma/De$ also varies over a much larger range, i.e. $3 < \Gamma\sigma/De < 5$. Table 5 shows comprehensive results for d for both the 0.5% and 1% solutions. We can see that increased values for $\Gamma\sigma/De$ are strongly correlated with larger values of the parameter d, at least over the range of values for $\Gamma\sigma/De$ that encompassed by our data. In spite of this correlation, however, it is not possible to interpret $\Gamma\sigma/De$ in a more definitive, physical manner than indicated above.

3.2.b. Drop Mobility

Figure 12(a) shows experimental results for drop mobility versus drop size for fixed values of the capillary number Γ, in this "large" Γ regime for the 0.5% drops.

In this case, drop mobility is essentially independent of λ, with the only exception being the smallest drop that, for each flow rate, moved along the test section with a drop mobility of approximately 10% larger than the

corresponding mobility of the larger drops. This is due to the fact that the undeformed radius is smaller than the constriction radius, which allows the drop to position itself entirely in a small region about the flow centerline at which the maximum flow velocity occurs. Drop mobility is an increasing function of Γ, and most probably is independent of the viscosity ratio, at least within the restricted limits of the range of viscosity ratio caused as a consequence of increasing flow rate in conjunction with the shear thinning properties of the viscoelastic drops. In support of this last argument is the known fact that similar Newtonian-Newtonian systems in earlier studies did not show a dependence of drop mobility on viscosity ratio, in spite of the extremely large range of the viscosity ratios, that were considered, ($0.7 < \sigma < 14.6$). The increase in mobility with Γ is correlated with the observation mentioned earlier and shown in Fig. 10, that the front edge of a moving drop becomes increasingly streamlined as the flow rate increases, favoring its motion through the constrictions of the wavy-wall tube, and thereby increasing its average absolute velocity through the test section.

3.2.c. Average Dimensionless Extra Pressure Drop, ΔP^+

Figure 12(b) shows the dependence of ΔP^+ versus drop size for the 0.5% solution at the higher flow rates corresponding to the larger values of Γ. ΔP^+ is a monotonically decreasing function of λ for the three largest flow rates whereas, for the lowest flow rate in these large Γ-systems (with a corresponding $\sigma = 0.92$), the dimensionless extra pressure drop begins with a positive value for $\lambda = 0.62$, takes on a maximum value for $\lambda = 0.77$, and then decreases monotonically for $\lambda > 0.77$.

For fixed values of Γ, $|\delta(\Delta P^{++})|$ increases with drop size until $\lambda \sim 1$ but for $\lambda > 1$, it no longer depends on λ. In addition, for $\lambda > 1$, $|\delta(\Delta P^{++})|$ is very small compared with the total value of the averaged extra pressure drop for all flow rates. Such behavior for $|\delta(\Delta P^{++})|$ is in clear contrast to its behavior for the small-Γ systems.

3.3 Experimental Results for 1% Polymer Concentration

Finally, we consider the results for drops that are made from a 1% solution of Separan AP-30 in distilled water. In presenting the experimental results for this solution, no distinction is needed between small Γ-systems and large Γ-systems (at least for the range of our experiments) because all of the results, even those corresponding to the smallest value of Γ, follow the same general trend. Increases in Γ (flow rate) produce a corresponding decrease in values for the viscosity ratio (due to shear-thinning effects), but all of the latter were estimated to be larger than unity (see Table 1(b).

The drop shape and drop deformation for this concentration were discussed earlier, in connection with a general evaluation of the effect of elasticity on drop deformation behavior. It was found, in that discussion, that the larger viscosity ratios for these more concentrated systems seemed to overshadow the expected increase in elastic response, which was, in fact, much more evident for drops made of the 0.5% polymer solution than for those made of the 1% polymer solution. In general, it appears as though the same general trend of large viscosity ratios masking increased elasticity also applies to the extra pressure drop ΔP^{+} and the mobility $\bar{u}/\bar{v}$. Figure 13 shows the experimental curves for ΔP^{+} versus λ, and Fig. 14 shows the corresponding results for $\bar{u}/\bar{v}$

versus λ (1% polymer concentration). ΔP^+ is a monotonically increasing function of λ for fixed Γ (and thus fixed σ), and a decreasing function of Γ. The latter is certainly due to both the increased deformation for increase of Γ and the accompanying decrease of σ due to shear thinning. The magnitude of the pressure oscillations $|\delta(\Delta P^{++})|$ was large when compared with the value of ΔP^+ for the smallest flow rate ($\Gamma = 0.77$), especially for the small λ values, but was not as important as for the 0.5% polymer solution. $|\delta(\Delta P^{++})|$ for the larger flow rates was negligible when compared with the total value of the average extra pressure drop, especially for $\lambda > 0.62$.

With respect to drop mobility, it may be seen from the plot of $\bar{u}/\bar{v}$ versus λ in Fig. 14 that $\bar{u}/\bar{v}$ is virtually independent of λ, for $\lambda \geq 0.77$ when $\Gamma \geq 0.26$ and virftually independent of λ, for $\lambda \geq 1.04$ when $\Gamma = 0.077$. We may note that, unlike the corresponding drop mobility for the 0.5% polymer solution discussed in Sect. 3.2, the drop mobility for the 1% polymer solution *does not* undergo any "jump" for drop sizes $\lambda > 1$. Rather, it appears asymptotic at its minimum for $\lambda > 1$. This resembles again the typical Newtonian drop behavior discussed in 3.1a (for small Γ) and sustains the earlier hypothesis that, for the 1% drops, the elastic effects are negligable compared to the viscous effects within the range of our parameters. Furthermore, Fig. 15 shows the photographic sequence for a 1% drop of 0.40 cc of volume ($\lambda = 1.44$) which is moving through the first constriction of the wavy wall tube at a flow rate of Q = 1.05 cc/min ($\Gamma = 0.077$). The similarity between drop configuration as seen in this sequence and that one shown in Fig. 5(b) for a Newtonian drop (same Γ, same λ) is just as remarkable as the difference found when the same comparison is made with

the drop configuration shown in Fig. 5(a) for a 0.5% drop. A similar result is obtained for the other values of λ.

In comparing $\bar{u}/\bar{v}$ versus λ curves for the 1% experiments with the corresponding curves for the 0.5% experiments, it may be seen that, in spite of the different polymer concentrations, $\bar{u}/\bar{v}$ has fairly equal values for most of the flow rates used in our experiments.

4. Conclusions

The motion of viscoelastic drops suspended within a Newtonian fluid has been studied for flow through a converging/diverging channel. Different flow rates were employed so that a wide range of capillary numbers could be investigated. Drastically different behavior regarding drop shape, drop deformation and drop breakup was found relative to the behavior of Newtonian drops suspended in a Newtonian suspending fluid flowing through the same geometry. For instance, at small-Γ values, breakup was observed for large viscoelastic drops (0.5% polymer cocentration), and this brought about important consequences on the time-dependent extra pressure signal. A striking example of this was observed for a particular drop size where the two daughter drops, after breakup, travel through the test section with different mobilities hence causing the time-dependent signal pressure to depend on their relative positions in the wavy-wall tube. On the other hand, for the equivalent Newtonian-Newtonian problem, drop breakup was not observed at all for small-Γ values. For large-Γ values, a very different situation prevailed, i.e. Newtonian-Newtonian systems undergo large deformation when the flow

increases and may eventually break up downstream of the test section in a constant radius tube section. At these large-Γ values, viscoelastic drops were found to resist deformation and breakup. The average of the time-dependent dimensionless extra-pressure drop, the magnitude of its oscillations, and the drop mobility were found, with the exception of some particular cases (usually related to drop breakup), to follow the same general trends with respect to Γ and λ as the Newtonian-Newtonian systems, but very different trends with respect to changes in σ (due to elastic effects). Viscoelastic drops were mainly made of two different polymer concentrations (1% and 0.5%), and it was found that the more dilute solution showed *relatively stronger elastic effects,* which in the more concentrated solutions seemed to be dominated by viscous effects due to the drastic increase in drop viscosity which accompanied the increase in polymer concentration, and seemed to overshadow elastic effects in spite of the fact that, in absolute terms, these must also become larger.

Our results show that at small-Γ values, drop breakup may occur causing important effects on the drop dynamics. Such behavior may be worth noticing when dealing with two-phase flows (viscoelastic-Newtonian) through porous structures if dispersion phenomena is undesirable.

Breakup mechanisms for viscoelastic drops were described in terms of the snap-off mechanisms in capillary tubes that have been studied by earlier researchers for the Newtonian case. The difference between breakup for a viscoelastic drop and no breakup for an equivalent Newtonian drop was evidently made by more acute interfacial differences for the viscoelastic case with respect to the Nerwtonian case. However, the cause of the different

configurations assumed by the drops remains without explanation.

Due to the importance of dispersion phenomena in practical applications, it is important to investigate further the viscoelastic-Newtonian systems at low values of Γ, especially to determine the conditions for the capillary number at which drop breakup occurs. At such Γ, different Deborah numbers should be studied to acquire a better insight of the role of elasticity. According to our experiences with the 1% and 0.5% polymer concentration, it seems that the best way to systematically evaluate elastic effects associated with variations in De (at low Γ) is by changing the strength of the unsteadiness of the flow (rather than changing the concentration of polymer) in such a way that dominating viscous effects can be minimized. A systematic change in the strength of the unsteadiness of the flow would be possible, for example, by systematically changing the ratio between the maximum area of the cross section to the minimum area in a converging/diverging channel geometry. In order to keep Γ constant, the flow rates need readjusting according to the new hydraulic radii produced by the different channels.

A summary of the major departure of viscoelastic drop behavior with respect to Newtonian drop behavior (Newtonian suspending fluid for both cases) flowing under similar conditions, as well as the major common features, was also included in this work.

Table 1. Values of Γ and σ and other flow parameters for the drop liquids (0.5% and 1% by weight aquous sol. of separan AP 30). μ_i and consequently σ depend on the flow rate. T=25°C.

(a)

Ucon oil 1715 LB as suspending fluid (μ_o = 6.54, $\rho \sim 1$).
0.5% AP-30 Separan in Distilled Water as drop liquid.

Flow Rates Q (cm^3/min and Systems	β_ω	μ_i	$\sigma = \frac{\mu_i}{\mu_o}$	Γ	N_{11}
System 1 1.058	0.711	11	1.68	0.077	8
System 2 1.63	1.076	9	1.37	0.11	14
System 3 3.82	2.55	6	0.92	0.26	27
System 4 4.9	3.29	5	0.76	0.34	30
System 5 8.4	5.64	4	0.61	0.58	50
System 6 15.96	10.71	3	0.46	1.12	85

(b)

Ucon oil 1715-LB as suspending fluid
1.0% AP-30 Separan in distilled water as drop liquid.

System 7 1.05	0.711	38	5.81	0.077	60
System 8 3.82	2.556	21	3.21	0.26	150
System 9 4.9	3.29	20	3.0	0.34	180
System 10 8.4	5.64	15	2.3	0.58	250
System 11 15.94	10.71	9	1.37	1.12	300

Table 2. Drop volume and corresponding λ, which is defined as radius of undeformed drop/characteristic radius (r_{HP}).

Drop Vol., c.c	λ
0.03	0.62
0.06	0.77
0.10	0.92
0.15	1.04
0.20	1.15
0.40	1.44
0.60	1.65
0.80	1.82

Table 3. *(a)* for 0.5% viscoelastic drops and (b) for 1% viscoelastic drops.They show values of Γ and De with respect to the flow rate.

(a)

0.5% Separan Solution		
Q	Γ	De
3.8	0.26	0.157
4.9	0.34	0.175
8.4	0.58	0.223
15.94	1.12	0.338

(b)

1.0% Separan Solution		
Q	Γ	De
3.8	0.26	0.259
4.9	0.34	0.262
8.4	0.58	0.304
15.94	1.12	0.320

Table 4. *(a)* shows for 0.5% solution how highly insensitive the parameter d (at the "crossroads") is with respect to the flow rate (or Γ). d is defined as d = maximum longitudinal measure of the drop along the flow centerline/wavelength of a single cell of the wavy wall. *(b)* show the larger variation of parameter d respect to flow rate for the 1% polymer concentration. *(c)* gives data for Newtonian systems. Note that d is very sensitive to changes in the flow rate (Γ).

(a)

Q (cc/min)→	3.8	4.9	8.4	15.94
Γ →	Γ = 0.26	0.34	Γ = 0.58	Γ = 1.12
	σ = 0.92	σ = 0.76	σ = 0.61	σ = 0.46
↓λ				
0.62	0.4	0.4	0.4	0.4
0.77	0.75	0.75	0.75	0.75
1.04	0.90	1.0	1.0	1.0
1.15	1.0	1.1	1.2	1.2
1.442	2.0	2.0	2.2	2.2
1.655	2.8	2.8	3.3	3.2

(b)

Q (cc/min)→	3.8	4.9	8.4	15.94
Γ →	Γ = 0.26	0.34	Γ = 0.58	Γ = 1.12
↓λ	σ = 3.21	σ = 3	σ = 2.3	σ = 1.37
0.62	0.4	0.4	0.4	0.5
0.77	0.75	0.75	0.75	1.1
1.04	1.0	1.0	1.6	3.0
1.15	1.0	1.2	1.8	3.1
1.442	2.1	2.3	3.5	4.5
1.655	3.2	3.8	4.5	6.0

(c)

	σ=0.72		σ=7.47		σ=14.6	
Q (cc/min)→	4.6	8.6	4.6	8.6	4.6	8.6
Γ→	1.34	2.54	1.34	2.54	1.34	2.54
↓ λ						
0.62	0.60	0.81	0.61	0.83	0.65	0.90
0.77	0.89	1.45	0.91	1.50	0.91	1.50
1.04	1.90	2.80	1.92	2.80	1.92	3.00
1.15	2.36	3.30	2.40	3.50	2.50	3.90

Table 5. Comprehensive data for both solutions. Those systems with the largest value for $\Gamma\sigma/De$ (ratio between deforming mechanisms to restoring mechanisms) undergo the most severe deformations.

Q→	3.8		4.9		8.6		15.94	
	0.5%	1.0	0.5%	1.0%	0.5%	1%	.5%	1%
$\Gamma\sigma/De$ →	1.46	3.21	1.47	3.87	1.58	4.35	1.52	4.8
↓λ								
0.62	0.4	0.4	0.4	0.4	0.4	0.4	0.4	0.5
0.77	0.75	0.75	0.75	0.75	0.75	0.8	0.75	1.1
1.04	0.90	1.0	1.0	1.0	1.0	1.16	1.0	3.0
1.15	1.0	1.0	1.1	1.2	1.2	1.8	1.2	3.1
1.442	2.0	2.3	2.0	2.3	2.3	3.5	2.1	4.5
1.655	2.8	3.2	2.9	3.8	3.2	4.5	3.0	6.0

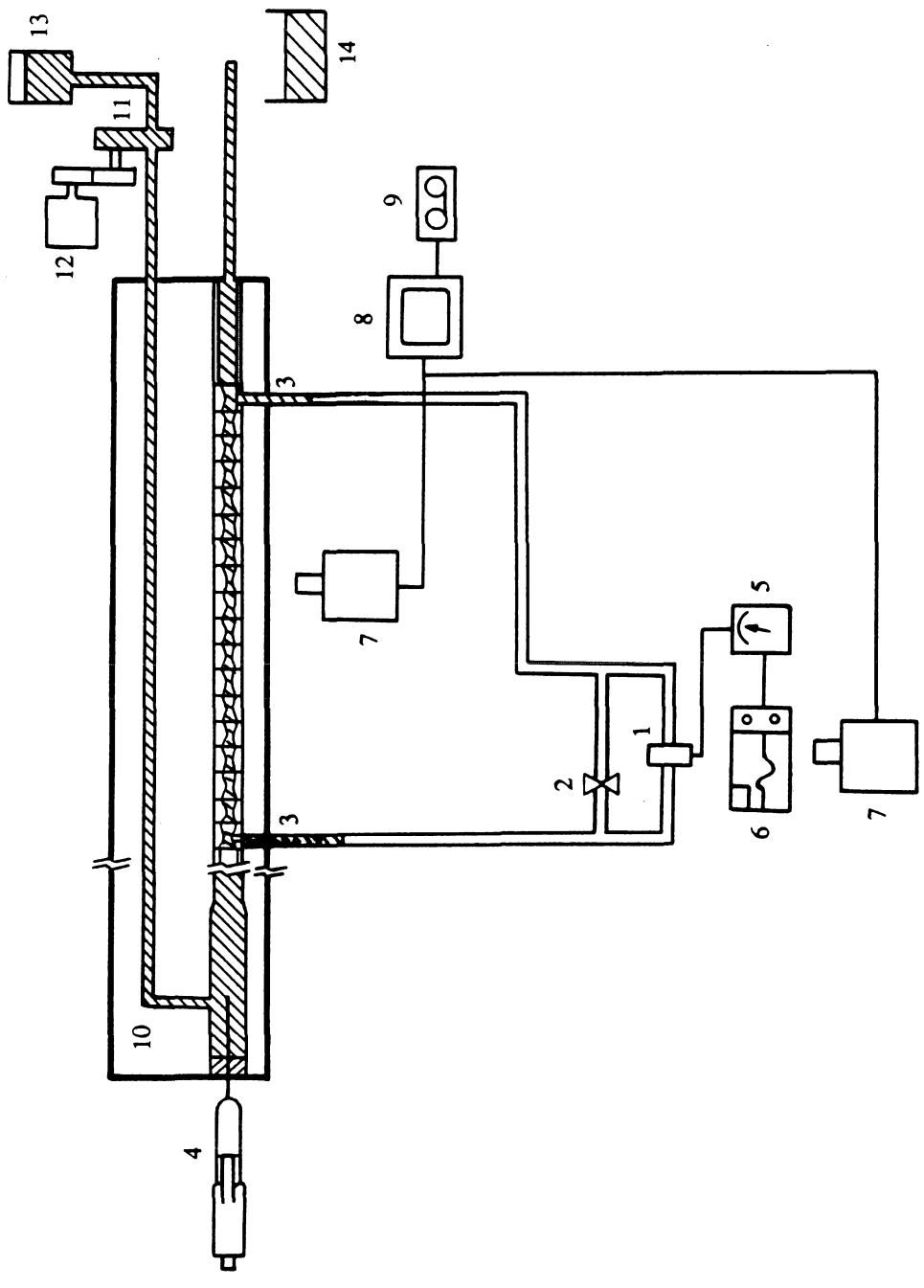

Figure 1. Experimental Setup: 1 Pressure transducer, 2 Manometer by-pass valve, 3 Pressure port, 4 Micrometer syringe, 5 Transducer indicator, 6 Strip chart recorder and timer, 7 Videocamera, 8 Monitor, 9 Videorecorder, 10 Constant temperature bath, 11 Gear pump, 12 Variable speed motor, 13 Suspending fluid reservoir, 14 Container.

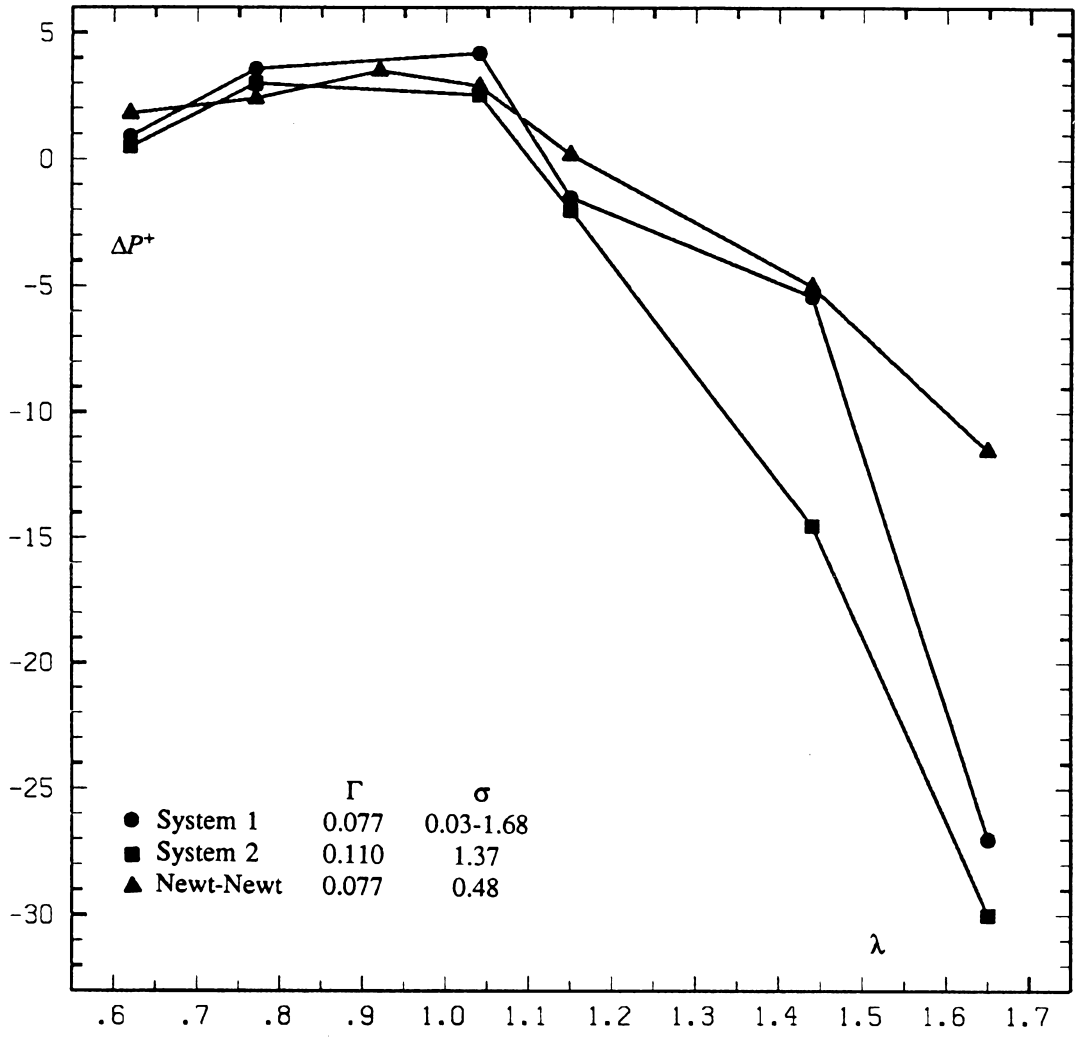

Figure 2(a). ΔP^+vs.λ, small-Γ systems. The curve for system 1 is valid for the three aqueous solutions of 0.01%, 0.10% and 0.50% of Separan AP 30 in distilled water. Notice the "off-trend" value for system 1 for λ=1.44 caused by the different mobility of the two drop caused by drop breakup.

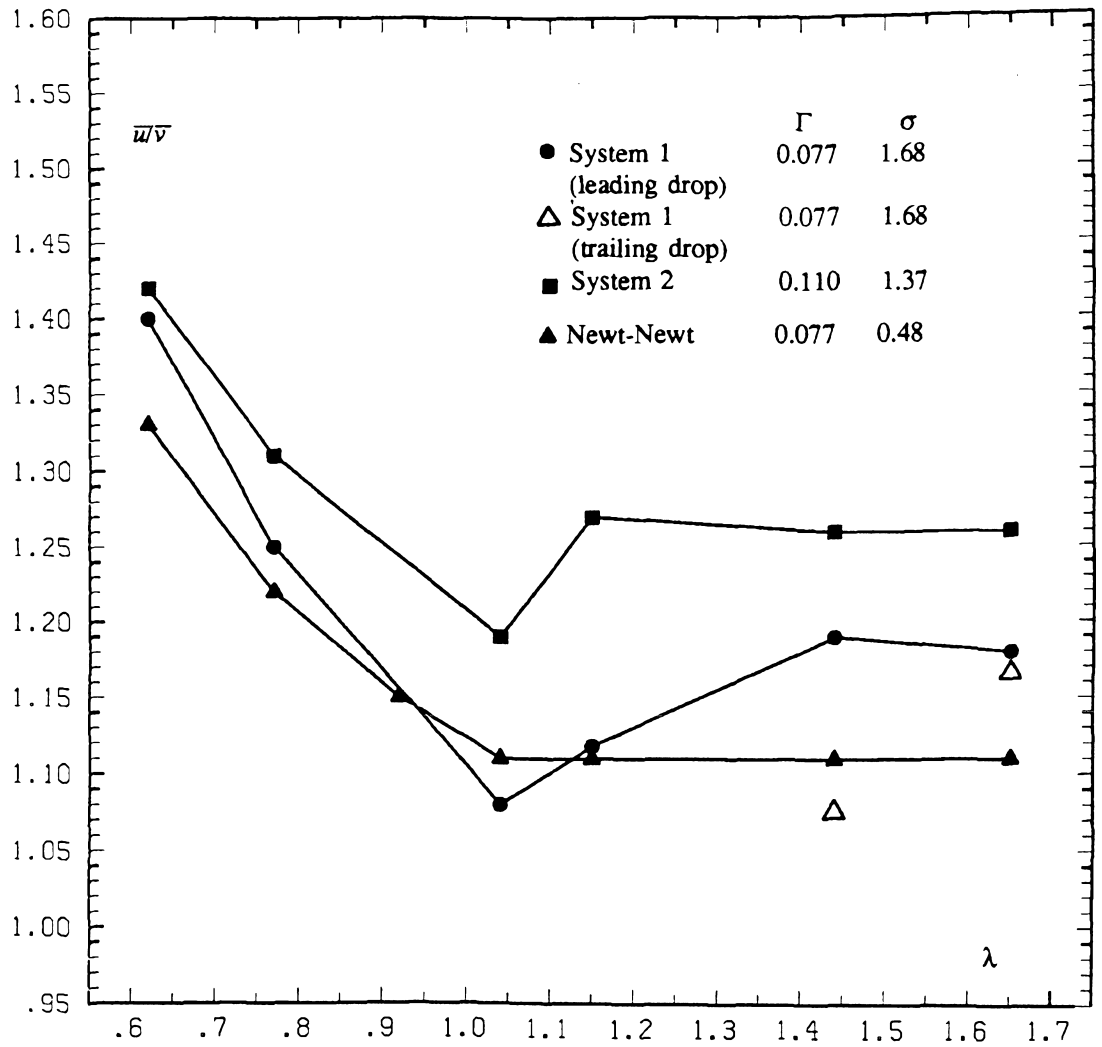

Figure 2(b). $\overline{u}/\overline{v}$ vs. λ, small-Γ systems. For system 1 drop breakup occurred for $\lambda \geq 1.44$, the data for these cases correspond to the leading drop after breakup. The Δ points correspond to $\overline{u}/\overline{v}$ of the trailing drop.

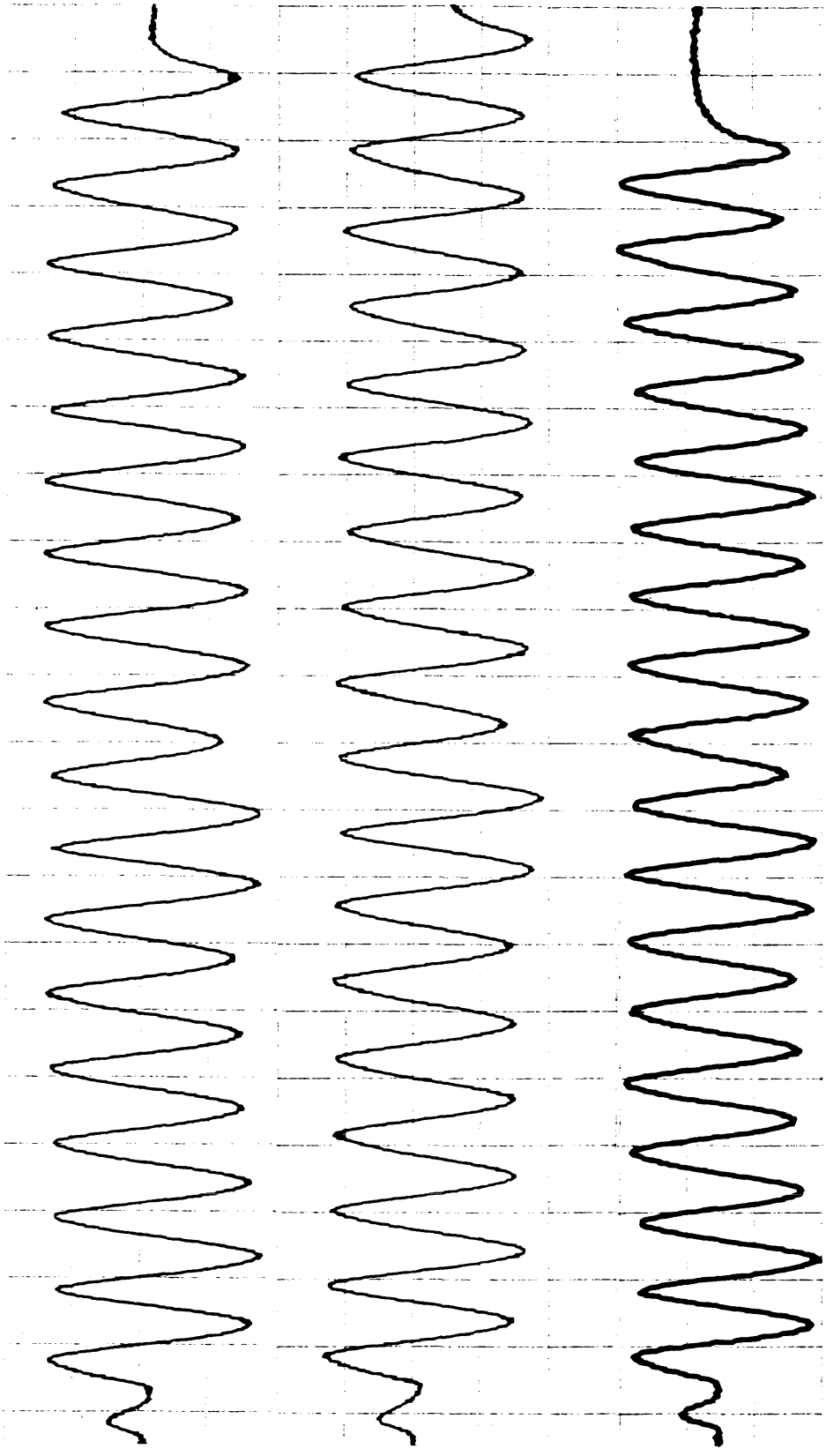

Figure 3. Pressure signal at Γ=0.077 for drops of equal size (λ=1.15) made of viscoelastic fluids of different polymer concentrations; (a) 0.01%; (b) 0.10% and (c) 0.50% by weight. The insensitivity of the pressure signal with respect to the viscosity ratio is clear. Similar results are obtained for all values of λ.

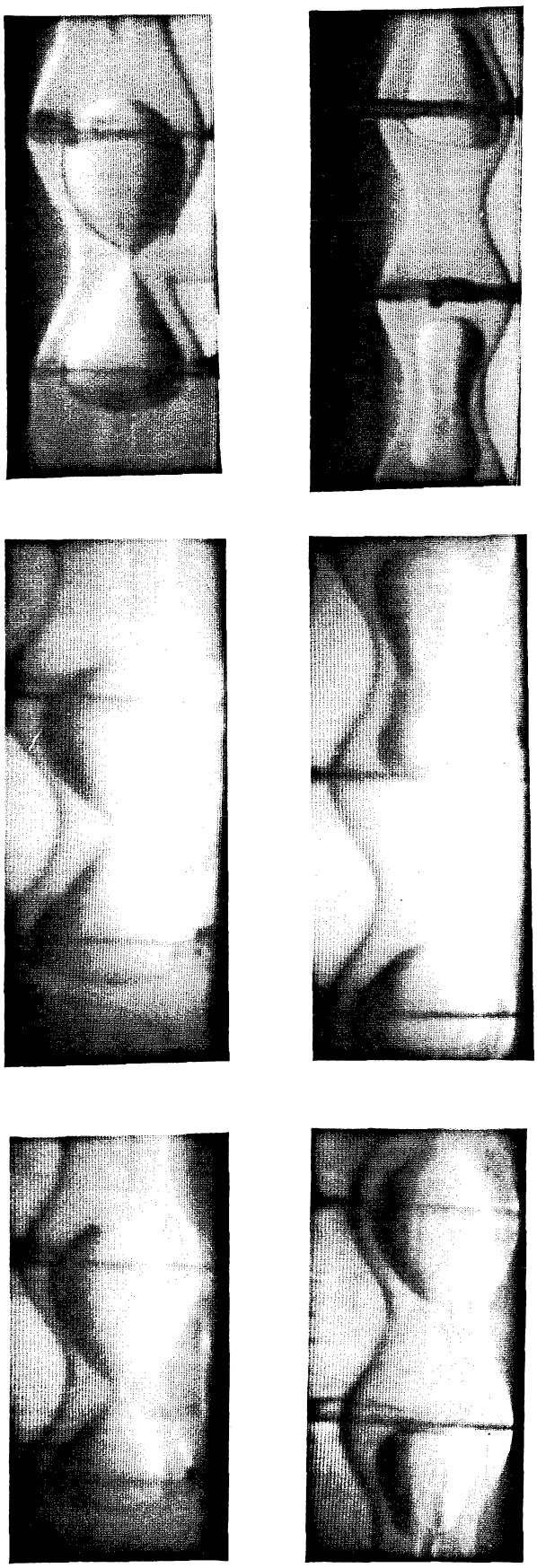

Figure 4. The first row of photographs shows three different viscoelastic drops (made of different polymer solutions) at the moment of breakup. The second row of photographs shows, correspondingly, the daughter drops produced by breakup at a moment when it is clear that the leading drop has moved faster than the trailing one. In each case, Γ=0.077 and λ=1.44. The different concentrations in the drop liquids are, from left to right, 0.01%, 0.10% and 0.50% by weight.

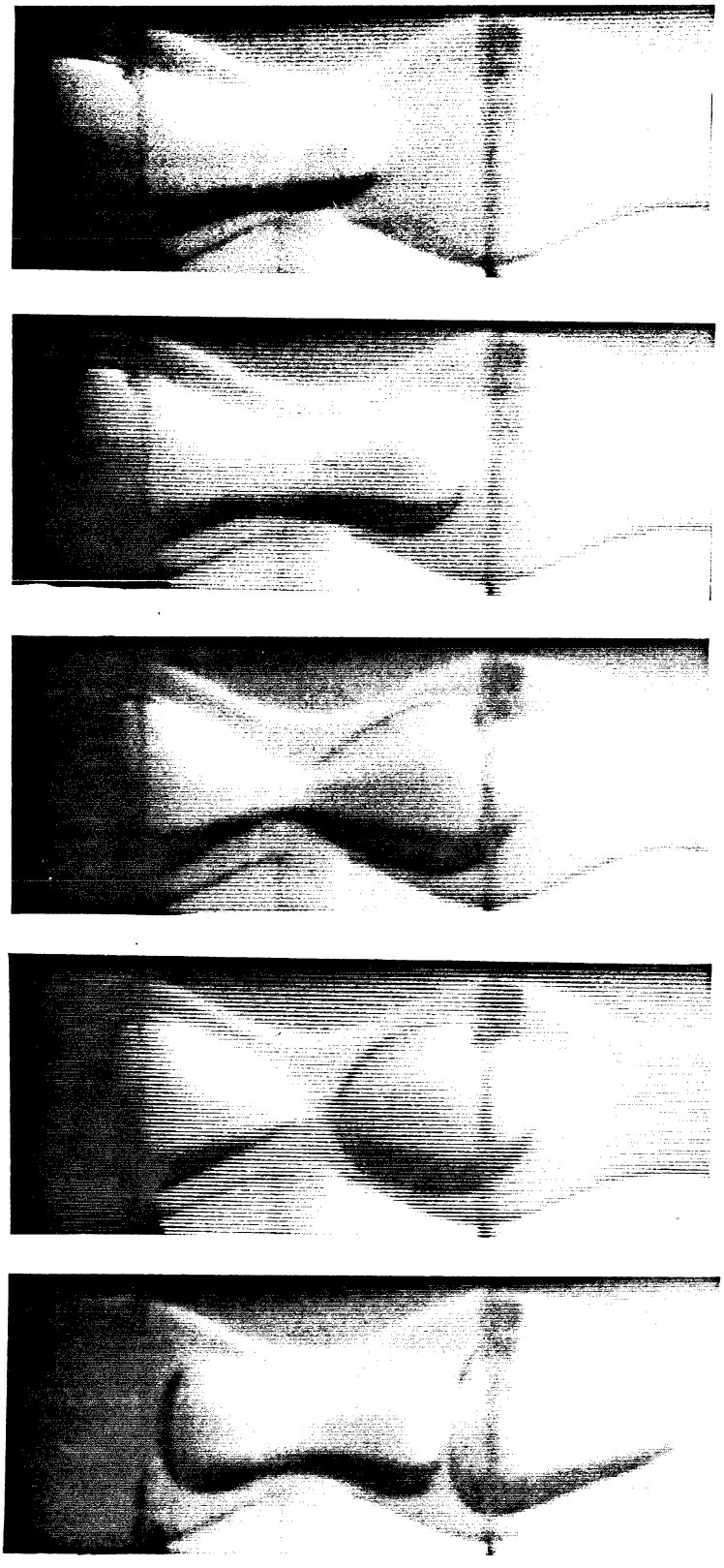

Figure 5(a). Sequence of drop breakup. Γ=0.077, σ=1.68, λ=1.44, 0.50% solution.

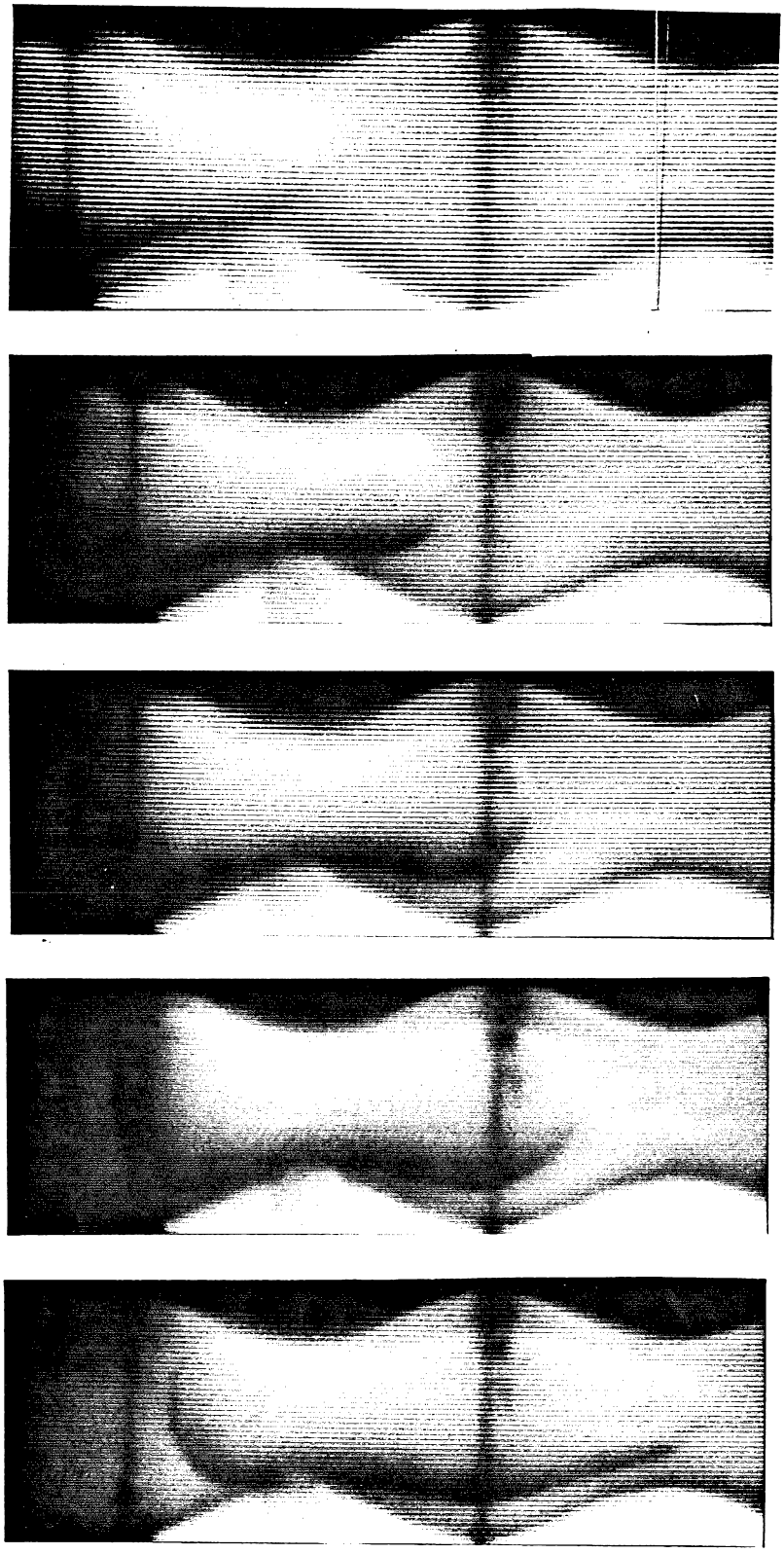

Figure 5(b). Newtonian drop, Γ=0.077, σ=1.4 and λ=1.44. See text.

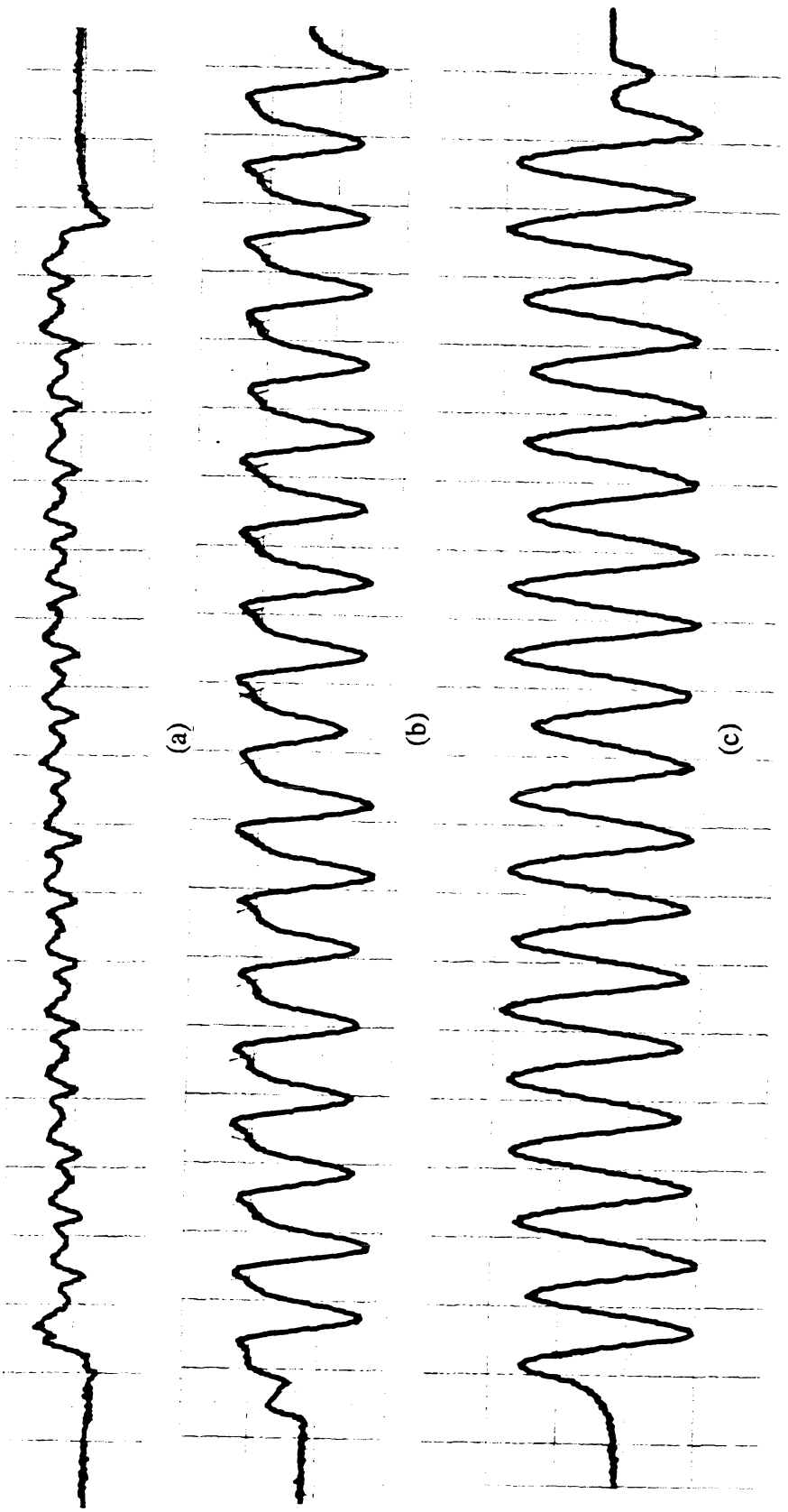

Figure 6. Pressure signal for Γ=0.077 (0.50% solution). For (a) λ=0.77, for (b) λ=1.04, for (c) λ=1.15. Note that for (b) and (c) $|\delta(\Delta P^{++})|$ is larger than the arithmetic average of the extra pressure drop, ΔP^{+}.

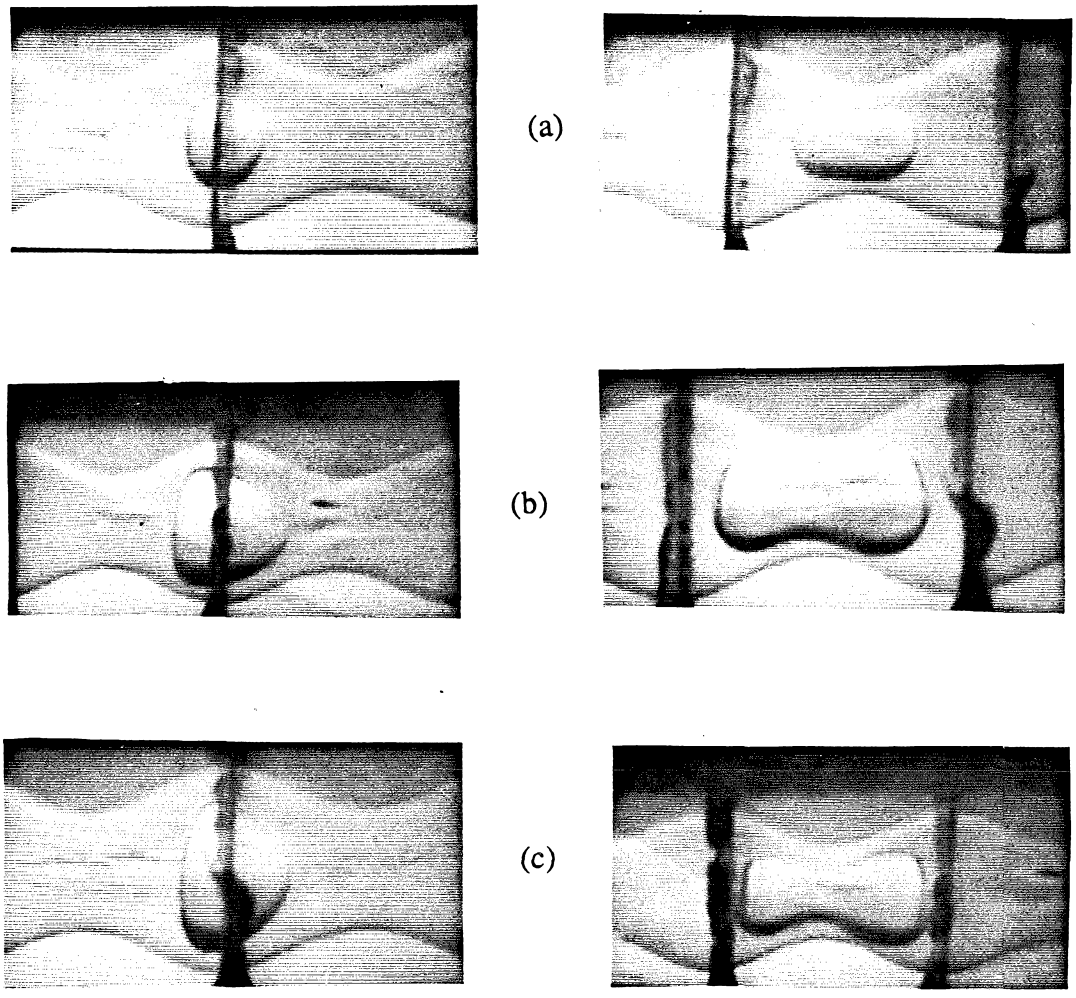

Figure 7. Drop shape at two different positions inside the test section for Γ=0.077 (0.50% solution). In (a), λ=0.77; in (b), λ=1.04; in (c), λ=1.15. The corresponding pressure signals are shown in Figure 6.

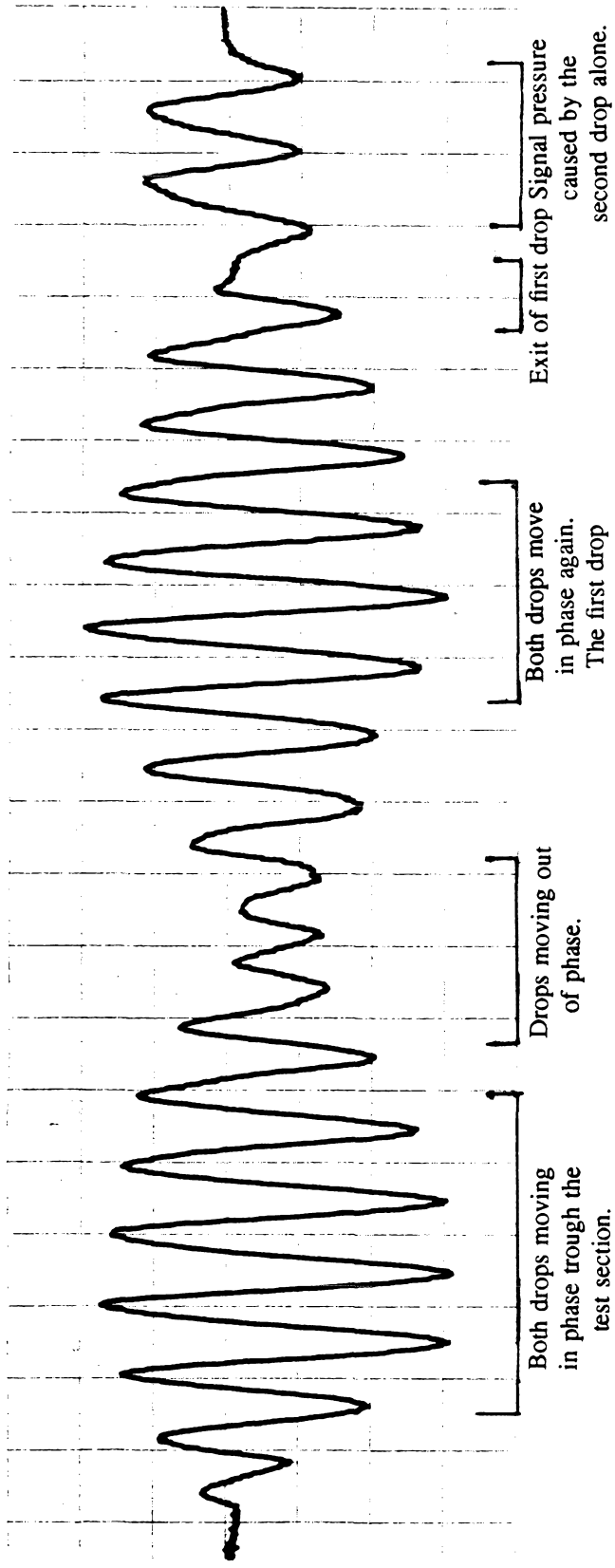

Figure 8. Pressure signal at Γ=0.077 and λ=1.442. For such conditions drop breakup was observed for the first time. Notice the large oscillations produced by the "in-phase" motion of the daughter drops as they move through the test section. The smaller oscillations are produced by the "out-of-phase" motion of the drops (see text).

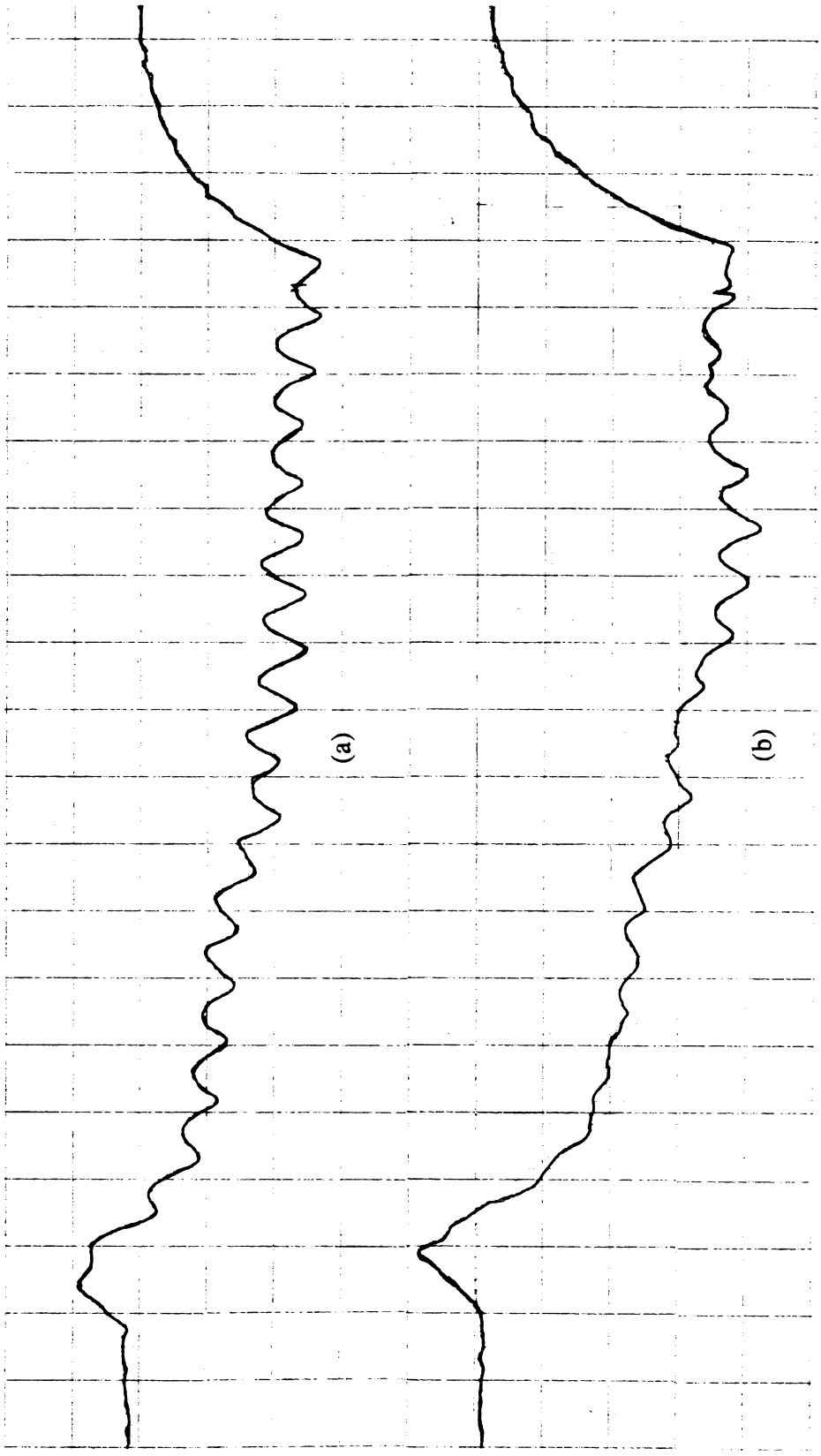

Figure 9. Pressure signals at Γ=0.058 for (a) λ=1.04 and (b) λ=1.15 (0.50% solution). The values for ΔP^+ were taken at the steady state value of the pressure signal for the final third of the test section. See text.

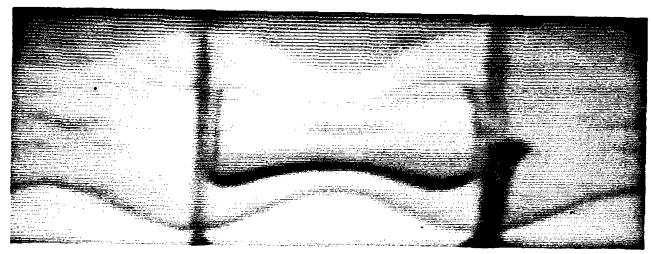

(a)

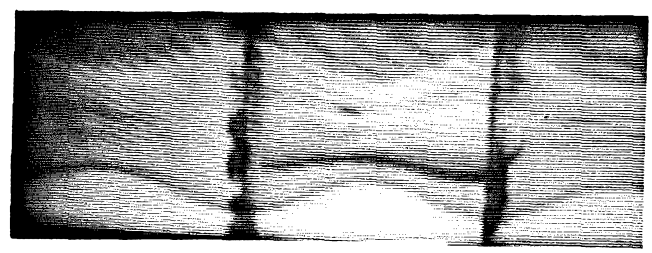

(b)

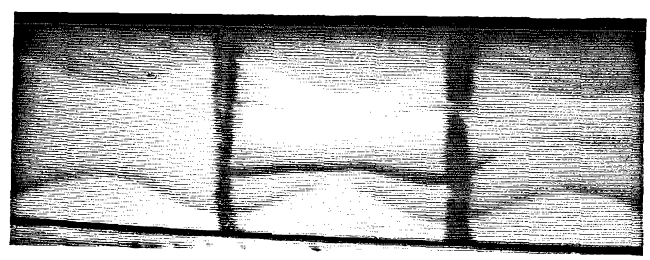

(c)

Figure 10. Effect on drop deformation of increases in flow rate (0.50%). λ=1.15 for the three cases shown. In (a), Γ=0.26; in (b), Γ=0.34; in (c), Γ=0.58. Notice the small variation of d (see text).

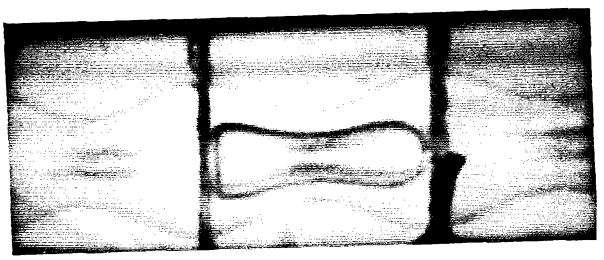

(a)

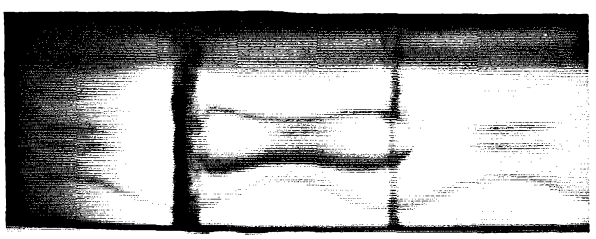

(b)

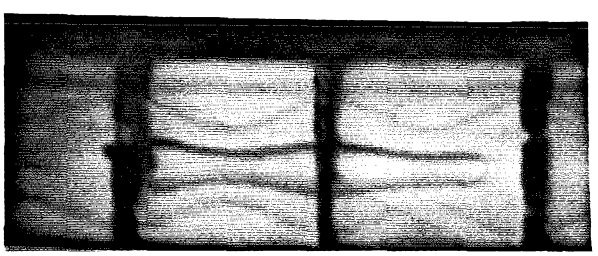

(c)

Figure 11. Effect on drop deformation of increases in flow rate (1% solution). λ=1.15 for the three cases shown. In (a), Γ=0.26; in (b), Γ=0.34; in (c), Γ=0.58. Notice the large variation of d (see text).

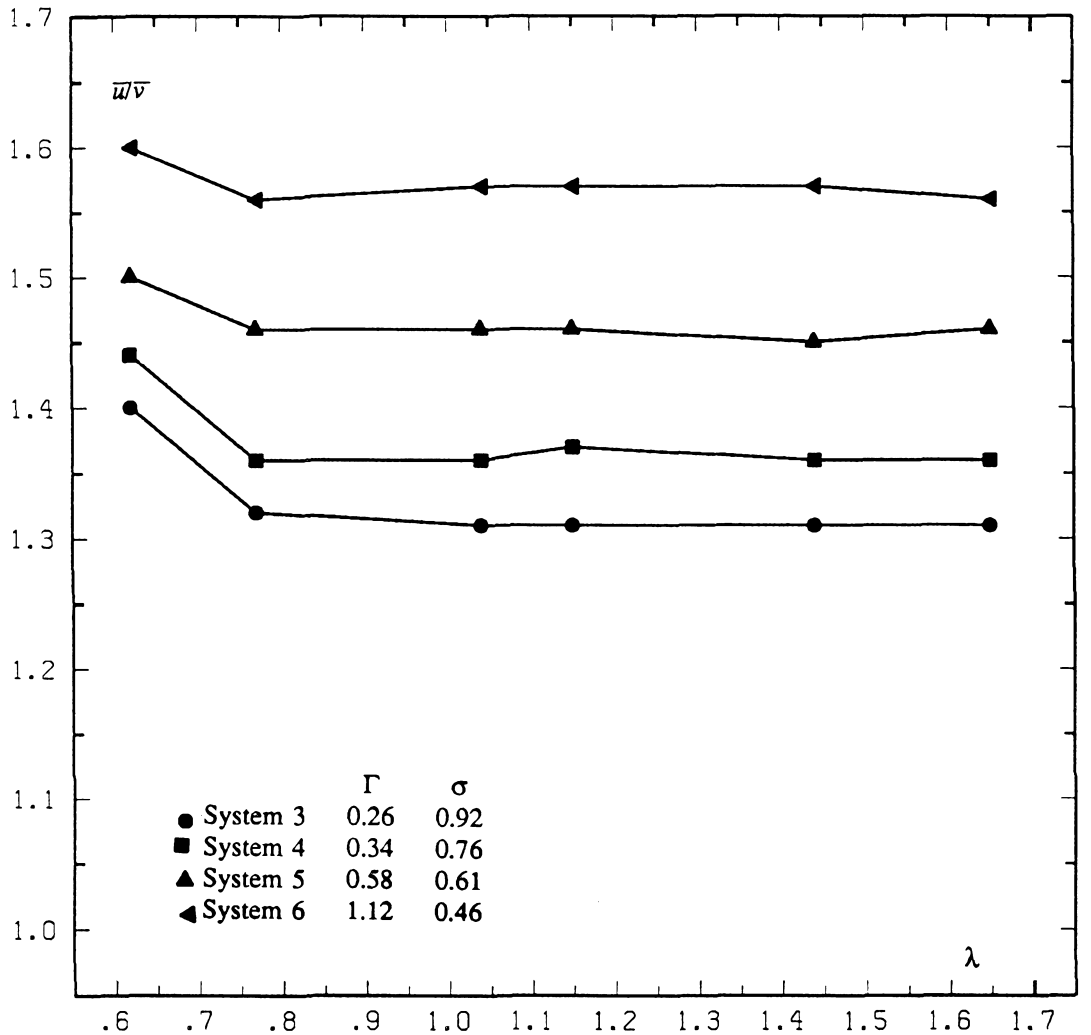

Figure 12(a). $\overline{u}/\overline{v}$ vs. λ, large-Γ systems (0.50% solution). Drop mobility is virtually independent of λ for most of its range.

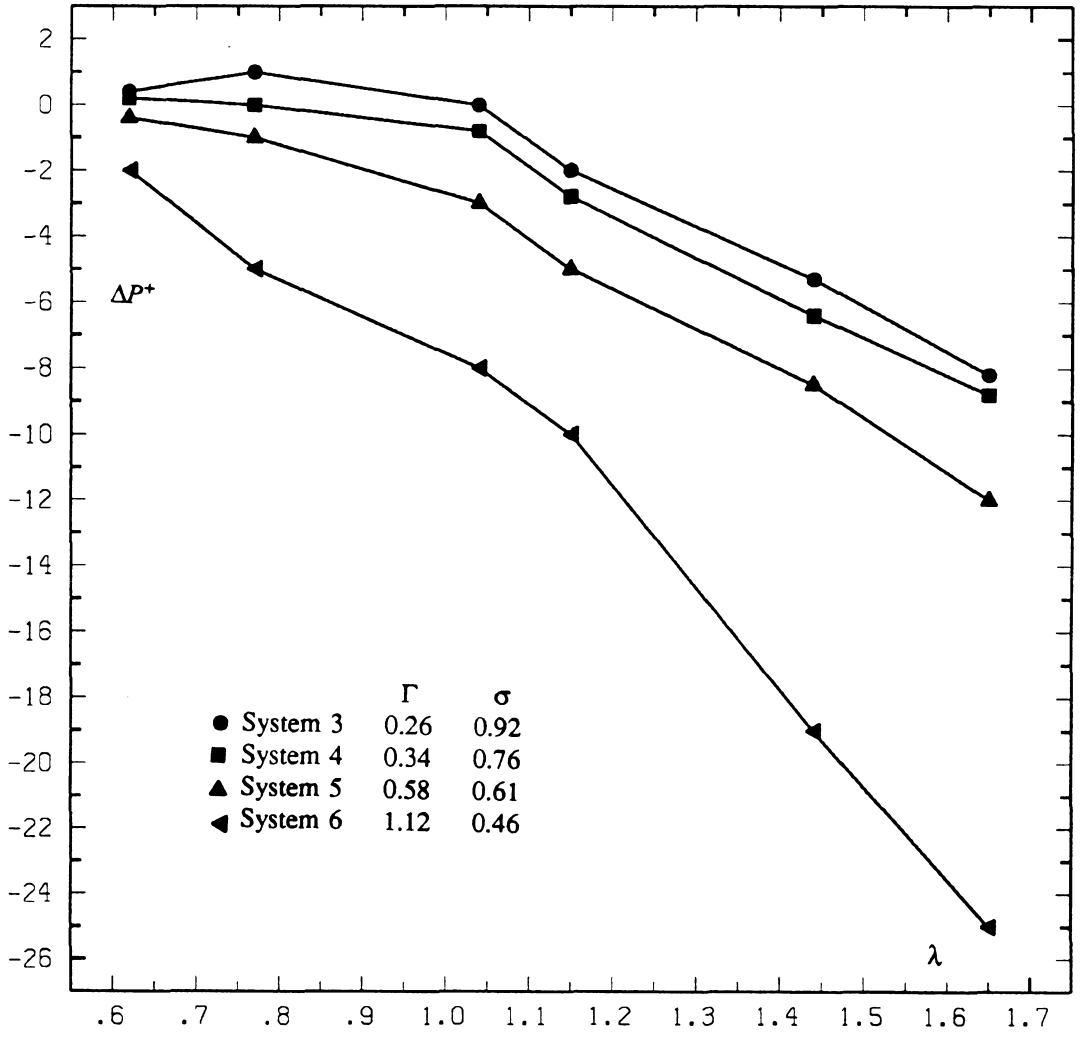

Figure 12(b). ΔP^{+}vs.λ, large-Γ systems (0.50% solution).

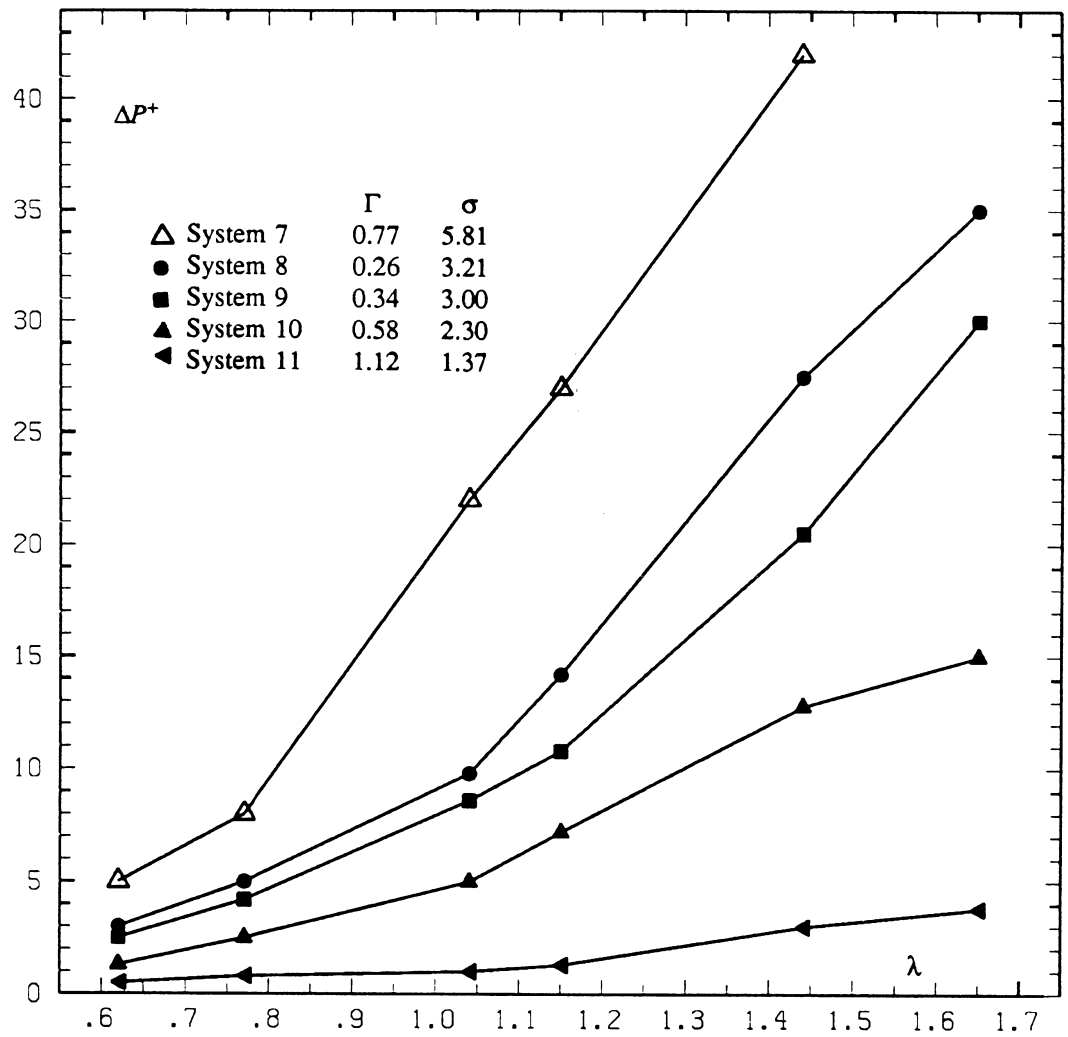

Figure 13. ΔP^{+}vs.λ, all values of Γ (1% solution).

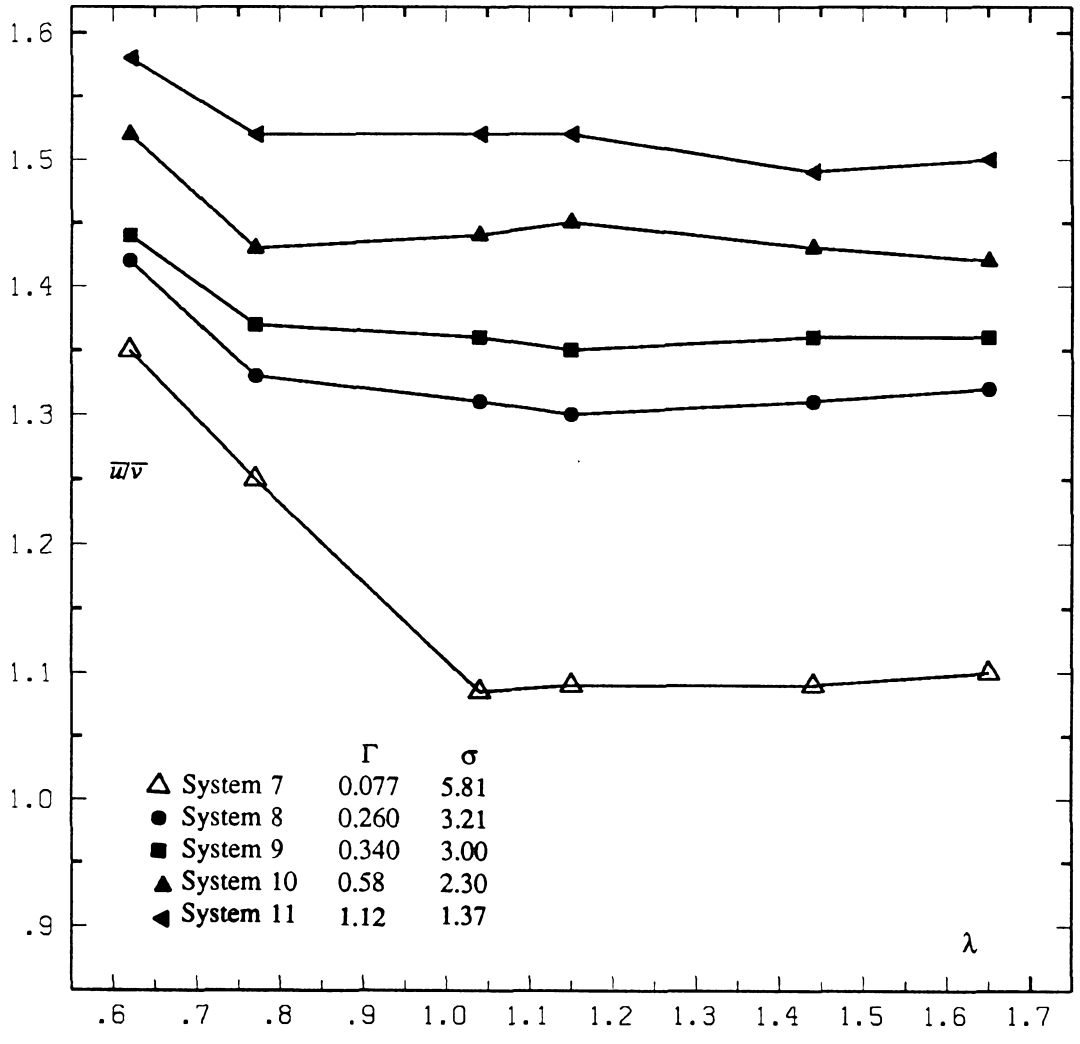

Figure 14. $\overline{u}/\overline{v}$ vs. λ, all values of Γ (1% solution).

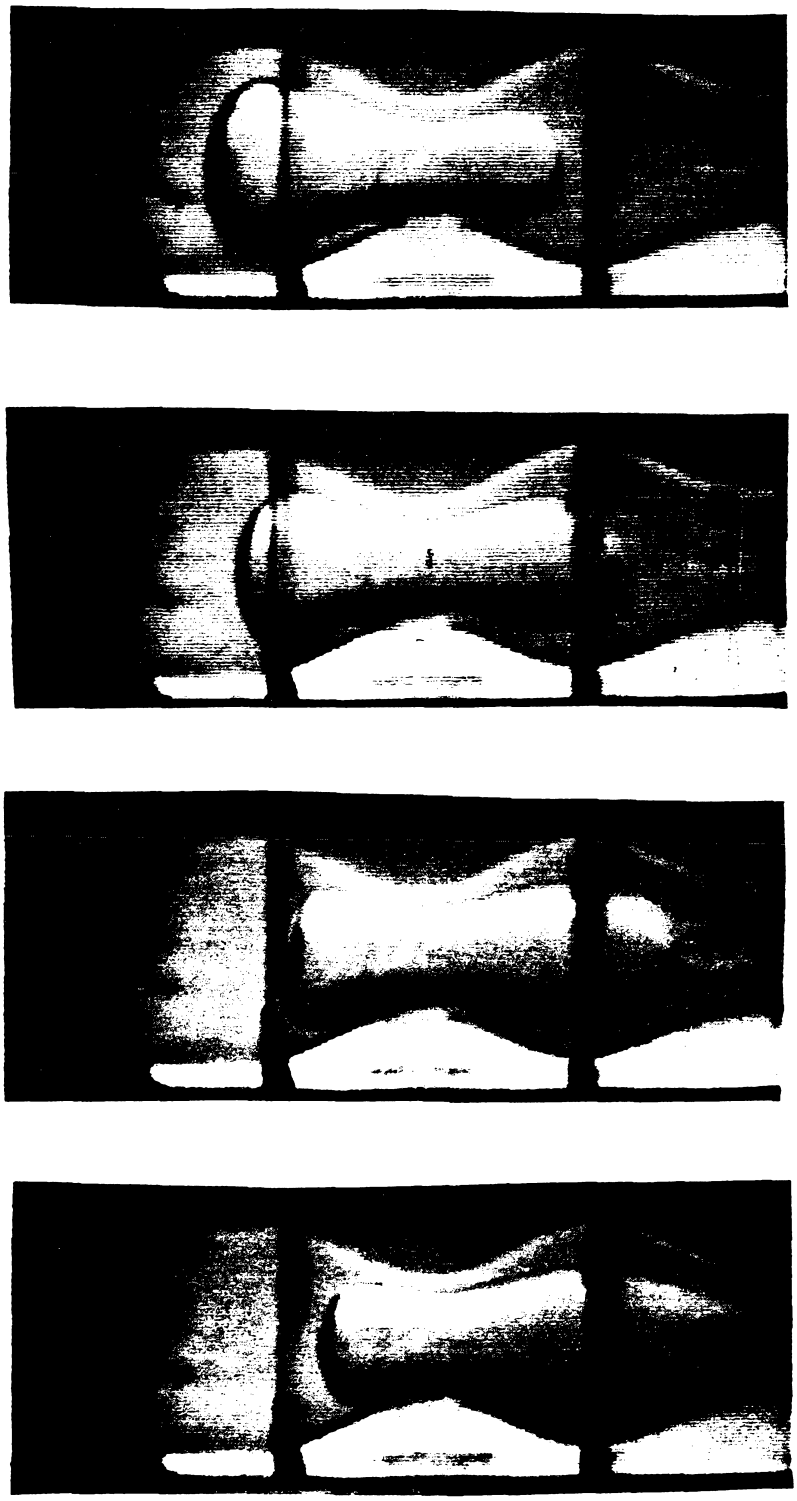

Fig. 15 shows the photographic sequence for a 1% drop of 0.40 cc of volume (λ=1.44) which is moving through the first constriction of the wavy wall tube at a flow rate of Q = 1.05 cc/min (Γ=0.077).

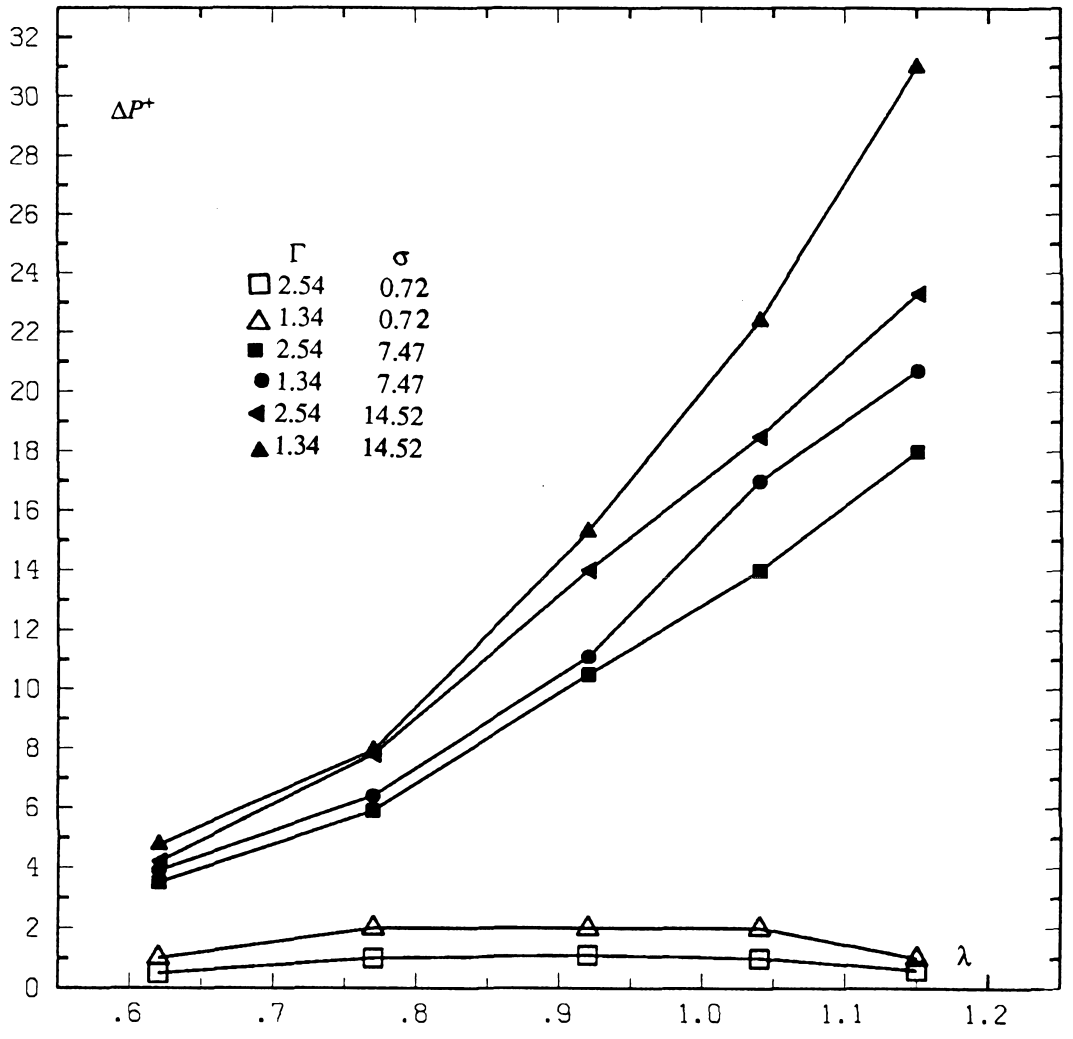

Figure 16. ΔP^{+}vs.λ, large values of Γ (Newtonian-Newtonian systems).

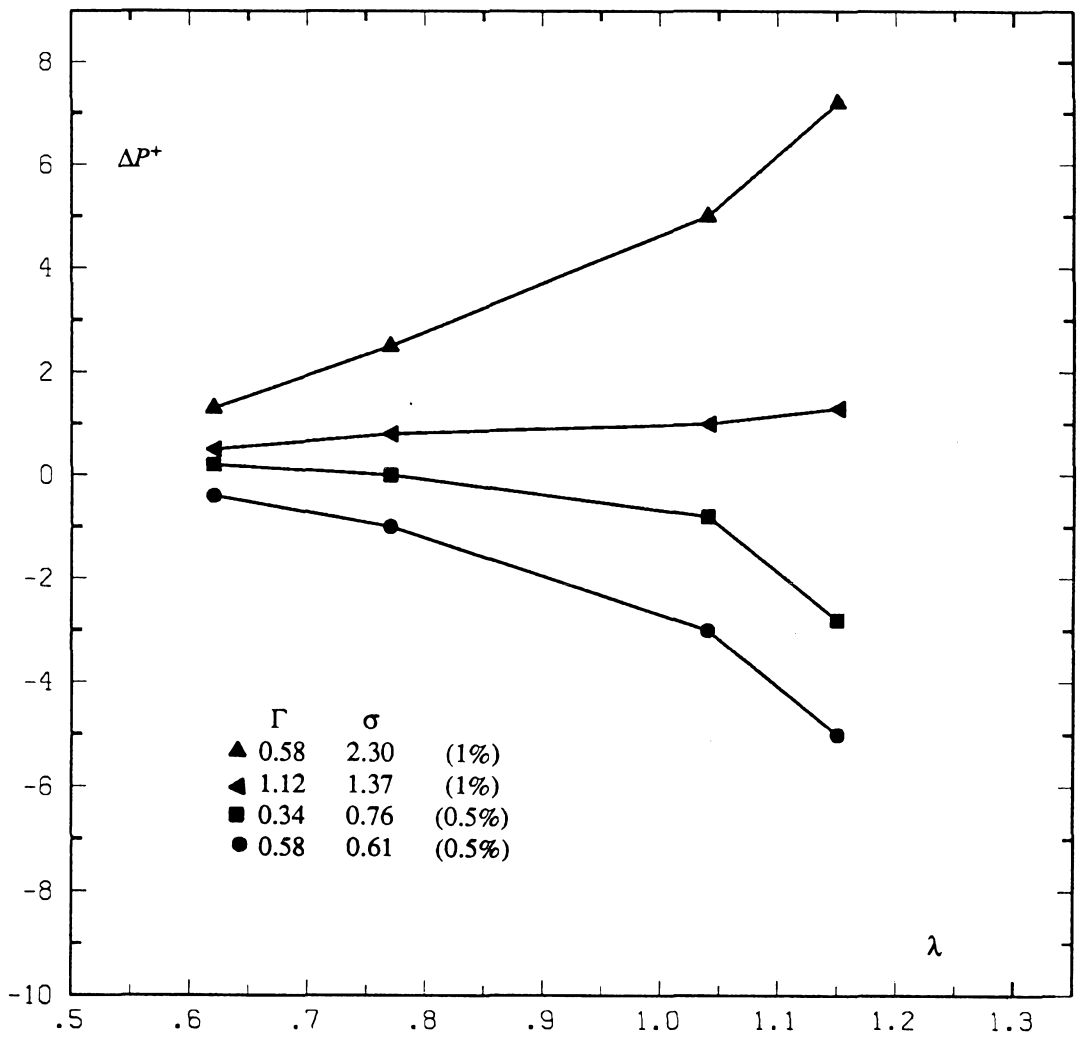

Figure 17. ΔP^{+}vs.λ, for some of the viscoelastic systems used in our experiments, large-Γ.

Appendix

Pressure Measuring System Calibration

It is important to realize that the pressure differences expected to occur during these experiments are extremely small and a very precise calibration for such range is necessary.

The standard arrangement of U-tube manometer with a bypass valve connected to the pressure transducer, fully described in (I), was used to perform this calibration. A strip chart recorder (Houston Instrument) was connected to the pressure indicator and was used to record the pressure output. This calibration was performed for a Validyne P90D variable reluctance pressure transducer (±1" water range) and scanned pressures from zero to about 300 dynes/cm^2 with average increments of about 18 dynes/cm^2.

Such small increments in the differential pressure fed to the pressure transducer were necessary so that we could have a number of data points that rendered a reliable calibration curve. We describe next the general procedure we followed in order to perform such calibration. The numbers and letters written between parentheses refer to Fig. A of the appendix.

With valve (V) open, the U-tube manometer was first filled to a certain height with carbon tetrachloride (1) making sure that no air remained trapped inside the system. Since valve (V) is open, the carbon tetrachloride produces no differential pressure across the pressure transducer but provides a convenient stand on which, once (V) is closed, a column of liquid of certain height may be built in either one of the legs of the U-tube manometer so that a differential pressure is fed to the pressure transducer. Note that if only distilled water is supplied into one leg of the U-tube manometer, a range from zero to 300 dynes/cm^2 would be entirely covered

by building a 0.3 cm height column of distilled water. This means that if a number of data points (say, 15) were required to construct a calibration curve within the pressure range of 0.3 cm column of water, then increments in differential pressure corresponding to 0.02 cm of height in the average would need to be taken. This small height corresponds to 20 divisions in the instrument we used to measure heights (micrometer cathetometer, 1 division = 0.001 cm, Fred C. Henson Co., Pasadena). However, for such small heights it is not possible to have a precise measurement since the uncertainty at each reading was found to be approximately ±0.005 cm (or five divisions of the instrument).

Because of the above, we opted to increase (by the same amount) the height of the column of liquid in both legs of the U-tube manometer using for this purpose two different liquids (one for each leg) of slightly different densities. Distilled water was put in one leg of the manometer (D. W. leg) and an aqueous solution of 23% glycerol in distilled water was put in the other leg (A.G. leg). The calibration was performed at 22.5°C. The densities of these liquids at that temperature were measured to be 0.998 gr/cm^3 for the distilled water, and 1.054 gr/cm^3 for the aqueous glycerin solution. In this way we were able to impose small differential pressures across the pressure transducer and at the same time have large increments in the height of the columns of liquid to be read (averaging 0.237 cm in height at each reading).

Many difficulties were found in obtaining sharp stable menisci between the liquid-liquid interfaces in both legs of the U-manometer due to the natural shape of the menisci, to the relatively large cross-sectional area of the U-tube (0.6361 cm^2) and to the small amounts of liquid involved in the calibration. This problem was

overcome by initializing our readings not from the interface between liquids but from a certain height (say, h_o), which allowed a convenient minimum amount of liquid sufficient for a good formation of menisci at the liquid-liquid interface in both legs. h_o was achieved by first adding a 0.254 cc volume of distilled water inside the D. W. leg (i.e. building up a 0.4 cm height column of water on top of the CCl_4) and then adding exactly the same volume of aqueous glycerin solution inside the A.G. leg. While these two steps were taken valuve (V) remained open. Those quantities of liquids remained there for 24 hours (wax paper was used to seal the manometer legs, and all liquid containers were perfectly closed in order to avoid evaporation or absorption of humidity), then the menisci in the liquid-liquid interface were sharp and stable. Valve (V) was then closed and the level of the A.G. leg was raised equal to the D.W. leg, this being our starting "zero" level (h_o) for our subsequent readings. At this moment, the pressure transducer indicator and the strip chart recorder were set to zero (their respective sensitivities being those expected to be used in the actual experiments), and recording of the calibration data points commenced. Each data point in our calibration corresponds to a small increment in column height above h_o. These increments were attained by alternatively adding up to each leg of the manometer equal small amounts of either distilled water or aqueous glycerin solution inside the corresponding leg of the manometer. A micrometer pipette was used for this purpose, and the equality in the height of each menisci (liquid-air) was always checked carefully with the cathetometer to rule out any possibility of having irregularities in the U-tube walls.

Full-scale deflection in both the pressure transducer indicator and the strip chart recorder was reached when the height of both columns was 5.555 cm,

representing an actual differential pressure of 305 dynes/cm^2. Sixteen data points were recorded by incrementing the height of the columns of liquid by approximately 0.34 cm at each reading. The calibration was performed twice under similar circumstances, obtaining the same results each time. The data points are plotted in Fig. B of this appendix.

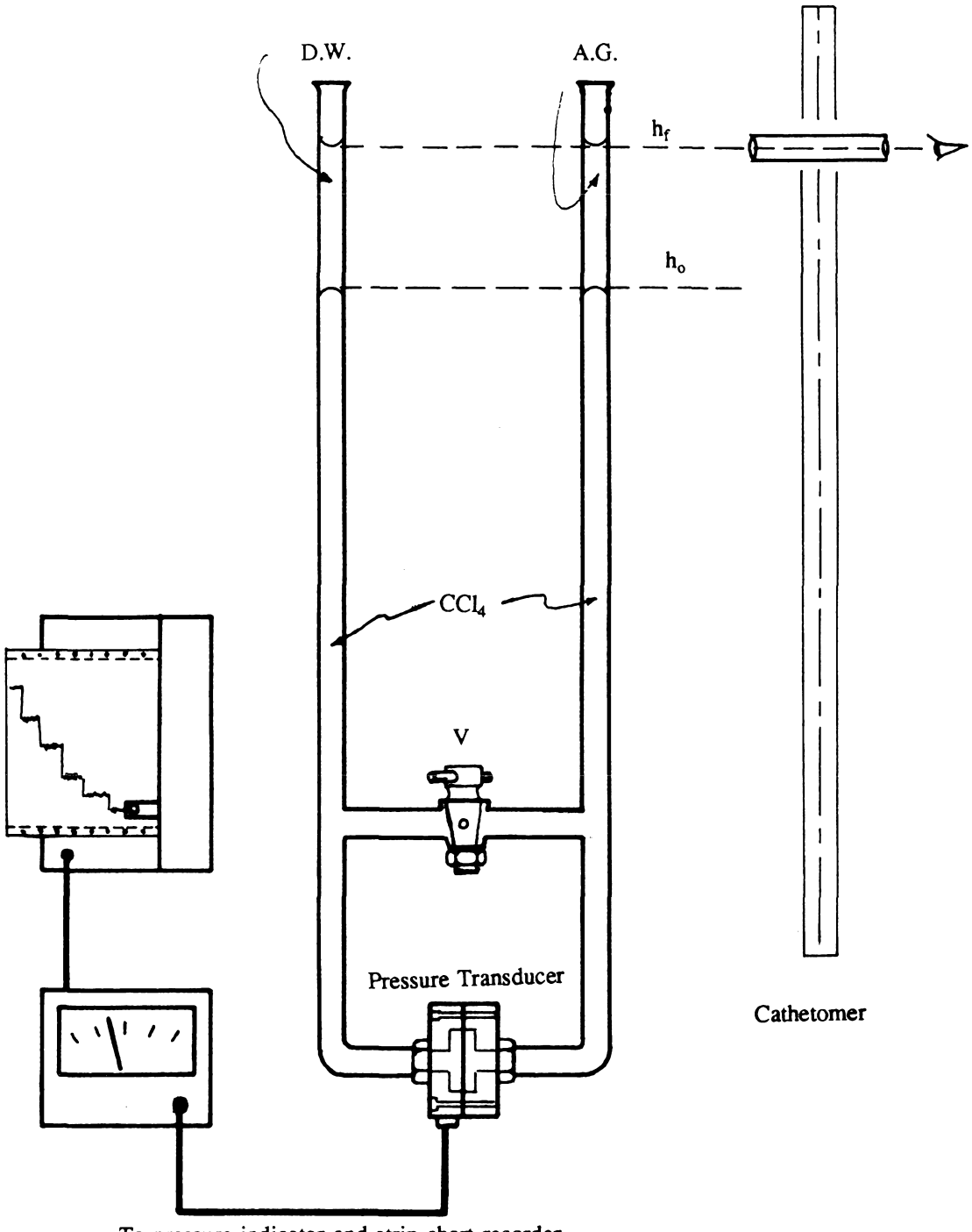
D.W.
A.G.
h_f
h_o
CCl_4
V
Pressure Transducer
Cathetomer
To pressure indicator and strip chart recorder

Figure A

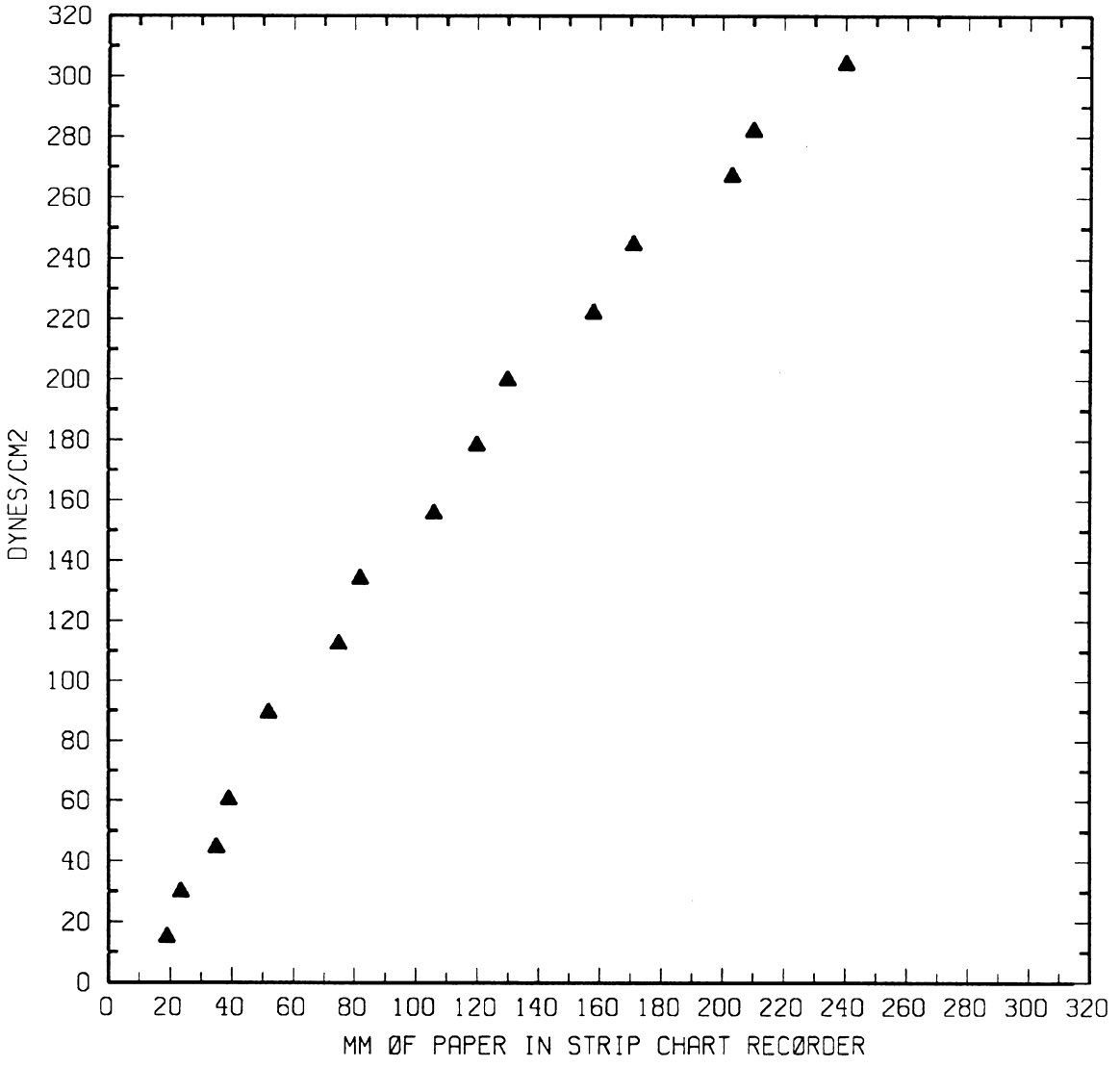
DYNES/CM2
0
20
40
60
80
100
120
140
160
180
200
220
240
260
280
300
320
MM ØF PAPER IN STRIP CHART RECØRDER

Figure B

Chapter 2

The Creeping Motion of Immiscible Drops Through a Converging/Diverging Tube in a Constant-Pressure Gradient-Driven Flow

1. Introduction

Measurements of the extra pressure drop caused by a drop and the drop mobility, have been taken in a number of different flow conditions. Ho and Leal (1975) studied a straight tube geometry with Newtonian drops moving in both Newtonian and viscoelastic suspending fluids (I). Olbricht and Leal (1981,1983) studied two tube geometries: a straight circular tube and a wavy-wall tube with Newtonian drops (both neutrally buoyant and non-neutrally buoyant) moving in both Newtonian and viscoelastic suspended fluids (III). The case of viscoelastic drops moving in a Newtonian suspending fluid through a wavy-wall tube has been presented by us in a study complementary to the present one (IV).

The above studies were made for constant flow rate conditions, with the flow generated by a gear pump. Under these conditions, drops moving in a two-phase flow through a test tube could not influence the volumetric flow rate at all. In order to study a condition that is more nearly representative of the local circumstances for a flow in a real porous media, where a constant pressure head is the driving force for flow, it is necessary to study the two-phase problem under the conditions of a constant pressure gradient as a driving mechanism for the flow, with the volume flow rate then varying as a function of time.

In the present study, we consider flow through a wavy-wall tube, brought about by imposing a constant pressure gradient. In so doing, the volumetric flow is allowed to change in response to any changes in flow resistance that may appear in the experimental setup. In particular, as a drop moves along the wavy-wall test section and causes a time-dependent periodic change in the total flow resistance, it will then simultaneously cause a time-dependent periodic change in the

instantaneous volumetric flow rate.

The different nature of the driving mechanisms, one allowing no variations in the flow rate (gear pump), the other being susceptible to changes in flow resistance (constant pressure gradient), may act on the whole two-phase problem in such a way that the drop dynamics may be substantially different depending which driving mechanism is being used. Understanding the different conditions imposed on the two-phase flow by the two different driving mechanisms and their effect on the drop dynamics at the level of a single drop in our simplified experimental model may be useful in the general context of understanding an actual two-phase flow through a real porous media,

We have measured the extra pressure drop, the drop mobility and the drop deformation for neutrally buoyant Newtonian drops moving within a Newtonian suspending fluid through a wavy-wall test section with a constant pressure gradient. Data from this experiment will be compared with corresponding data available from experiments which were carried out at a constant flow rate for equivalent values of independent flow variables such as the capillary number, the viscosity ratio and the drop size. In so doing, we will be able to analyze how the change in the nature of the driving mechanism may affect the drop dynamics.

2. Definition of Flow Variables and Mathematical Model

The experimental results will be analyzed in terms of several basic dimensionless parameters.

Since the early work by G. I. Taylor (1934) on the deformation of single drops subjected to a simple shear flow, the importance of the capillary number in the

deformation of Newtonian drops in a Newtonian fluid has been well established. In the present study, the capillary number is defined as $\Gamma = (\mu_o \bar{v}/\gamma)$, where μ_o is the viscosity of the suspending fluid, γ is the interfacial tension (measured by the pull-ring method) between suspended and suspending fluids, and $\bar{v}$ is the average flow velocity defined as the ratio of the volumetric flow rate Q to the effective cross sectional area for the wavy-wall tube, i.e. $\bar{v} = Q/\pi r_{HP}^2$, where r_{HP} is the effective radius for the wavy-wall tube (cf. Olbricht and Leal, 1983). The viscosity ratio is defined as $\sigma = \mu_i/\mu_o$ where μ_i is the viscosity of the suspended fluid. Numerical values of the above quantities are given in Table 1. Drop size is defined in terms of the ratio λ of the undeformed radius of the drop to the effective tube radius r_{HP}. The different drop volumes used in our experiments, and the corresponding values of λ are given in Table 2. In addition to the time-dependent drop shape which is recorded on magnetic videotape, we are interested in data for the dimensionless extra pressure drop ΔP^{++}, the dimensionless magnitude of the periodic part of the pressure signal $\delta(\Delta P^{++})$, and the drop mobility $\bar{u}/\bar{v}$. ΔP^{++} is the measured change in the pressure drop caused by the drop in its passage through the test section made dimensionless by the quantity $\mu_o \bar{v}/r_{HP}$. For practical purposes, our results are presented here in terms of ΔP^{+}, defined as the arithmetic average of the maximum and minimum value of the periodic pressure signal, i.e. $\Delta P^{+} = \frac{1}{2}(\Delta P^{++}_{max} + \Delta P^{++}_{min})$. The drop mobility $\bar{u}/\bar{v}$ is defined as the average velocity of the center of the drop as it passes through the test section (i.e. the distance between two fixed marks, located at the entrance and exit of the test section, divided by the elapsed time for the center of the drop to go from one mark to the other), relative to the average velocity of the flow. We also define a parameter d, associated with drop deformation, as being the ratio of the maximum

longitudinal length of the drop measured along the center line of the flow to the wave length of a single period of the wavy-wall tube. Also, the following abbreviations will be used henceforth: CFR will be used when refering to a constant-flow-rate experiment as provided by a constant-flow gear pump; CPG will be used when referring to a flow which is being driven by a constant pressure gradient.

It is important to emphasize that in a CFR experiment, changes in flow rate are not allowed regardless of the fact that the total flow resistance may change, whereas in a CPG experiment the flow rate varies according to any change in flow resistance.

A schematic representation of the pressure distribution in the complete flow system for a CFR experiment is shown in Fig. 1, while a similar plot for the pressure distribution in a CPG experiment is sketched in Fig. 2. For simplicity in constructing these figures, we assume that the flow system exhibits the same flow-rate/pressure-drop relationship at all points. Hence, referring to Fig. 1, we represent the pressure distribution in the absence of a drop as a straight line extending from the entry region at point c to the exit at point d. When a drop is put into this CFR system, the volumetric flow rate remains the same. Hence, the pressure profile upstream and downstream must retain the same *slope* as before. On the other hand, the drop corresponds to a pressure "jump" on the scale of Fig. 1 at point b. Since the exit pressure is fixed at p_{atm} in our flow system, the pump in this CFR experiment simply compensates for the drop by increasing the inlet (pump outlet) pressure by ΔP^{+}_{CFR}, while retaining the same flow rate (and thus the same slope for P from point a to point b). In a CPG experiment with the same flow rate in the *absence* of a drop, the total pressure drop is fixed at the exact same level as in the

CFR case, and p again varies linearly with position in the flow system from point a to point c. However, when a drop is introduced in the CPG system, the extra resistance to motion (i.e. ΔP^{*}_{CPG}) can only be accommodated by a change in flow rate. The total pressure drop from a to c is *fixed.* The sketch in Fig. 2 shows a typical instantaneous pressure profile — note that the slopes upstream and downstream of the drop are still equal, but decreased in value as a consequence of the reduction in flow rate.

It is useful to reflect briefly on the implications of Figs. 1 and 2 for measurement of the extra pressure drop associated with the presence of the droplet, i.e. ΔP^{++}. In the CFR case, this quantity can be measured by simply determining the *change* in the total pressure drop between any two convenient points provided only that one is upstream and the other downstream of the drop. Measurement in the CPG system is more complicated, and the result will differ from the CFR case for two reasons. One is that the flow rate, for the same initial ΔP, will differ when the droplet is "added" in the two systems. This is the dynamical difference of interest that we are trying to measure, and it will be reflected not only in the *mean* values of ΔP^{+}, but also (and probably more importantly) in the variations with time of the instantaneous values ΔP^{++}. The second is, however, spurious. In a CPG experiment, accurate measurement of ΔP^{+} (or ΔP^{++}) requires that the pressure sensor upstream and downstream be as close to the drop as possible. From a practical standpoint, however, the pressure measurement system must span at least a portion of the wavy-wall test section (in our case, in fact, it generally encompassed this complete section), and this is indicated symbolically by the measuring points 1 and 2 in Fig. 2. So see the problem: we can refer to Fig. 3 which represents only the difference

in the pressure distribution with the drop present relative to that without the drop (with the manometer-transducer system described later, this is what we actually see). Clearly, the quantity that we wish to measure is the difference at point c. However, the "apparent" value measured is the difference $p_2 - p_1$ and this differs from ΔP^{++} because of the change in slope in the upstream and downstream regions.

To demonstrate these facts more clearly, we can actually derive expressions for the instantaneous, time-dependent extra-pressure signal that is measured in the two idealized experiments that are represented in Figs. 1-3, i.e. ΔP^{++}_{CFR} and ΔP^{++}_{CPG}. If no drop is present in a CFR experiment, the constant volumetric flow rate given by the gear pump is

$$Q^{(0)}_{CFR} = \frac{\alpha \Delta P^{(0)}_{CFR}}{L_1 + L_2} , \tag{1}$$

where $\alpha = \frac{\pi R_0^4}{8\mu_o}$, R_0 being a global equivalent radius for the whole experimental system, $\Delta P^{(0)}_{CFR}$ is the total pressure drop across the whole experimental setup, and $(L_1 + L_2)$ is the total length of the experimental setup, as indicated in Figs. 1 and 2. We use a superscript 0 to indicate quantities defined in the absence of the drop. Since the flow rate is the same everywhere in the system, it may be noted that

$$Q^{(0)}_{CFR} = \frac{\alpha \Delta P_1}{L_1} = \frac{\alpha \Delta P_2}{L_2} , \tag{2}$$

where ΔP_1 and ΔP_2 are the pressure drops acrosss the lengths L_1 and L_2, respectively, such that $\Delta P_1 + \Delta P_2 = \Delta P^{(0)}_{CFR}$.

where ΔP_1 and ΔP_2 are the pressure drops across the lengths L_1 and L_2 such that

$$\Delta P^{(0)}_{CFR} = \Delta P_1 + \Delta P_2 . \tag{3}$$

Now, when the drop is added, the volume flow rate remains fixed, but the total pressure drop increases by an amount ΔP^{++}_{CFR} which is sufficient to maintain this flow rate, i.e.

$$\Delta P_{CFR} = \Delta P^{(0)}_{CFR} + \Delta P^{++}_{CFR}$$

$$= \Delta P_1 + \Delta P_2 + \Delta P^{++}_{CFR} \, . \tag{4}$$

Since the flow rate is fixed, it is evident from Eq. (2) that ΔP_1 and ΔP_2 remain at the same values as before (cf. Fig. 1).

Now let us suppose that the extra-pressure drop ΔP^{++}, to push the drop at a speed consistent with a total volume flow rate Q, can be expressed in the form

$$\Delta P^{++} = \beta(Q) \cdot Q \tag{5}$$

where β is a coefficient whose value depends on Q (since the drop may deform by different amounts at different values of Q). Then, since Q in the CFR experment is constant at $Q^{(0)}_{CFR}$, we see from Eqs. (1) and (5) that

$$\Delta P^{++}_{CFR} = \beta^{(0)} \frac{\alpha}{(L_1 + L_{2)}} \Delta P^{(0)}_{CFR} \, . \tag{6}$$

In contrast, in a CPG experiment, it is the overall pressure drop which remains fixed. Let us suppose that we begin with an overall pressure drop $\Delta P^{(0)}_{CPG}$ which is equal to $\Delta P^{(0)}_{CFR}$ so that the volume flow rate in the absence of a droplet is the same in the two experiments, i.e.

$$Q^{(0)}_{CPG} = \frac{\alpha \Delta P^{(0)}_{CPG}}{L_1 + L_2} = \frac{\alpha \Delta P^{(0)}_1}{L_1} = \frac{\alpha \Delta P^{(0)}_2}{L_2} \, . \tag{7}$$

However, in this case, when a drop is added, the flow rate Q and the pressure drop in the two legs upstream and downstream must decrease to maintain the overall

pressure drop at $\Delta P^{(0)}_{CPG}$, i.e.

$$\Delta P^{(0)}_{CPG} = \Delta P_1 + \Delta P_2 + \Delta P^{++}_{CPG} . \tag{8}$$

Hence, the volumetric flow rate decreases to

$$Q_{CPG} = \frac{\alpha \Delta P^{(0)}_{CPG}}{L_1 + L_2 + \alpha\beta(Q_{CPG})} \tag{9}$$

and the extra-pressure drop ΔP^{++}_{CPG} is

$$\Delta P^{++}_{CPG} = \beta(Q_{CPG}) \cdot Q_{CPG}$$

or

$$\Delta P^{++}_{CPG} = \frac{\alpha\beta(Q_{CPG})\Delta P^{(0)}_{CPG}}{L_1 + L_2 + \alpha\beta(Q_{CPG})} . \tag{10}$$

Since $\Delta P^{(0)}_{CPG} \equiv \Delta P^{++}_{CFR}$, it follows from EQ. (10) that

$$\Delta P^{++}_{CPG} = \Delta P^{++}_{CFR} \left[\frac{\beta(Q_{CPG})/\beta^{(0)}}{1 + \dfrac{\alpha\beta(Q_{CPG})}{L_1 + L_2}} \right] . \tag{11}$$

As noted earlier, the extra-pressure drop occurring in the two experiments differs because of the change in volume flow rates. We may note that if β is nearly constant (i.e. small changes in drop deformation are small so that $(\beta(Q_{CPG}) \sim \beta(Q^{(0)}_{CPG}) = \beta^{(0)}$, then

$$\Delta P^{++}_{CPG} = \Delta P^{++}_{CFR} \left[\frac{1}{1 + \dfrac{\alpha\beta^{(0)}}{L_1 + L_2}} \right] . \tag{12}$$

All of the above refers to the actual value of ΔP^{++} which exists in the system. However, in the case of the CPG experiment, this is not precisely what is measured and account must be taken of the finite distances l_1 and l_2 between the points of

pressure measurement and the drop. When no drop is present in a CPG experiment, the pressure difference actually measured between points 1 and 2 is

$$\Delta P_{21}^{(0)} = P_2^{(0)} - P_1^{(0)} = \frac{\Delta P^{(0)}(l_2 + l_1)}{L_1 + L_2} \quad . \tag{13}$$

Note that $l_1 + l_2)$ and $(Ll_1 + L_2)$ vary with time as the drop moves through the test section, but the quantities $(l_1 + l_2)$ and $(L_1 + L_2)$ are independent of time and have to do only with geometrical characteristics of the experimental system (see Fig. 2). On the other hand, when a drop is present in a CPG experiment, one has

$$\frac{(P_2 - P_1)}{l_2 + l_1 + \alpha\beta} = \frac{\Delta P^{(0)}}{(L_1 + L_2 + \alpha\beta)} \quad . \tag{14}$$

From Eq. (14), one arrives at

$$\Delta P_{2\,1} = P_2 - P_1 = \Delta P_{CPG}^{++}\left[1 + \frac{l_2 + l_1}{\alpha\beta}\right] \tag{15}$$

where use has been made of the fact that $\Delta P_{CPG}^{++} = \dfrac{\alpha\beta\Delta P_0}{L_1 + L_2 + \alpha\beta}$.

The measuring apparatus senses only the difference between ΔP_{21} with and without the drop. Therefore, the output signal from the differential pressure transducer system is the difference between Eq. (15) and Eq. (13):

$$\Delta P_{CPG\ measured} = \Delta P_{2\,1} - \Delta_{21}^{(0)} = \Delta P_{CPG}^{++}\left[1 - \frac{l_1 + l_2}{L_1 + L_2}\right] . \tag{16}$$

$\Delta P_{CPGmeasured}^{++}$ is the quantity being measured by the pressure transducer system which is represented in Fig. 3 by the pressure drop $P_A - P_B$. One can see in Fig. 3 that $P_A - P_B$ is a fraction of the real extra pressure drop caused by the drop in a CPG experiment, (i.e. $P_C - P_D$), and that it depends on the real lengths of the experimental

setup. Equation (16) provides a means to evaluate the real influence of the drop. For our particular experiment, we have estimated that

$$\Delta P^{++}_{CPG\ measured} \sim 0.95\ \Delta P^{++}_{CPG}\ . \tag{17}$$

Equation (17) will be used to estimate the real values of the average dimensionless extra-pressure drop in a CPG experiment.

Experimental

The basic apparatus used to carry out the experiments under CPG conditions is shown in Fig. 4. Two pressure regulators (50 psi) were connected in series to our laboratory constant-pressure supply line. The first regulator decreased the pressure to approximately 40 psi; the second regulator maintained pressure at 20 psi. A third precision nillmatic pressure regulator (0.5 psi to 15 psi, Moore Products Co, PA) was used to supply the constant driving pressure head. The suspending fluid was kept in a pressurized container. The hydrostatic pressure within this container was kept constant by continuously pumping fluid into it at a required constant flow rate. The level of the fluid in the container could be checked visually at all times by means of a transparent thin pipe connected to the container which served as a level indicator. Between the precision regulator and the suspending fluid container, a large air accumulator was placed to ensure damping of any possible pressure variation from the pressure supply. The differential pressure transducer connected to the test section was used to verify the constancy of the driving pressure head in the case of single-phase flow of the suspending fluid alone.

The experiments were carried out in a similar fashion to those described in (III) and (IV), i.e. the suspending fluid was forced through a long pipe (0.90 cm I.D.) prior to the wavy-wall test section inside a constant temperature bath at 25°C.

Transit time through the bath was always sufficiently long so as to assure thermal equilibrium of the suspending fluid and the bath. Another straight section (0.90 cm I.D.) followed the test section. In this final section of the pipe line, the drops relaxed and returned to their original shapes. Detailed characteristics and dimensions of the test section may be found in (III).

The experiments were performed in the following way. The pressure-measuring system is allowed to reach equilibrium, and the valve in the upper branch of the U-pipe manometer (see Fig. 4) is then closed to allow the differential pressure transducer connected to the lower branch to sense any change in pressure across the test section. The signal from the pressure transducer is then amplified via the pressure indicator (CD 25 Validyne) and recorded on a stripchart recorder (omniscriber, Houdson Instruments). The drops were injected manually, one by one, using a Gilmont micrometer syringe (0.001 cc accuracy). The drops detached from the needle, presenting no difficulty, and traveled along the centerline of the tube.

One RCA TC 1000 video camera recorded the drops as they moved through the test section, while another identical camera recorded both the pressure signal being recorded in the stripchart recorder and the actual time as indicated by a lab timer. The images from the video cameras were then combined electronically so that the moving drop, its extra pressure signal and the actual time taken by the drop to move through the test section can be seen together on a single screen (Sanyo Videomonitor) and recorded on a magnetic tape by a videotape recorder (Panatomic Omnivision II).

Measurements were taken for five Newtonian-Newtonian systems encompassing a wide range of material parameters (see Table 1). The Newtonian suspending fluids used were Ucon oil LB 1715 and 95.2% aqueous glycerin solution, with viscosities of 6.54 and 3.94 poises, respectively. The Newtonian drop liquids were: different grades of Dow Corning silicon oil fluid 510, and mixtures of Dow Corning silicon oil fluid 200, to which carbon tetrachloride was added, as necessary, to produce the required density. The fluids 510 were used as a suspended phase within Ucon oil LB 1715. These pairs produced viscosity ratios of σ= 0.75, 7.50 and 14.6. The mixtures of silicon oil fluid 200 and carbon tetrachloride were used as suspended phase within the aqueous solution of glycerol. These pairs produced viscosity ratios of σ = 0.40 and σ = 0.60. Experiments were performed for two flow rates: 4.6 and 8.6 cc/min.

4. Experimental Results

The motion of Newtonian fluid drops within a Newtonian suspending fluid through a wavy-wall tube exhibits some general characteristics common to all systems under study. For example, periodicity of the pressure signal, increase of the dimensionless extra pressure drop with increasing viscosity ratio, increase of drop mobility with increasing flow rate, and increase of drop deformation with increasing capillary number. Obviously, drop deformation also increases with increasing drop size.

According to previous experimental results, the data may be separated into two categories: small-Γ systems and large-Γ systems. This classification also has the advantage of allowing direct comparison of our data with that obtained previously

for a CFR experiment.

For small-Γ systems, glycerol (p = 1.248 gr/cc and μ = 3.94 poises) was used as the suspending fluid and different mixtures of silicon DC 200 (to which carbon tetrachloride had been added) provided the drop fluids. For large-Γ systems, Ucon oil LB 1715 (p = 0.998 gr/cc and μ = 6.54 poises) was used as the suspending fluid and different grades of silicon oil DC 510 provided the drop liquids.

4.1 Small-Γ Systems

Systems 1 and 2 were tested in a CPG experiment at two different flow rates, yielding Γ = 0.043 and Γ = 0.083, respectively.

4.1.a Drop Deformation

Drop breakup was not observed for any drop in small-Γ systems. Drops deform to squeeze through the constrictions of the wavy-wall tube following the tube contour closely as they move into the ample parts of the wavy-wall tube. The maximum deformation is attained when the drop is positioned approximately mid-way through the cross section of the minimum area (at this moment, the maximum value of the time-dependent pressure signal is also attained). Table 3 shows values for the parameter d associated with drop deformation. One can see that d is virtually independent of σ for both Γ = 0.043 and 0.083 and that d increases (moderately) as Γ increases.

4.1.b Average Dimensionless Extra Pressure Drop and Drop Mobility

Figure 5(a) shows values for ΔP^+ vs λ vs. λ for small-Γ systerms in a CPG experiment. ΔP^+ is first an increasing function of λ (fixed values of Γ and σ) until it takes on a maximum value and then it becomes a decreasing function of λ. ΔP^+

decreases as Γ increases due to an increase in flow rate. [Since drop deformation d is observed to change moderately with respect to flow rate (Table 3), then ΔP^+ must be extremely sensitive to changes in d produced by changes in Q.) One can also see that ΔP^+ is an increasing function of σ (fixed values of Γ and λ).

Figure 5(b) shows the corresponding values for $\bar{u}/\bar{v}$ vs. λ. We can see that the mobility of the drop is a decreasing function of λ, up to $\lambda \sim 1$, and takes on a constant value for $\lambda \geq 1$. $\bar{u}/\bar{v}$ is an increasing function of Γ (for fixed values of λ and σ), and it decreases slightly with decreasing σ (for fixed Γ and λ). Note in Table 3 that because of the restricted range of the viscosity ratio, virtually no dependence of d on σ was observed. For small-Γ systems, the general trends of the average dimensionless extra pressure drop, the drop mobility and the drop deformation within the context of a CPG experiment follow the same general trends of their corresponding quantities in the context of a CFR experiment. However, differences in their magnitudes (as predicted by Eq. 13) will be found when comparing results between CPG and CFR experiments, all other flow parameters being equivalent.

4.2 Large-Γ Systems

Systems 3, 4 and 5 were tested in a CPG experiment with two different flow rates, yielding $\Gamma = 1.34$ and 2.54.

4.2.a Drop Deformation

For large-Γ systems with $\sigma = 0(1)$, no drop breakup was observed either inside or outside of the test section. In these systems, a small drop ($\lambda < 0.92$) passes through the test section undergoing periodic deformation as it goes from a constriction to a bowed section of the wavy-wall tube. On the other hand, a larger drop ($\lambda \geq 0.92$) deforms more and more at each constriction of the wavy-wall tube as it

passes through the first six or ten constrictions, depending on the drop size and the magnitude of Γ (flow rate). After this transition stage, such drops are observed to attain a constant longitudinal length (constant d).

Table 4 shows values of the deformation parameter d for drops moving in a CPG experiment for large-Γ systems (Γ = 1.34 and 2.54). We can see that d strongly depends on the viscosity ratio (as opposed to the trend seen for small-Γ systems), i.e. drop deformation increases with increasing σ (fixed values of Γ and λ) and this dependence seems to have an effect on the drop mobility, as will be discussed below. Also, we can see the strong influence of the capillary number (flow rate) on d; obviously, d increases with drop size.

4.2.b Average Dimensionless Extra Pressure Drop and Drop Mobility

Figures 6(a) and 6(b) show, respectively, values for ΔP^+ vs. λ and $\bar{u}/\bar{v}$ vs. λ for large-Γ systems in a CPG experiment. For $\sigma > 1$, ΔP^+ is an increasing function of λ (for fixed values of Γ and σ), whereas it seems to slowly decrease with λ for $\sigma < 1$. ΔP^+ is an increasing function of σ (for fixed values of Γ). ΔP^+ decreases with increasing Γ (increasing flow rate) and, hence, it can also be said (as was the case for small-Γ systems) that ΔP^+ decreases with increasing drop deformation. The average dimensionless extra pressure drop follows the same general trend as its counterpart in a CFR experiment. But the numerical values for ΔP^+ vs. λ will shortly be seen to fall under the corresponding curves for the CFR case, in agreement with Eq. (13). On the other hand, our results show that drop mobility depends on viscosity ratio, this apparently being a consequence of increased drop deformation since d was observed to increase with σ. Drop deformation, though, was never strong enough to cause dispersion phenomena.

Figure 6(b) shows that the mobility of the drop is an increasing function of Γ, nearly independent of λ (for fixed values of Γ and σ), and an increasing function of the viscosity ratio. It is apparent from our CPG experimental results that there is a correlation among drop mobility, viscosity ratio and drop deformation for these large-Γ systems with $\sigma \sim 1$ and $\sigma > 1$. As shown in Table 4, d increases with σ for both $\Gamma = 1.34$ and 2.54. On the other hand, $\overline{u}/\overline{v}$ is observed to increase with σ. It seems then, as the drop deformation increases because of an increase in viscosity ratio, drop mobility also increases. As will be seen in Sect. 5, this is not the case at all in a CFR experiment.

5. Comparison Between CPF and CPG Experiments

A convenient way to analyze the basic difference between CPG and CFR experimental results is to organize them according to the magnitude of the capillary number. As stated earlier, the magnitude of the flow rate for the suspending fluid alone, the ratio of viscosities and the drop size are equivalent in magnitude for both experiments, and only the nature of the driving force for the flow is changed. Differences between these results may be attributed to the different character of the driving mechanism. Values for drop deformation, average dimensionless extra pressure drop and drop mobility in a CFR experiment have been presented in III and reproduced in IV. Henceforth we compare our results for a CPG experiment with our results for CFR experiments, which were carried out and reported in IV. The numerical values given for the average dimensionless extra pressure drop for a CPG experiment are the *real* values as estimated according to Eq. (18). In order to distinguish results for the two types of experiment, the subindexes CPG and CFR will

be attached to the flow variables.

5.1 Small-Γ Systems

Experimental data for Systems 1 and 2 taken from a CPG experiment was compared with data for equivalent systems taken from a CFR experiment.

5.1.a Drop Deformation

At small capillary numbers, equivalent drops moving in either a CFR or a CPG experiment move through the wavy-wall test section in a very similar fashion. They closely follow the tube walls, obtaining their maximum deformation and maximum values for the corresponding pressure drop when located approximately midway through the region of minimum cross-sectional area in the wavy-wall tube. However, Table 5 shows a very consistent trend regarding the drop deformation parameter when changing from a CPG to a CFR experiment, all other flow variables being equivalent. That is, the magnitude of d_{CFR} is larger than that of d_{CPG}. It appears then that a CFR flow is more efficient in effecting deformation of the drop than a CPG flow, and in this sense may be referred to as being potentially stronger.

At first it may seem surprising that drop deformation may undergo such increments solely on the basis of changes in the nature of the driving mechanism for the flow, particularly because in the context of either a CFR or a CPG experiment, a large change in the total flow rate would be necessary to produce equivalent changes in d (see for example Tables 3 and 4). However, it looks intuitively correct that a CFR flow causes greater drop-tube wall interaction and consequently greater deformation of the drops, or, conversely, that in a CPG flow the effect of restoring mechanisms is being favored by the release of the constant flow condition and thus may act more effectively against drop deformation.

5.1.b Average Dimensionless Extra Pressure Drop and Drop Mobility in CPG and CFR

Figure 7(a) shows comparison of ΔP^+_{CFR} with ΔP^+_{CPG} as a function of λ for σ = 0.40 and 0.60 at Γ = 0.043. All curves representing the average dimensionless extra pressure drop ΔP^+ for a CPG experiment fall under the corresponding curves for CFR experiments in qualitative agreement with Eq. (13). Correspondingly, Fig. 7(b) shows a similar comparison for the numerical values of the drop mobility vs. λ (same systems). $(\overline{u}/\overline{v})_{CPG}$ values are fairly equal for most λ's than those for $(\overline{u}/\overline{v})_{CPR}$. Figures 8(a) and 8(b) show the corresponding information for the same systems but at Γ = 0.083.

5.2 Large-Γ Systems

Experimental data for Systems 3, 4 and 5 taken from a CPG experiment is compared with data for equivalent CFR experimental systems.

5.2.a Drop Deformation

Within the context of a CFR experiment, drop deformation and drop breakup develop according to the following mechanism. (i) For $\lambda < 0.77$, drops undergo periodic deformation while passing through the wavy-wall tube; (ii) For $\lambda > 0.72$, drops deform continuously while passing through the first half of the wavy-wall tube until an equilibrium shape is attained; and (iii) For the largest values of λ, drops are observed to exit the test section before reaching a steady shape. Some of these drops form strands or filaments which remain stable while in the test section, but later break up in the straight-wall relaxation section that followed the test section generating several equal sized droplets.

The dispersion phenomena for a CFR experiment was promoted by changes in the following variables: an increase in λ, fixed σ and Γ; an increase in Γ, fixed σ and λ; and, to a lesser extent, an increase in σ, fixed λ and Γ (note the relatively weak dependence of d_{CFR} on σ in CFR, as shown in Table 6).

On the other hand, within the context of a CPG experiment, drop deformation develops following steps (i) and (ii), but drop breakup was never observed to occur either inside or outside the wavy-wall tube. Even more d_{CPG} was less than d_{CFR} for both Γ = 1.34 and 2.54.

Drop deformation d_{CPG} in a CPG experiment was promoted by changes in the following variables: an increase in λ, σ and Γ fixed; an increase in Γ, λ and σ fixed; and an increase in σ, λ and Γ fixed. It is important to realize that the dependence of d_{CPG} on σ for both Γ = 1.34 and 2.54 is much stronger in a CPG experiment than the dependence of d_{CFR} on σ in a CFR experiment, as shown in Table 6. There, it can also be noted for these large-Γ systems that values for d_{CFR} were found to be consistently larger than those for d_{CPG} for equivalent flow conditions and in this sense we may again refer to a CFR flow as being stronger than a CPG flow.

Here again, equivalent changes to those brought about by a mere change in the nature of the driving mechanisms for the flow would require, in either a CPG or a CFR experiment, a large change in the flow rate. It thus seems once more that the combined effect of both the change in flow rate due to the obstructing action of the drop and the increase in the effect of the restoring mechanism produced by removal of the constant flow condition has produced a stronger than expected effect.

It will be shown below as we compare drop mobilities in the two different types of flows that drop mobility seems to reflect the changes in drop deformation.

First, the most highly deformed drops caused by a CFR flow (i.e. largest values for d_{CFR}) correspond to the largest drop mobilities and, conversely, smaller drop deformation (smaller values for d_{CPG}) corresponds to smaller values of drop mobility. Second, the relatively slight dependence of d_{CFR} on σ corresponds to a single $\overline{u}/\overline{v}$ vs. λ curve for a very wide range of viscosity ratios in the CFR experiment and, conversely, the strong dependence of d_{CPG} on σ corresponds to a strong dependence of $(\overline{u}/\overline{v})$ with respect to σ in the CPG case.

5.2.b Average Dimensional Extra Pressure Drop and Drop Mobility

In Fig. 9(a), ΔP^{+}_{CFR} vs. λ is compared with ΔP^{+}_{CPG} as a function of λ for $\sigma = 7.5$ and 14.6 at $\Gamma = 1.34$. Figure 10(a) shows similar data for the same values of the viscosity ratio but at $\Gamma = 2.54$. All curves that represent the average extra pressure drop for a CPG experiment fall below the corresponding curves for the CFR experiment, in qualitative agreement with Eq. (13).

Figures 9(b) and 10(b) show numerical values for the $(\overline{u}/\overline{v})_{CPG}$ vs. λ and $(\overline{u}/\overline{v})_{CFR}$ vs. λ for corresponding fluid systems. The curves for $(\overline{u}/\overline{v})_{CFR}$ vs. λ at either $\Gamma = 1.34$ or $\Gamma = 2.54$, each good for a large range of viscosity ratio ($0.7 < \sigma < 15$), constitute an upper boundary for $(\overline{u}/\overline{v})_{CPG}$ vs. λ (one curve for each value of the viscosity ratio) at the same capillary numbers.

As mentioned in Sect. 5.1.a, the behavior of the drop mobility with respect to σ reflects the behavior of drop deformation with respect to σ, i.e. $(\overline{u}/\overline{v})_{CFR}$ is independent of σ for a CFR experiment (where d_{CFR} was found to depend only very slightly dependent on σ). On the other hand, $(\overline{u}/\overline{v})_{CPG}$ shows a significant dependence on σ for a CPG experiment (where d_{CPG} was found to be strongly dependent on σ).

6. Conclusions

We have studied here the effects on drop dynamics produced by a change in the nature of the driving mechanism from a CFR flow to a CPG flow.

The deformation undergone by drops flowing in a two-phase flow in a CPG experiment is less than the deformation undergone by equivalent drops flowing in a CFR experiment, particularly so at large capillary numbers. Moreover, in a CPG experiment, drop breakup was eliminated for the large-Γ system drops [with $\sigma \sim 0(1)$ and >1], in contrast to the fact that equivalent drops flowing in a CFR experiment do break up as they exit the wavy-wall test section. This difference between the two types of flows may be of considerable interest depending on whether dispersion of the suspended phase is desirable or not for a given process.

Also, for CPG conditions, drop deformation depended very strongly on viscosity ratio whereas that dependence was very weak in the CFR case. The drop mobility for large-Γ systems was found to be larger in a CFR experiment than in a CPG experiment. Indeed, the $(\bar{u}/\bar{v})_{CFR}$ vs. λ curves for the CFR experiment appeared to represent an upper limit for the corresponding experimental $(\bar{u}/\bar{v})_{CPG}$ vs. λ curves for a CPG experiment. In addition, it may be noted that $(\bar{u}/\bar{v})_{CFR}$ was independent of viscosity ratio for a large range of σ, whereas $(\bar{u}/\bar{v})_{CPG}$ depended on it. Large values of $(\bar{u}/\bar{v})_{CPG}$ (vs. λ) corresponded to larger values of viscosity ratio and vice-versa. This last effect seems to correlate with the degree of drop deformation in a CPG experiment where d_{CPG} was found to increase as viscosity ratio increased. Hence, it appears that larger values of $(\bar{u}/\bar{v})_{CPG}$ may be a consequence of increased drop deformation.

Due to the large change in flow rate required to produce relatively small changes in d in either CFR or CPG experiments, it seems unlikely that the changes observed in d (and other variables) are solely caused by the small change in flow rate due to the obstructing effect of the drop. Apparently, the release of the constant flow condition in a CPG promotes a more efficient action of the restoring mechanisms against deformation forces or, conversely, that a CFR causes greater interaction between the drop and the tube wall, hence causing larger drop deformation and larger drop mobility.

From a general point of view, and within the range of our experiments, a CFR flow may be considered as a potentially stronger flow compared with a CPG flow in the sense that it causes larger extra pressure drop, larger drop deformation, and, for large-Γ systems, larger drop mobility which is *independent* of viscosity ratio. On the other hand, a CPG flow may be considered a relatively weaker flow in the sense that it produces less extra pressure drop, less drop deformation, and, for large-Γ systems, less drop mobility which is *dependent* on viscosity ratio.

Consequently, under some particular circumstances, a CFR flow promotes breakup of the drop, whereas a CPG flow actually inhibits drop breakup for equivalent flow conditions.

Table 1. Properties of Systems.

System	Suspension Fluid	Drop Fluid	γ	σ	Γ	Γ
1	95.2 Glycerol	DC 200 + CCl_4	22	0.40	0.043	0.083
2	95.2 Glycerol	DC 200 + CCl_4	22	0.60	0.083	0.083
3	Ucon Oil LB 1715	DC 510	1.3	0.75	1.34	2.54
4	Ucon Oil LB 1715	DC 510	1.3	7.52	1.34	2.54
5	Ucon Oil LB 1715	DC 510	1.3	14.6	1.34	2.54

Table 2. Drop Volumes and Corresponding λ values.

Volume CC	λ
0.03	0.61
0.06	0.77
0.10	0.92
0.15	1.04
0.20	1.15

Table 3. The magnitude of the deformation parameter d_{CPG} is given at the intersection of columns representing drop size and rows representing viscosity ratio. d_{CPG} is defined as the ratio between the maximum longitudinal length of the drop measured along the flow center line to the wave length of one period of the wavy-wall tube.

CPG		Small-Γ		Γ = 0.043	
σ↓, λ→	0.62	0.77	0.92	1.04	1.15
0.40	0.28	0.38	0.51	0.66	0.78
0.60	0.28	0.38	0.51	0.66	0.80
				Γ = 0.083	
0.40	0.29	0.41	0.53	0.70	0.81
0.60	0.29	0.41	0.54	0.70	0.81

Table 4. The magnitude of the deformation parameter d_{CPG} is given at the intersection of columns representing drop size and rows representing viscosity ratio. d_{CPG} is defined as the ratio between the maximum longitudinal length of the drop measured along the flow center line to the wave length of one period of the wavy-wall tube.

CPG		Large-Γ		Γ = 1.34	
σ↓, λ→	0.62	0.77	0.92	1.04	1.15
0.75	0.47	0.66	1.00	1.43	1.75
7.50	0.54	0.84	1.18	1.84	2.16
14.6	0.54	0.87	1.21	1.86	2.23
				Γ = 2.54	
0.75	0.47	0.78	1.14	1.74	2.0
7.50	0.80	1.14	1.85	2.25	3.0
14.6	0.90	1.30	1.90	2.50	3.5

Table 5. Small-Γ Numbers. The magnitude of the deformation parameter d for both CPG and CFR experiments is given at the intersection of columns representing drop size and rows representing viscosity ratio for two small-Γ numbers. See text.

CPG Γ = 0.043					
σ↓, λ→	0.62	0.77	0.92	1.04	1.15
0.40	0.28	0.38	0.51	0.66	0.78
0.60	0.28	0.38	0.51	0.66	0.80
CFR Γ = 0.043					
0.40	0.29	0.41	0.52	0.66	0.80
0.60	0.29	0.41	0.52	0.67	0.80
CPG Γ = 0.083					
σ↓, λ→	0.62	0.77	0.92	1.04	1.15
0.40	0.29	0.41	0.53	0.70	0.81
0.60	0.29	0.41	0.54	0.70	0.81
CFR Γ = 0.083					
0.40	0.30	0.44	0.58	0.72	0.83
0.60	0.30	0.45	0.59	0.73	0.84

Table 6. Large-Γ Systems. The deformation parameter d for both CPG and CFR experiments is given at the intersection of columns representing drop size and rows representing viscosity ratio for two large-Γ numbers. See text.

			CPG Γ = 1.34		
σ↓, λ→	0.62	0.77	0.92	1.04	1.15
0.75	0.47	0.66	1.0	1.43	1.75
7.50	0.54	0.84	1.18	1.84	2.16
14.6	0.54	0.87	1.21	1.86	2.23
			CFR Γ = 1.34		
0.72	0.60	0.89	1.22	1.90	2.36
7.47	0.61	0.91	1.24	1.92	2.40
14.6	0.65	0.91	1.25	1.92	2.50
			CPG Γ = 2.54		
0.75	0.47	0.78	1.14	1.74	2.0
7.50	0.80	1.14	1.85	2.25	3.0
14.6	0.90	1.30	1.90	2.50	3.5
			CFR Γ = 2.54		
0.72	0.81	1.45	1.95	2.80	3.3
7.47	0.83	1.50	2.0	2.80	3.5
14.6	0.90	1.50	2.0	3.00	3.9

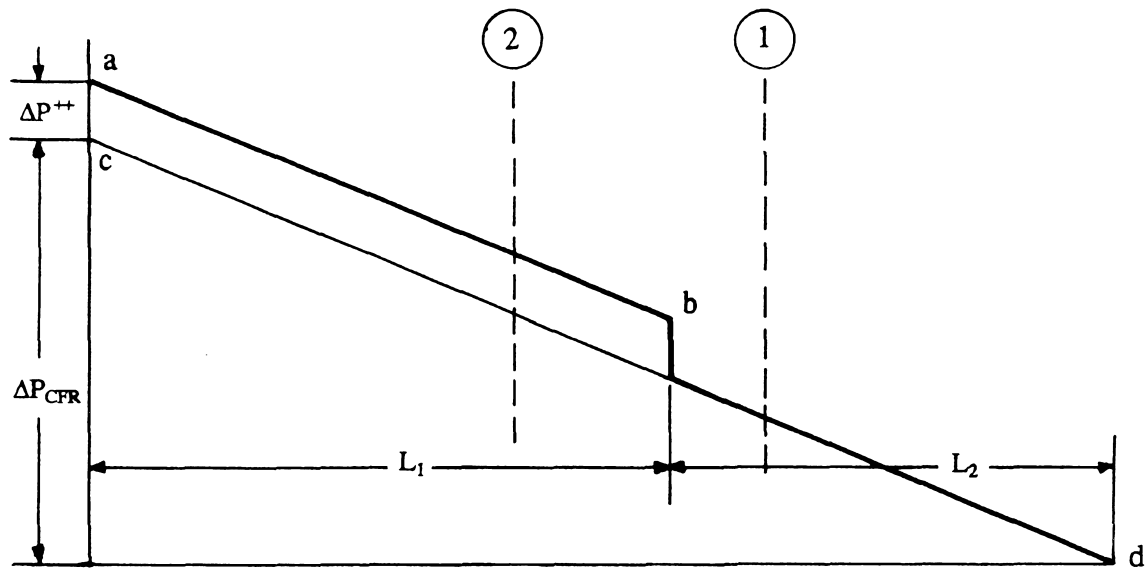

Figure 1. Schematic representation of the pressure distribution in the complete flow system for a constant flow rate (CFR) experiment.

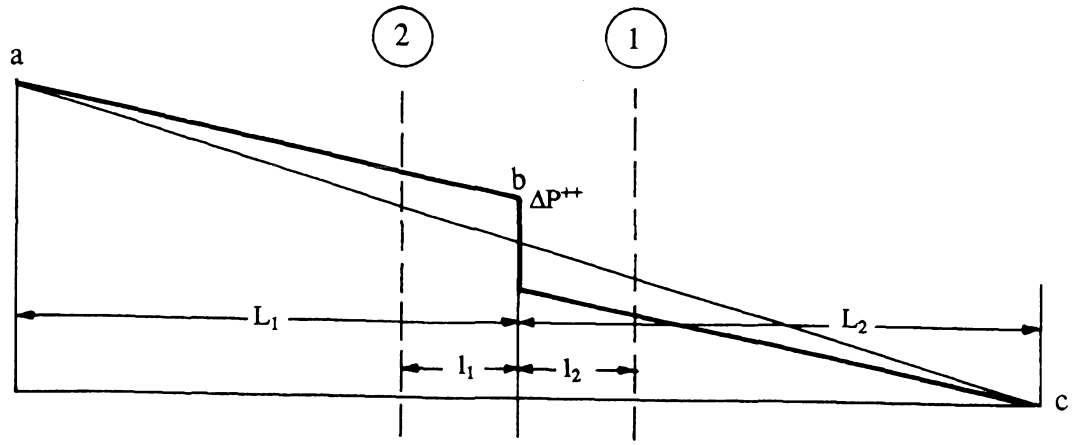

Figure 2. Schematic representation of the pressure distribution in the complete flow system for a constant pressure gradient (CPG) experiment.

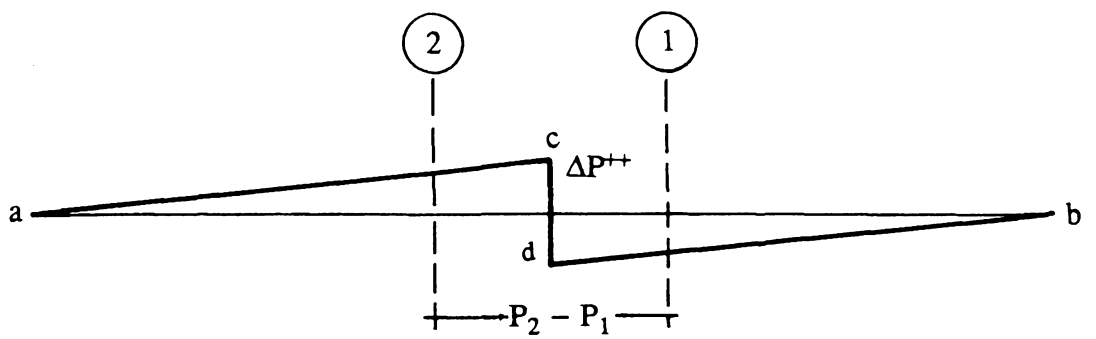

Figure 3. Representation of the difference in the pressure distribution with the drop present relative to that without the drop. The entrance and exit of the test section are indicated with numbers 2 and 1, respectively. $P_2 - P_1$ is the apparent value measured by the pressure transducer which differs from ΔP^{++} (at point c) because of the change in slope in the upstream and downstream region.

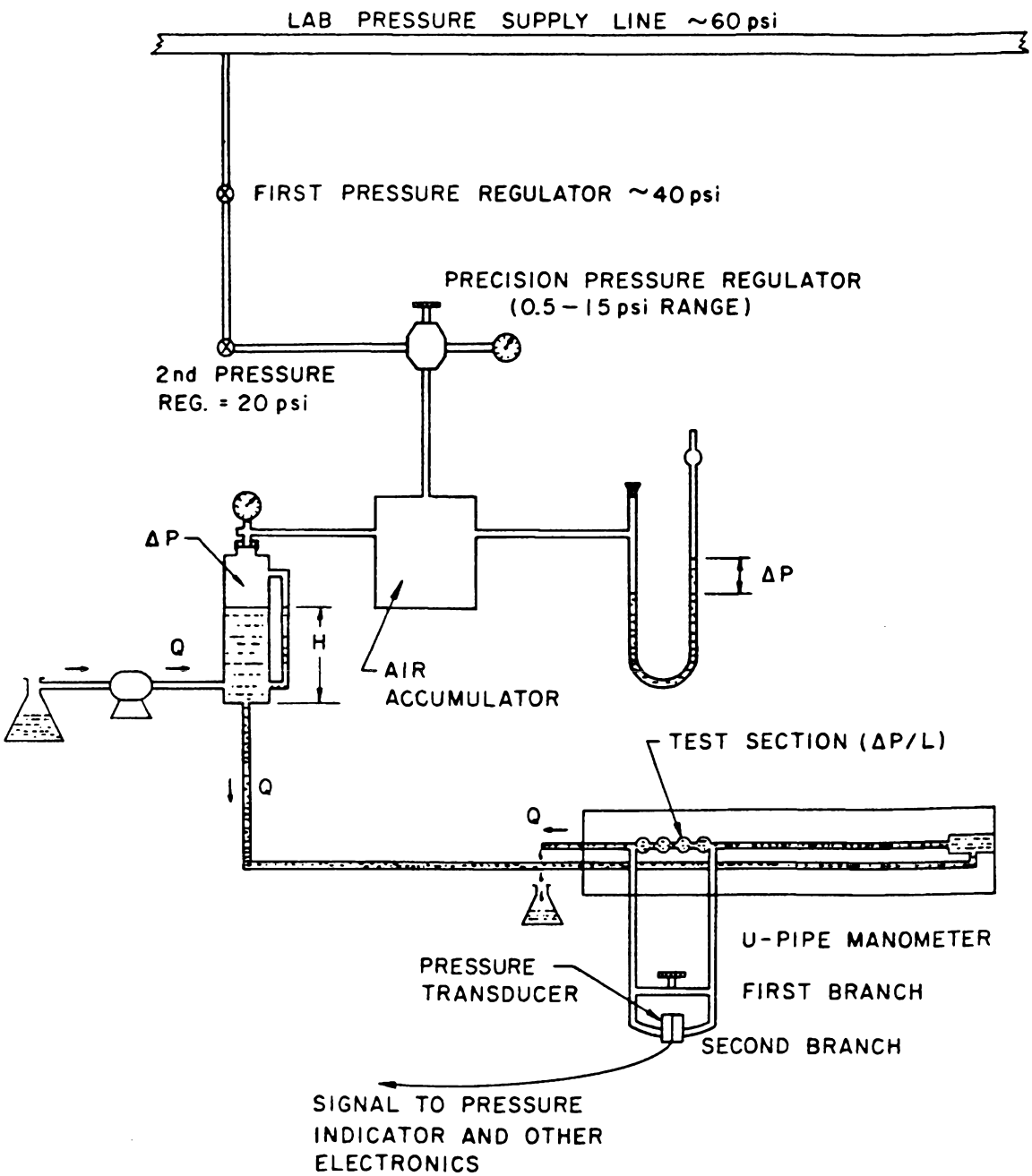

Fig. 4. The basic apparatus used to carry out the experiments under CPG conditions

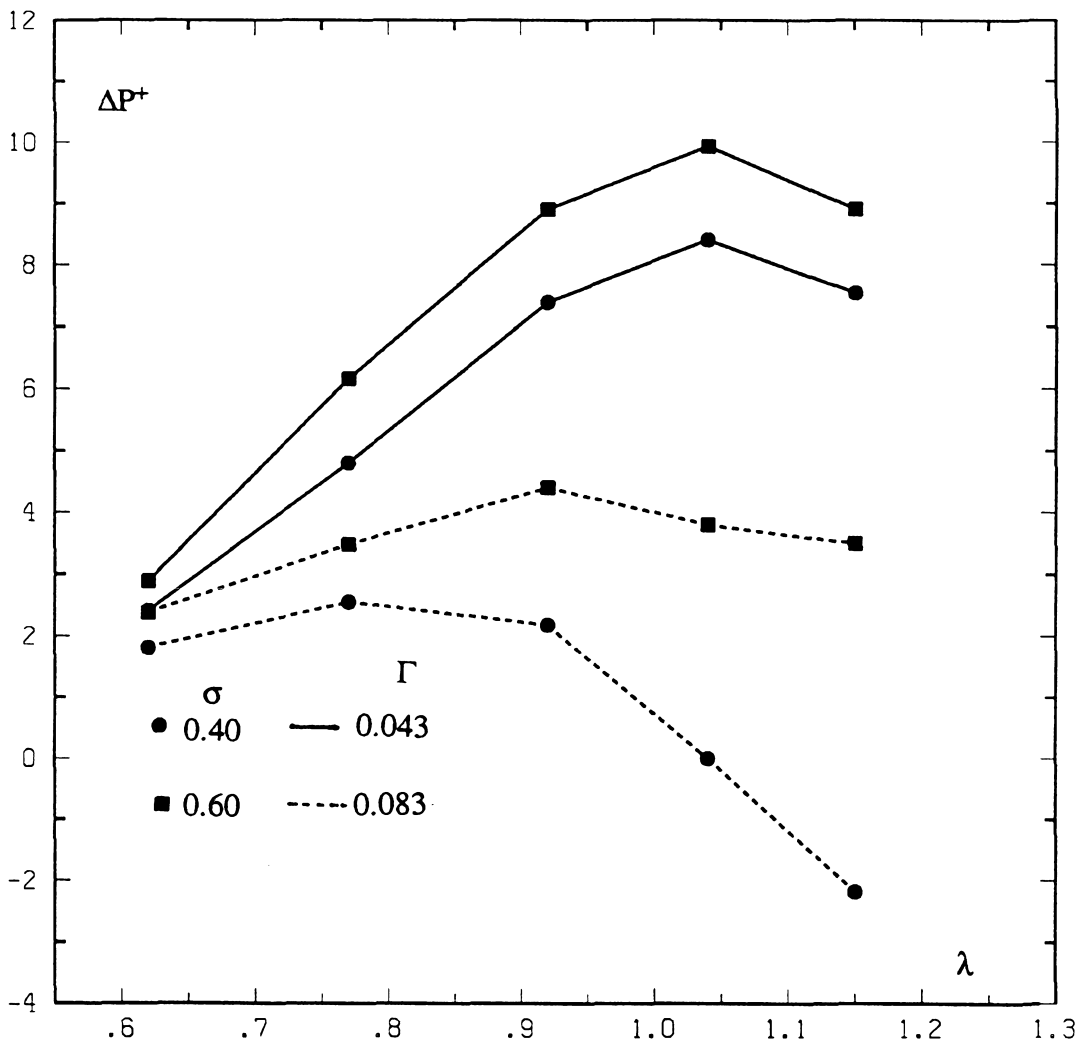

Figure 5(a). ΔP^+ vs. λ, small-Γ systems in a CPG experiment.

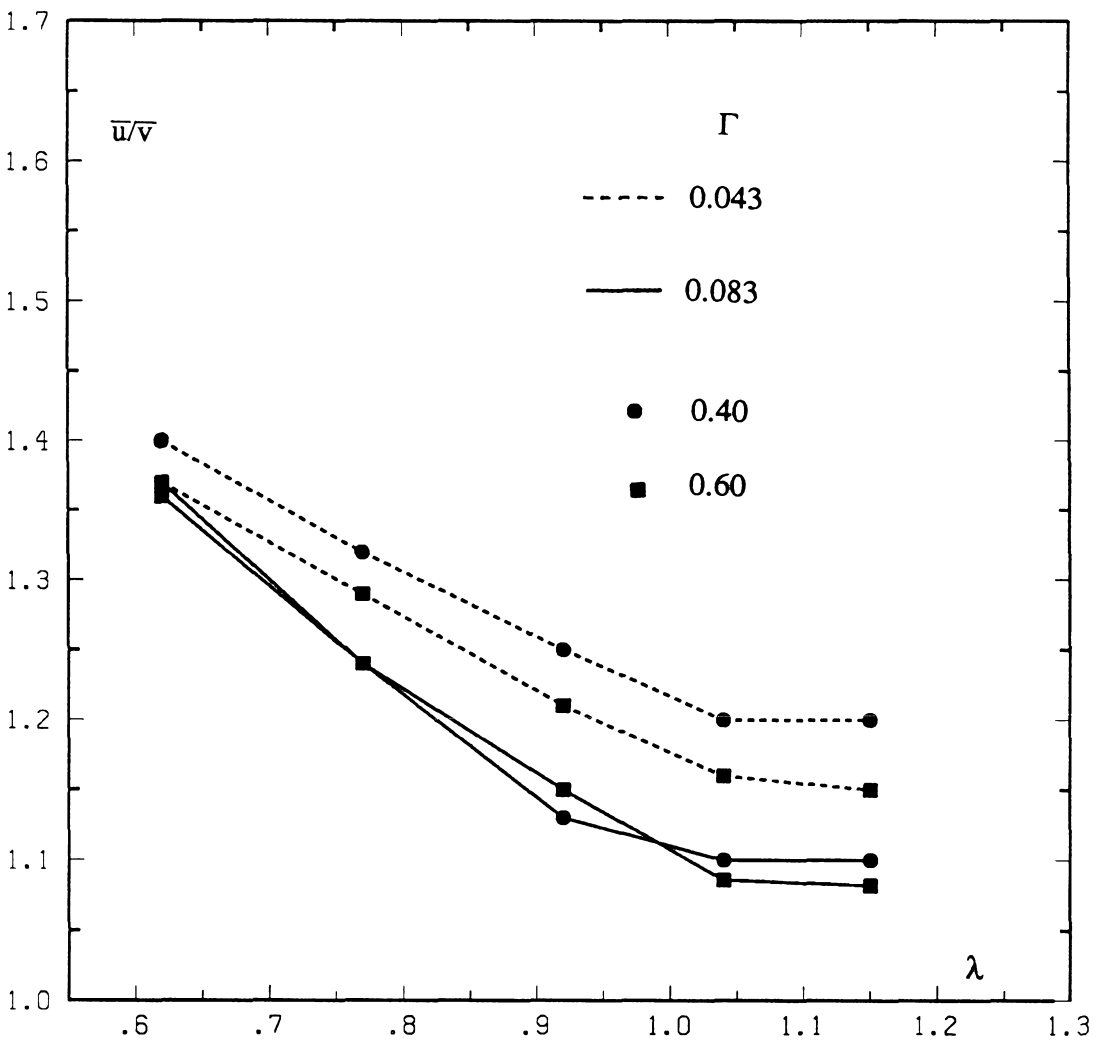

Figure 5(b). $\overline{u/v}$ vs. λ, small-Γ systems in a CPG experiment.

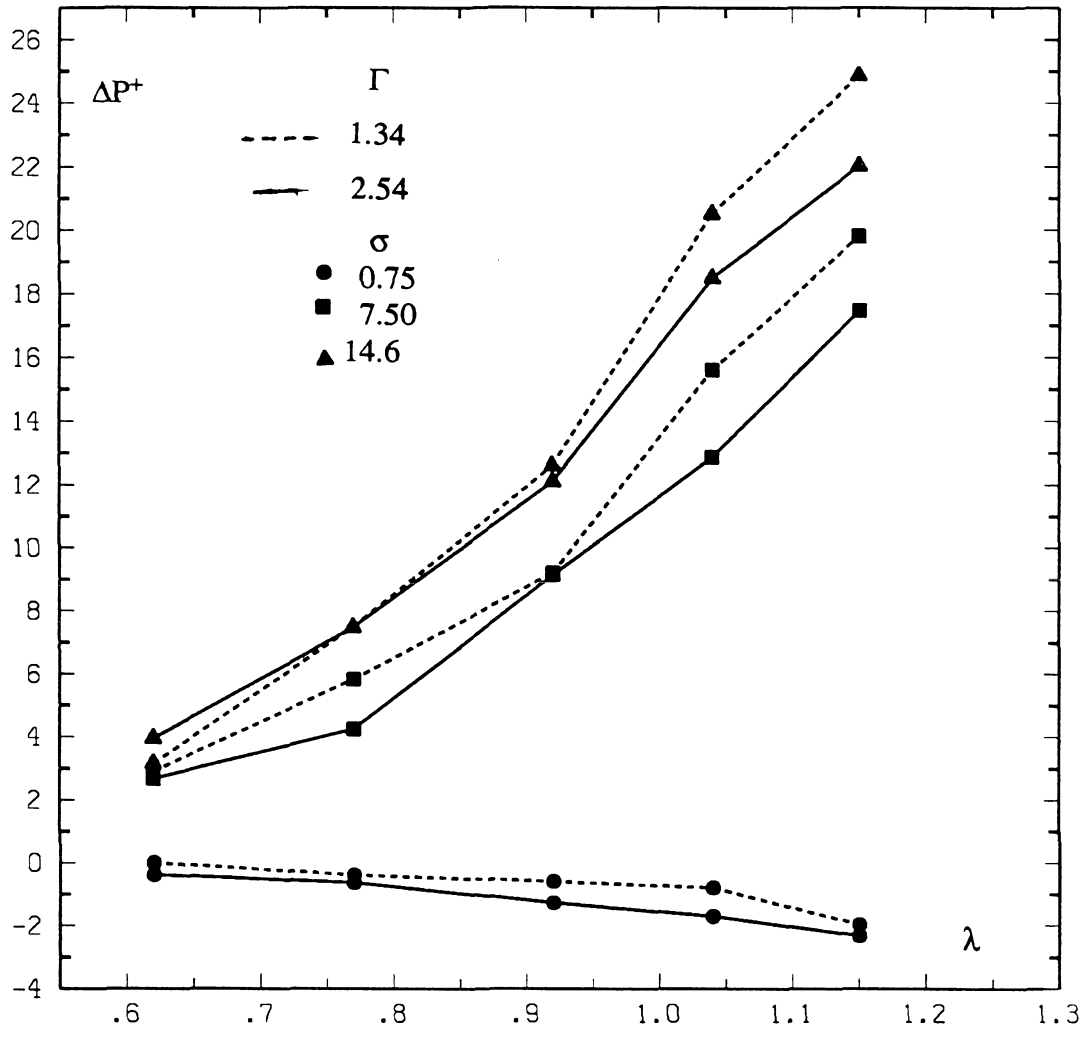

Figure 6(a). ΔP^+ vs. λ, large-Γ systems in a CPG experiment.

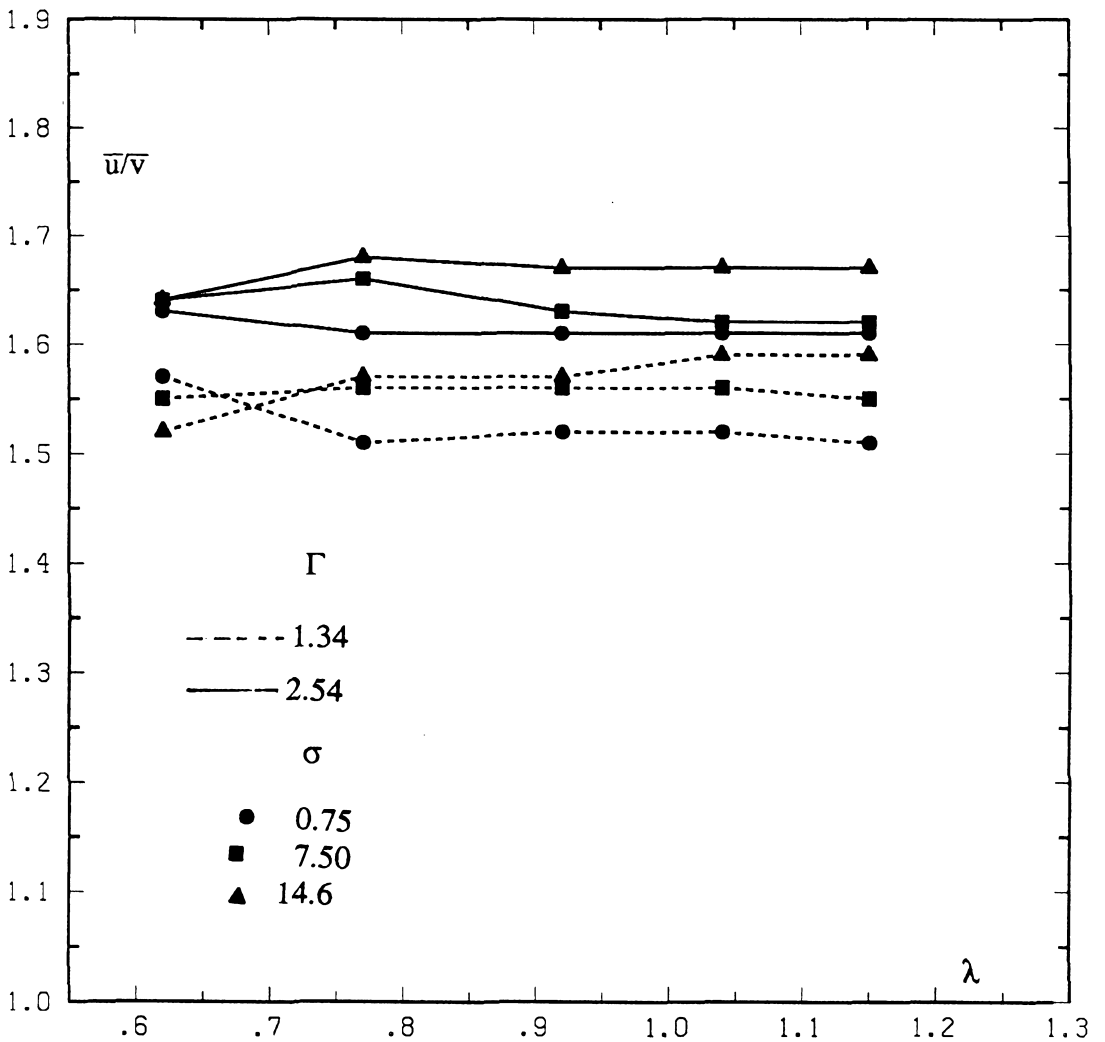

Figure 6(b). $\overline{u/v}$ vs. λ, large-Γ systems in a CPG experiment.

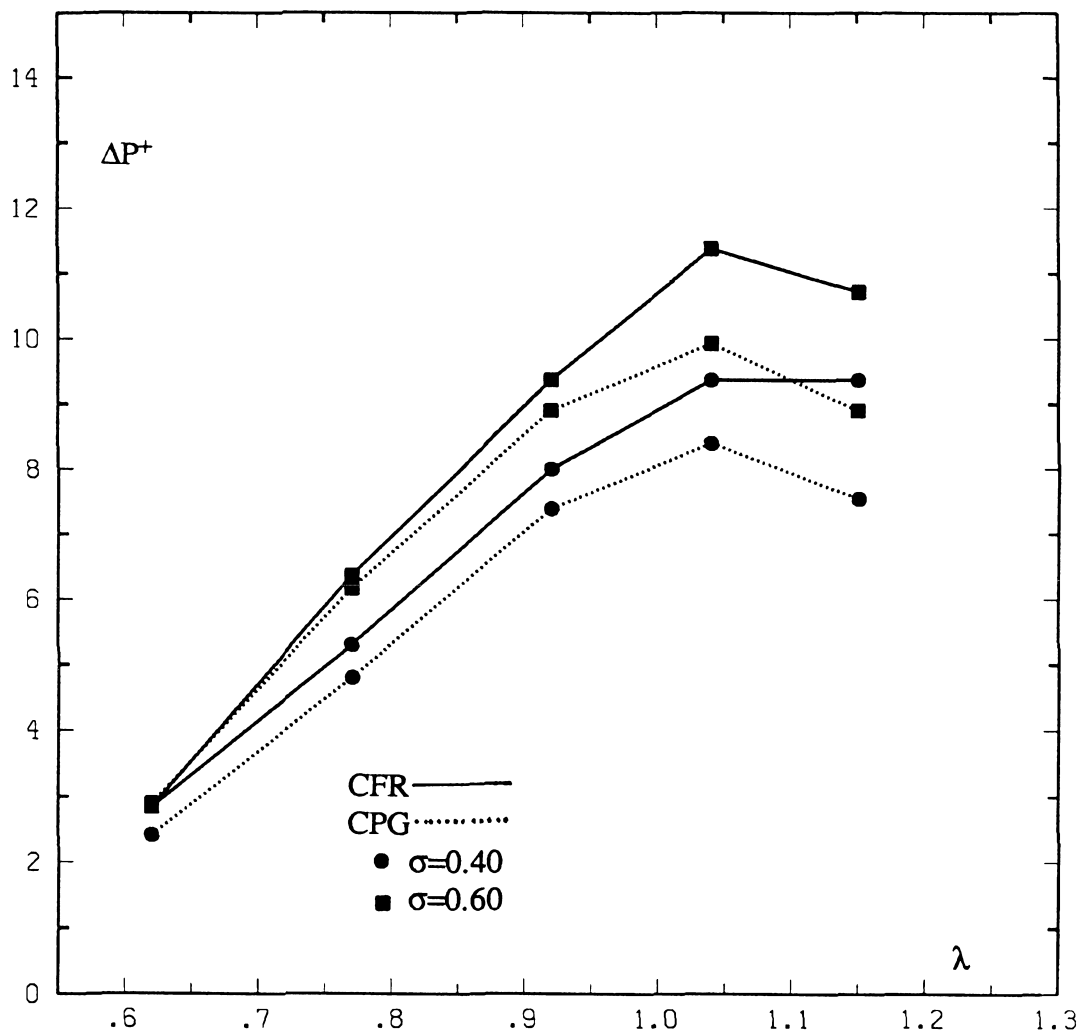

Figure 7(a). Comparison of ΔP^{+}_{CFR} with ΔP^{+}_{CPG} as a function of λ at Γ=0.043.

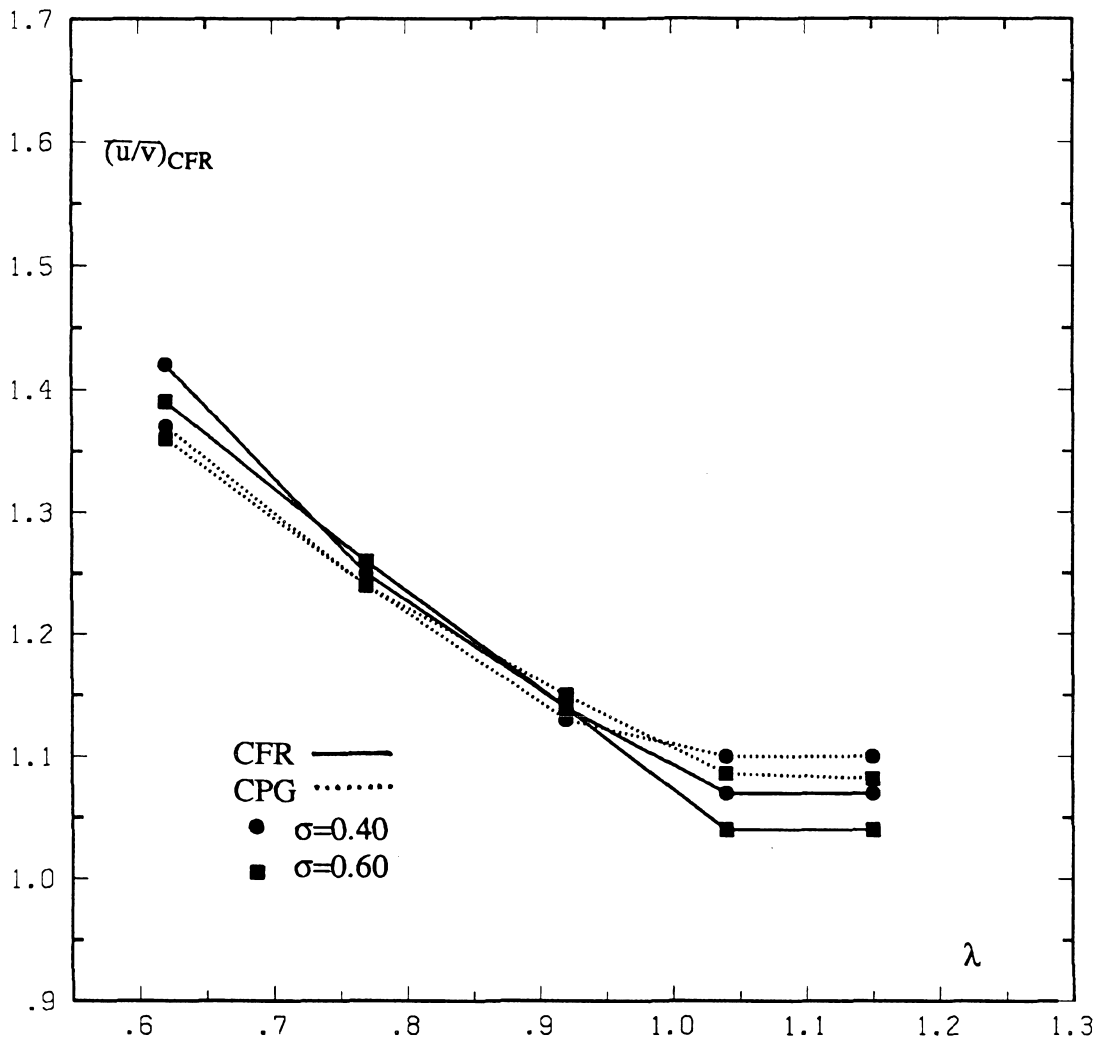

Figure 7(b). Comparison of $(\overline{u/v})_{CFR}$ with $(\overline{u/v})_{CPG}$ as a function of λ at Γ=0.043.

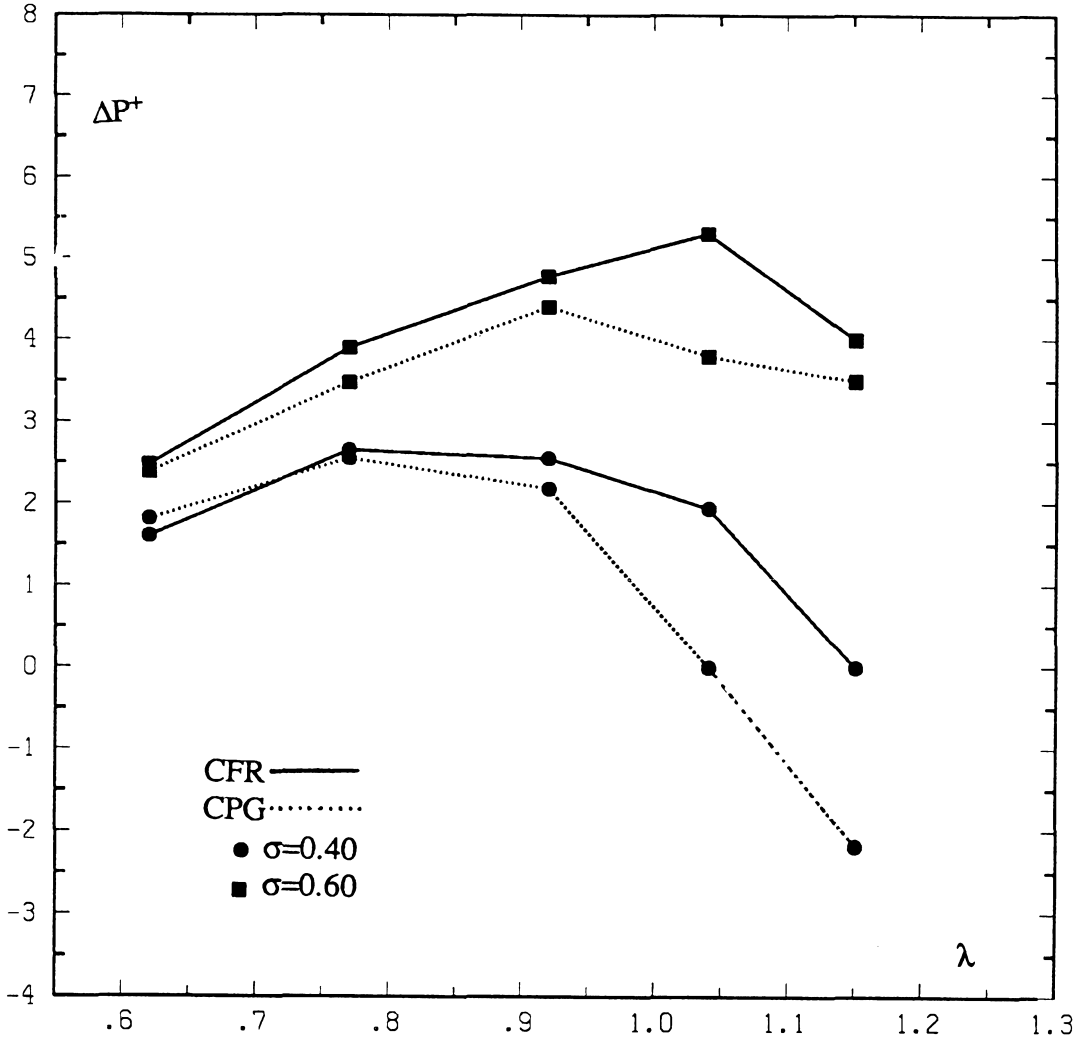

Figure 8(a). Comparison of ΔP^{+}_{CFR} with ΔP^{+}_{CPG} as a function of λ at Γ=0.083.

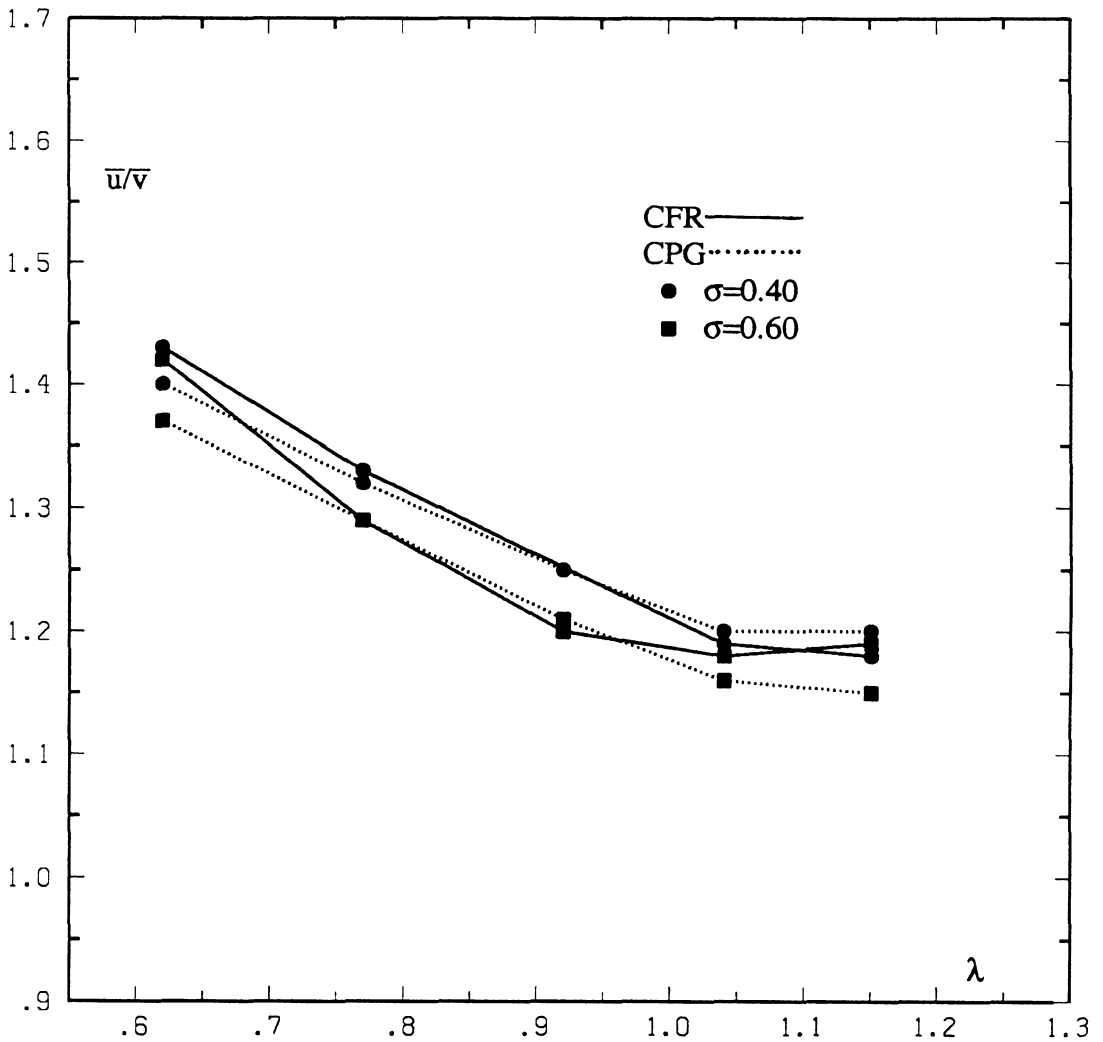

Figure 8(b). Comparison of $(\overline{u}/\overline{v})_{CFR}$ with $(\overline{u}/\overline{v})_{CPG}$ as a function of λ at Γ=0.083.

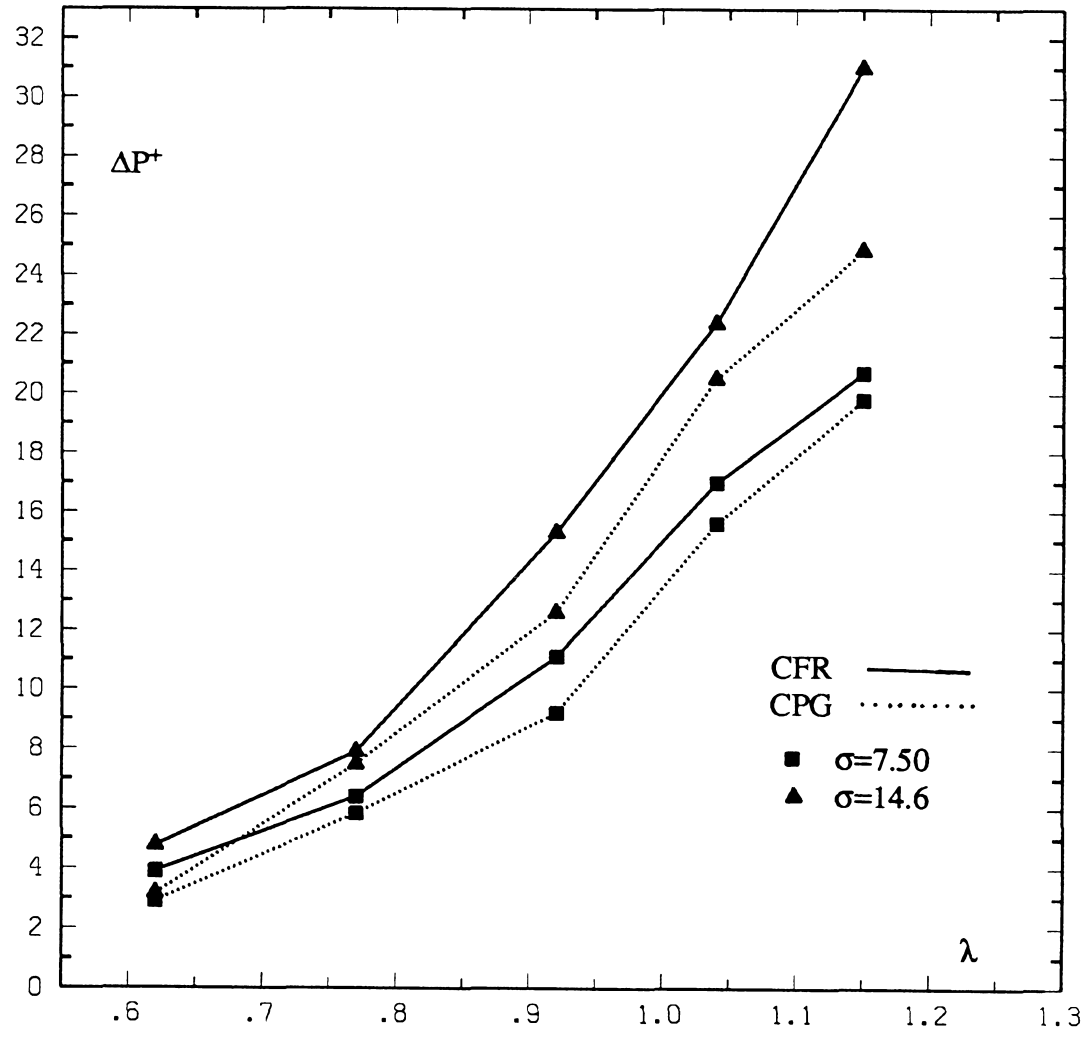

Figure 9(a). Comparison of ΔP^{+}_{CFR} with ΔP^{+}_{CPG} as a function of λ at Γ=1.34.

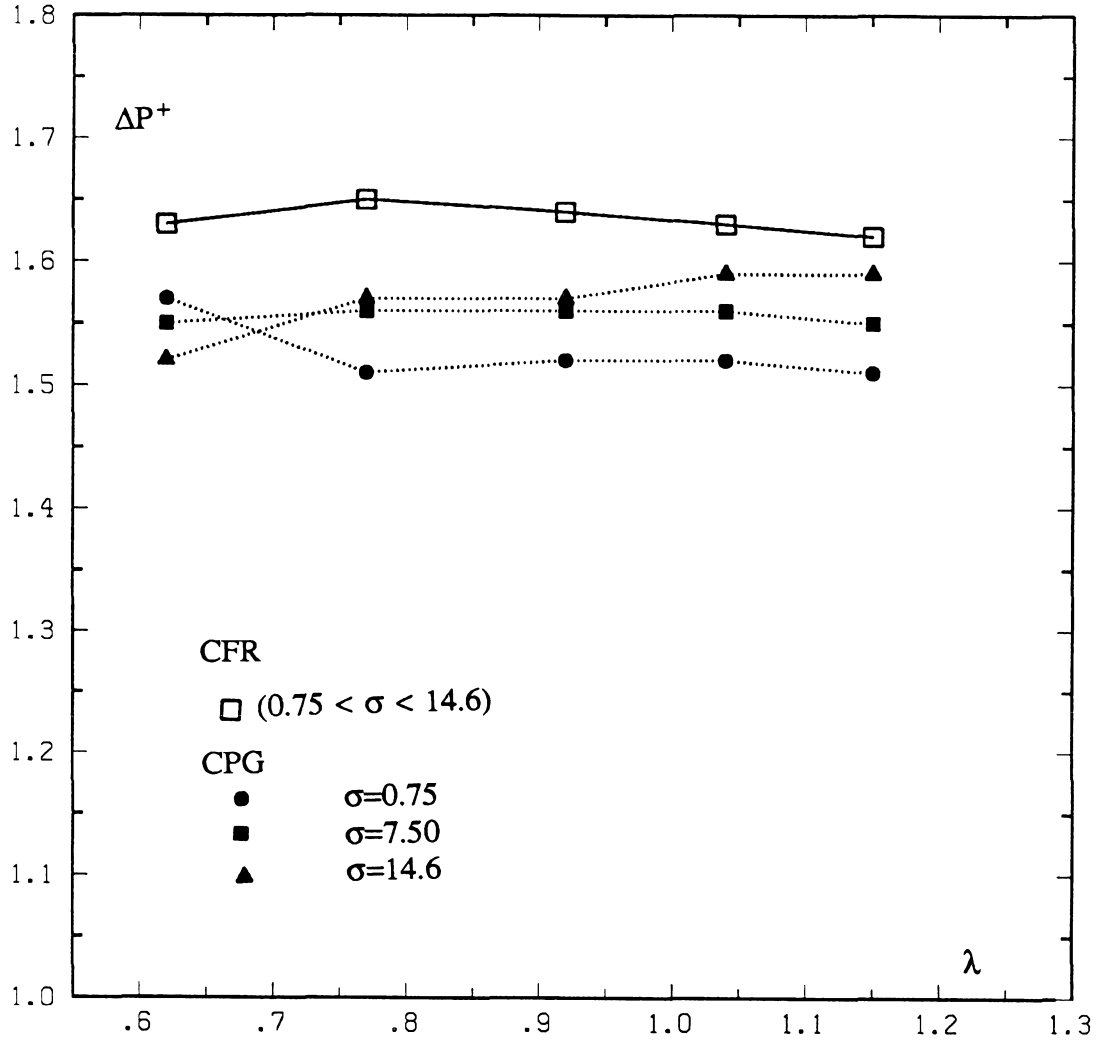

Figure 9(b). Comparison of $\overline{(u/v)}_{CFR}$ with $\overline{(u/v)}_{CPG}$ as a function of λ at Γ=1.34.

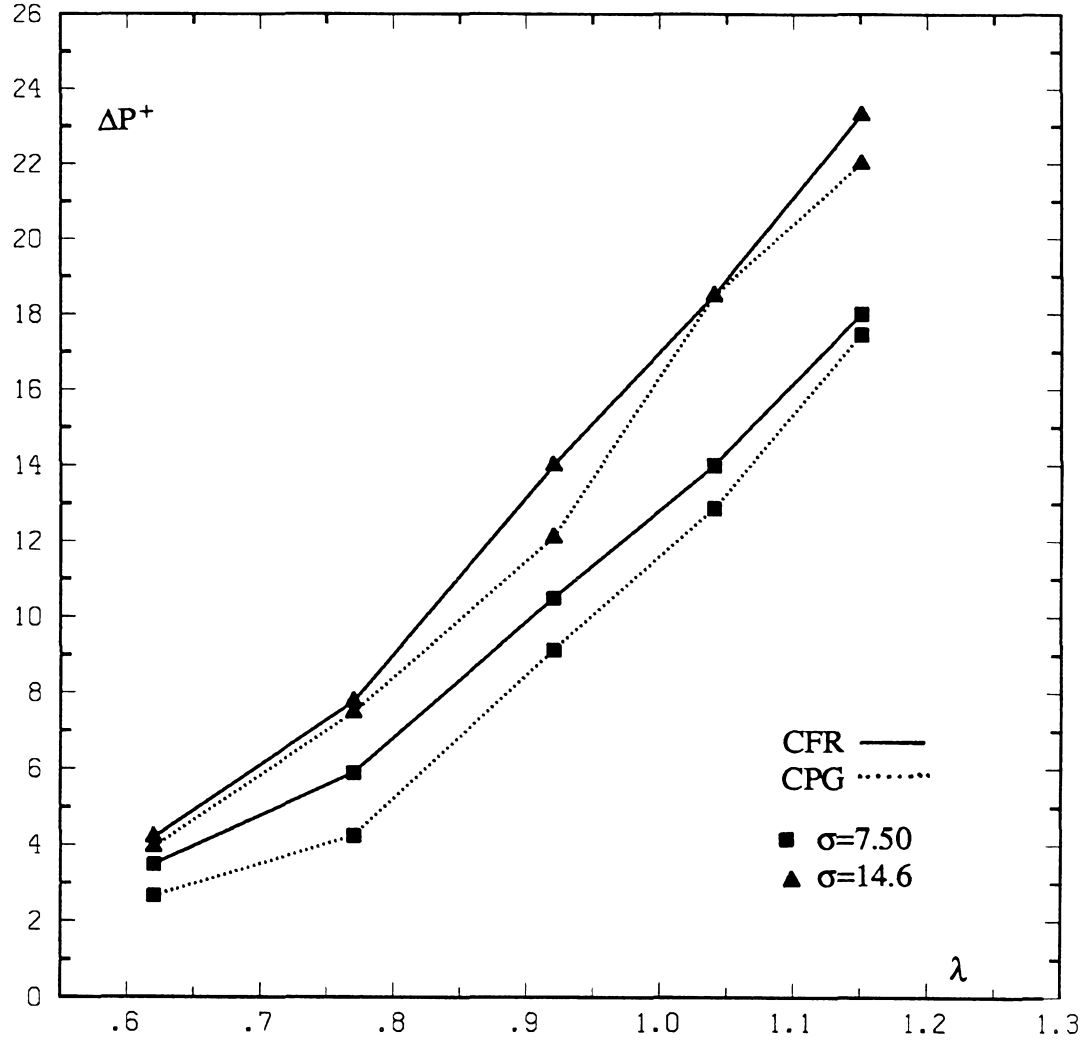

Figure 10(a). Comparison of ΔP^{+}_{CFR} with ΔP^{+}_{CPG} as a function of λ at Γ=2.54.

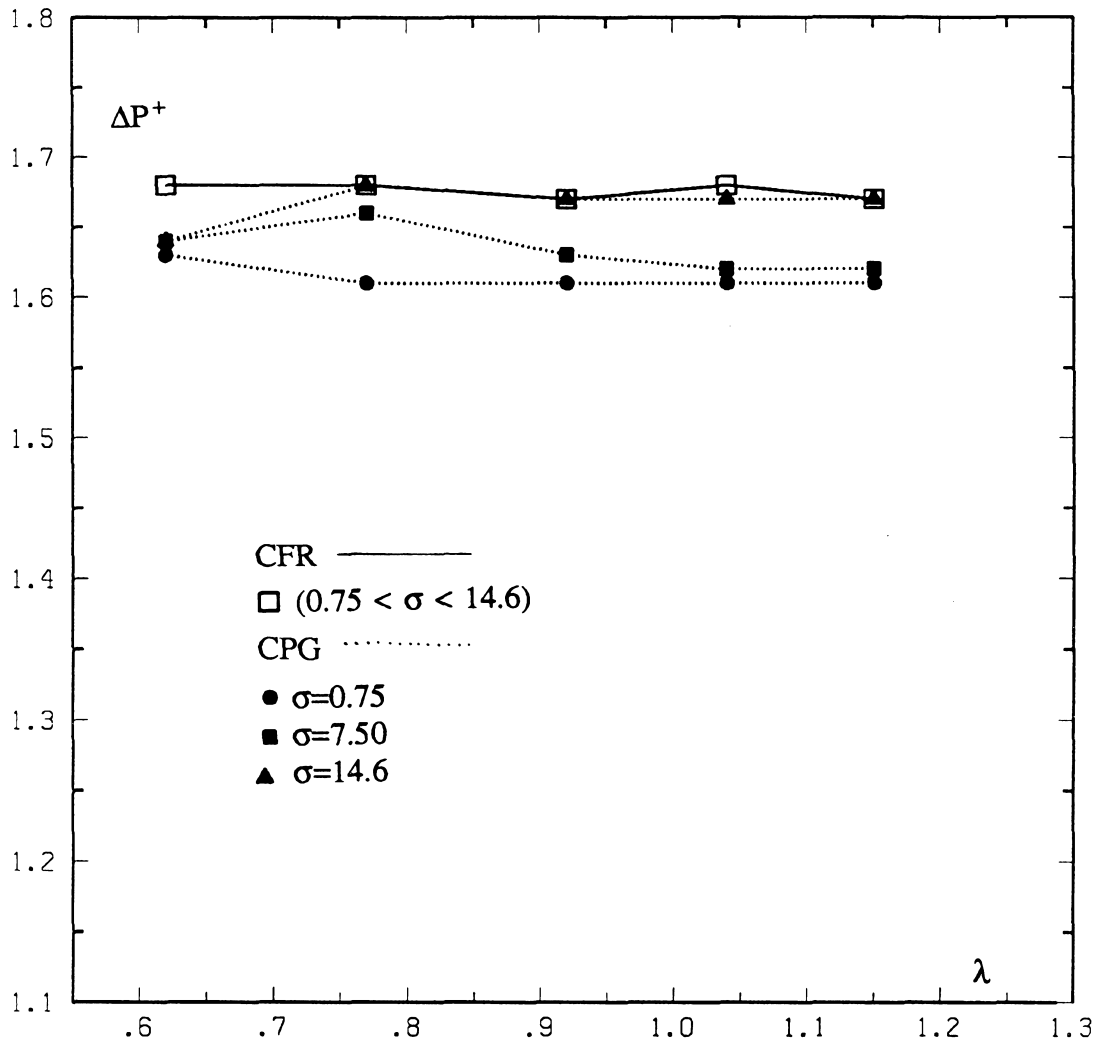

Figure 10(b). Comparison of $(\overline{u}/\overline{v})_{CFR}$ with $(\overline{u}/\overline{v})_{CPG}$ as a function of λ at Γ=2.54.

Chapter 3

Creeping Motion of Immiscible Drops Through a Parallel Channel in a Constant Pressure Gradient-Driven Flow

1. Introduction

Several different experimental studies regarding creeping motion of immiscible liquid drops moving within a suspending fluid through a tube have been carried out in our laboratory. These studies were directed toward a better understanding of the relationship between "independent variables" such as the physical properties of fluids, the volumetric flow rate and the geometrical characteristics of the experimental system, and "dependent variables" such as the extra-pressure drop, drop mobility and drop deformation.

Until now, the experimental models in these studies have consisted of two different channel geometries, a straight circular tube and a wavy-wall tube, and the experiments have been performed with different combinations of Newtonian and non-Newtonian fluids. Ho and Leal (1975) studied a straight-tube geometry with Newtonian drops moving in both Newtonian and non-Newtonian suspending fluids (I). Olbricht and Leal (1981,1983) investigated the effect of tube geometry on the time-dependent drop shape and its relation to the extra-pressure drop, using for this purpose both a straight-circular tube (II) and a converging/diverging tube (III). Their experiments were performed for Newtonian drops moving in both Newtonian and non-Newtonian suspending fluids, and they also included a systematic study the effects of buoyancy forces. Finally, the creeping motion of viscoelastic drops in a Newtonian suspending fluid has been studied earlier in this work for a converging/diverging tube (IV).

The effect on the drop dynamics caused by a change in the nature of the driving mechanisms was also studied here (V) (from one mechanism providing a constant flow rate to another based upon a constant overall pressure drop). In these

studies, the general effect of each type of flow on the motion of the suspended drop was given. However, no experimental measurement of the reciprocal action of the drop on the entire flow was possible because of the geometrical characteristics of the experimental apparatus, which limit the drop to a very small fraction of the overall pressure losses. A palpable effect of such action is provided in the present work. For this purpose, a constant pressure gradient flow similar to that studied in (V) was effected through an experimental apparatus consisting of a long, straight-circular tube in which a section (53 cm in length) was removed and replaced by a pair of parallel channels. This was done to provide a more realistic simulation of dynamics in porous media where a change in resistance to motion can produce dramatic variations in the motions of a suspended drop, including the possibility of complete immobilization as the flow shifts to "channels" which offer less resistance. Such changes could not be simulated in a single, long-cylinder system because the drop never contributes more than a small fraction of the total resistance to motion, and there is no alternative pathway available for flow. Both arms of the channel were provided with differential pressure-measuring devices in order to register, at both arms, the change in total flow resistance caused by the drop in its passage through one arm.

2. Experimmental

2.1 Apparatus

The parallel-channel apparatus was composed of a main, straight-circular pipe (0.9 cm I.D.) to which a bypass lucite tube (0.60 cm I.D.) was connected as shown in Fig. 1. One section (18 cm in length) of the main tube was removed and

replaced by a wavy-wall tube composed of 13 individual periodic units (each 1.5 cm in length), held together by means of two stainless steel brackets. The details of the individual units may be found in (III). A pressure tap was located at each end of this wavy-wall section. The bypass tube was also provided with pressure taps in order that a second differential pressure-measuring device could be connected to it. Thus we have what may be called a Test Section 1 (the wavy-wall test section) and a Test Section 2 (the bypass test section).

In a constant pressure-gradient flow (CPG), when a drop passed through Test Section 1, changing the total flow resistance to the flow and therefore changing the flow rate through it, its effects were also noticed in Test Section 2. Figure 1 shows a schematic representation of the parallel channel setup. The total length of the parallel channel is 53 cm; Test Sections 1 and 2 are each 18 cm in length. The pressure taps in Test Section 1 are located at the middle of the first and thirteenth units (spanning 18 cm between them). The equivalent radius of the wavy-wall tube that constitutes Test Section 1 is $r_{HP} = 0.316$ cm. Test Section 2 is a section of the bypass lucite tube and, hence, its internal radius is $r = 0.3$ cm. Its pressure taps are each located 18 cm apart at correspondingly equivalent positions with those in Test Section 1. The total length of the bypass tube is 55 cm, including the elbows connecting it to the main pipe. The upstream juncture of the bypass tube to the main pipe is located 24.5 cm upstream of the entrance to Test Section 1, and the downstream juncture to the main pipe is located 10.5 cm downstream from the exit of Test Section 1. To avoid collision of the drops against the tube walls at the junctures, the drops must be injected inside the parallel channel at a location downstream of the upstream juncture. Thus, an adequate span of time is allotted for the

electronics to return to the zero position after the unavoidable disturbance created by the injection of a drop (this is why a relatively long pipe was fitted between the upstream juncture of the bypass tube and the entrance to Test Section 1). When drops were injected well upstream of the first juncture of the parallel channel, they invariably collided with the tube walls of the juncture producing a train of drops (different sizes) going through Test Section 2 and one or two other small drops going through Test Section 1. Therefore, the drops were injected approxmately 2 cm downstream of the first juncture of the parallel channel. In order to do so, a long needle was constructed from a regular hypodermic needle and a 70 cm length of stainless steel tubing (0.055" I.D., 0.072" O.D.). The hypodermic needle was cut into half, and the tubing soldered between each half. A differential pressure-measuring device [U-tube manometer coupled with a differential pressure transucer, described in detail in (I) and (II)] was connected to each arm of the parallel channel. A P90D differential pressure transducer was used in the measuring system connected to Test Section 1 at pressure ports A and B of Fig. 1. Its calibration curve for the range of the differential pressures measured in the present work gave a slope of 2 dynes/cm^2 per cm [details are found in (V)]. A DP103 differential pressure transducer was used in the differential pressure-measuring system connected to Test Section 2 at ports D and C in Fig. 1. The DP103 pressure transducer was calibrated according to the calibration procedure described in (V). This calibration spanned a range from zero differential pressure to 150 dynes/cm^2 for the full range of the pressure indicator and stripchart recorder, and was found to be linear (38 data points recorded). The slope of this curve was equal to 0.287 dynes/cm^2 per cm of stripchart paper. The differential pressure signal emitted from Test Section 1

was amplified in a Validyne Co. CD12 pressure indicator. The differential pressure signal emitted from Test Section 2 was amplified by a Whittaker Co. CD25 pressure indicator. The output pressure signal of these two instruments was recorded by a two-pen Houston Instruments stripchart recorder, and here the magnitude of the average differential pressure was read. Figure 2 shows a typical signal pressure from the stripchart recorder. As in previous works, the drop shape and deformation were recorded on magnetic tape, as was the the actual time-dependent pressure signal and the actual experimental time.

2.2 Volumetric Flow Through both Arms of the Parallel Channel

The total volumetric fow rate Q_T is divided at the first juncture of the parallel channel into two other flows: Q_1, which continues straight ahead through Test Section 1, and Q_2, which deviates through the bypass tube and through Test Section 2. It is necessary to assess the magnitude of these flows for the suspending fluid alone since this will provide a measure of the average velocity of the flow through both test sections. $\bar{v}_{AV1}$, the average velocity of the flow through Test Section 1, will be defined $\bar{v}_{AV1} = Q_1/\pi r_{HP}^2$, where r_{HP} is the equivalent radius of the wavy-wall Test Section 1. $\bar{v}_{AV2}$, the average velocity of the flow through Test Section 2, will be defined $\bar{v}_{AV2} = Q_2/\pi r_{HP}^2$, where r is the radius of the straight-circular bypass tube. $\bar{v}_{AV1}$ and $\bar{v}_{AV2}$ will be used as characteristic velocities for nondimensionalization purposes.

In order to determine the magnitude of Q_1 and Q_2 for single-phase flow, several readings of the pressure drop-flow rate were taken at our bypss tube (points c and d in Fig. 1) for steady-state conditions, and the Poiseuille law was applied. It was found that $Q_2 = 0.2841Q_T$ and, hence, $Q_1 = 0.7158Q_T$ and $Q_2/Q_1 = 0.39$.

2.3 Flow Parameter and Materials Used

We have presented our experimental results in terms of familiar parameters such as capillary number, viscosity ratio and drop size. The capillary number is defined here as $\Gamma = \mu_o \bar{v}_{AV1}/\gamma$, where μ_o is the viscosity of the suspending fluid, $\bar{v}_{AV1}$ is the average flow velocity through Test Section 1 (as defined earlier), and γ is the interfacial tension between the two phases when measured by the full-ring method. The viscosity ratio is defined as $\sigma = \mu_i/\mu_o$, where μ_i is the drop fluid viscosity. The drop size is defined as $\lambda = r_D/r_{HP}$, where r_D is the undeformed radius of the drop (r_{HP} was defined earlier).

In the parallel-channel experiment, the passage of the drop was monitored through the constrictions of Test Section 1 by two means: directly, precisely at Test Section 1 (by measuring the direct influence of the drop on the pressure drop in the test section, and indirectly at Test Section 2 (by measuring the change in differential pressure drop due to the change in flow rate through the bypass tube that was caused by the presence of the drop in the wavy-wall Test Section 1. ΔP_1^{++} is termed the time-dependent extra-pressure drop caused by the passage of the drop through Test Section 1 made dimensionless by the quantity $\mu_o \bar{v}_{AV1}/r_{HP}$. Likewise, ΔP_2^{++} is termed the time-dependent pressure drop monitored at Test Section 2, made dimensionless by the quantity $\mu_o \bar{v}_{AV2}/r$, where r is the radius of the bypass straight-circular tube. As usual in the presentation of results, a more convenient parameter was used, namely the arithmetic average of the dimensionless extra-pressure drop defined as $\Delta P_1^{+} = \frac{1}{2}(\Delta P_{1\,max}^{++} + \Delta P_{1\,min}^{++})$; similarly, $\Delta P_2^{+} = \frac{1}{2}(\Delta P_{2\,max}^{++} + \Delta P_{2\,min}^{++})$. Drop mobility for the parallel-channel experiment was defined as $\bar{u}/\bar{v}_{AV1}$, where $\bar{u}$ is the average velocity of the drop through the wavy wall, i.e. $\bar{u}$ is the distance between the fixed

marks located at the entrance and exit of Test Section 1, divided by the elapsed time the center of the drop takes to go from one mark to another.

A deformation parameter d, which accounts qualitatively for the magnitude of drop deformation, is introduced here for comparison purposes. d is defined as the ratio of the maximum longitudinal length of the drop along the center line to the wavelength of one simple periodic unit of Test Section 1.

Two flow rates were tested in our experiments: Q_T = 4.6 cc/min, and Q_T = 2.46 cc/min. The first flow rate produced Q_1 = 3.2931 cc/min and Q_2 = 1.3068 cc/min; consequently, $\bar{v}_{AV1}$ = 0.1749 cm/sec and $\bar{v}_{AV2}$ = 0.077 cm/sec, respectively. The second flow rate gave Q_1 = 1.7611 and Q_2 = 0.698; consequently, $\bar{v}_{AV1}$ = 0.0935 cm/sec and $\bar{v}_{AV2}$ = 0.0411 cm/sec, respectively.

Union Oil LB 1715 and an aqueous glycerol solution were used as suspending fluids. With LB 1715, distilled water and various grades of silicon oil (Dow Corning fluid 510) were used as drop fluids, while different mixtures of silicon oils were used as drop fluids when the suspending fluid was the aqueous glycerol solution. These mixtures were made of different grades of Dow Corning silicon oil 200 to which carbon tetrachloride had been added previously so as to match the glycerol density. When the different silicon oil-carbon tetrachloride solutions attained the required density, they were mixed so as to give the desired viscosities. Numerical values for the capillary number, viscosity ratio and other physical properties are given in Table 1; the drop volumes tested and their corresponding λ's are given in Table 2.

3. Experimental Results

The extra-pressure drop measured at Test Section 2 gives a tangible indication of the effect of the suspended drop on the entire flow; i.e. an increase in flow resistance, caused by passage of a drop through the wavy-wall tube (Test Section 1), causes an increase in flow rate in the bypass tube (Test Section 2), or a decrease in the total flow resistance (produced, for example, by a low-viscosity fluid drop, as will be shown later) will actually increase the flow rate through the wavy-wall tube at the expenses of the flow through the bypass tube.

Our experimental data show that for the range of our parameters, the ratio of the average dimensionless extra-pressure drop measured at Test Section 2 to that measured at Test Section 1 is approximately equal to the ratio of the deviated flow through the bypass arm of the parallel channel to the flow through the straight arm. That is, $\Delta P_2^+/\Delta P_1^+ \sim Q_2/Q_1 = 0.39$. This ratio is persistent independent of viscosity ratio, drop size or total flow rate.

The flow through the parallel channel, itself a constant pressure-gradient experiment, shows the basic characteristics discussed in (V) for a similar type flow. Indeed, the behavior regarding drop deformation and mobility, with respect to viscosity ratio, reported in (V) was also found in the present experiment.

The presentation of our experimental results is organized, as in the previous works in this series, according to the value of the capillary number. Systems for which $\Gamma < 0.031$ are considered small-Γ systems, all other capillary numbers are defined as large-Γ systems.

3.1 Small-Γ Systems

Systems 2 and 3 with $\sigma = 0.40$ and 0.60, respectively, were tested at two different total flow rates yielding, at the test sections, $\Gamma = 0.0167$ and 0.031,

respectively. The results for these systems regarding drop deformation, mobility and average dimensionless extra-pressure drop are discussed next.

(a) Drop Shape and Deformation

The typical drop deformation behavior for small-Γ systems found in a constant pressure-gradient experiment [reported in (V)] is also followed by the drop deformation in a constant pressure-gradient flow through a parallel-channel setup. Drops pass through the wavy-wall tube closely following the contour of the tube walls (with the maximum value of the time-dependent extra-pressure drop caused by the passage of the drop attained midway through the constrictions). The deformation parameter d gives a qualitative account of the narrowing of the gap between tube walls and the drop surface. Obviously, as d decreases with decreasing Γ (fixed values of λ and σ), the drop surface has to approach more and more to the tube walls. Table 3 shows values of parameter d according to capillary number drop size and ratio of viscosities. It will be noted in Table 3, that parameter d is nearly independent of σ and this fact will be reflected in the independence of drop mobility with respect to d.

(b) Drop Mobility

Figure 3 shows $\bar{u}/\bar{v}_{AV1}$ vs. λ for small-Γ systems with σ = 0.40 and 0.60. We can see that drop mobility is a decreasing function of λ until $\lambda \sim 1$. For $\lambda > 1$, it takes on a constant value. Such behavior was also found in previous works for both constant flow-rate and constant pressure-gradient experiments. However, it was found in this work that for the smallest flow rate (Γ = 0.0167) the larger drops (both viscosity ratio) move through the wavy-wall tube with an average velocity less than the average velocity of the flow, i.e. $\bar{u}/\bar{v}_{AV1} < 1$ (λ = 1.04 and 1.15). It

seems intuitively correct that such behavior is due to the following: drop mobility was defined earlier as $\bar{u}/\bar{v}_{AV1}$, where $\bar{v}_{AV1}$ is the average flow velocity of the suspending fluid alone (no-drop conditions). But the actual average flow velocity of the two-phase flow (drop conditions), namely $\bar{v}_{AV1}$ (REAL) is less in magnitude than $\bar{v}_{AV1}$ since a fraction of Q_1, say ΔQ_1, is deviated through the bypass tube as a consequence of the passage of the drop through Test Section 1. That is, $\bar{v}_{AV1}$ (REAL) = $(Q_1 - \Delta Q_1)/\pi r_{HP}^2$ with $\Delta Q_1 = (\pi(0.3)^4 \Delta P_2^+)/(8\mu_o)(18)$. However, ΔQ_1 does not seem to be enough to account for such a decrease in drop mobility because it was estimated that eventhough $\bar{u}/\bar{v}_{AV1} < \bar{u}/\bar{v}_{AV1}$ (REAL), still $\bar{u}/\bar{v}_{AV1}$ (REAL) < 1. Therefore, it must also happen that the drop itself (for large λ) diminishes its average velocity through Test Section 1 with respect to both $\bar{v}_{AV1}$ and $\bar{v}_{AV1}$ (REAL) . Implicitly, the above assumes that, for these small-Γ systems (systems with large interfacial tension), the smaller the flow rate the more difficult for the drop to squeeze through the constrictions of the wavy-wall tube and, hence, they lag with respect to the average velocity of the flow. Figure 5 also shows that drop mobility is nearly independent of σ, just as is the case for d.

(c) Average Dimensionless Extra-Pressure Drop Measured at Both Arms of the Parallel Channel

Figure 4 shows ΔP_1^+ vs. λ and ΔP_2^+ vs. λ for $\sigma = 0.60$ at $\Gamma = 0.0167$ and 0.031. For these small-Γ systems, ΔP_1^+ and ΔP_2^+ are increasing functions of λ. We can also see that ΔP_1^+ and ΔP_2^+ vs. λ decrease as Γ increases because, as has been pointed out in earlier works, larger flow rates cause larger drop deformation. The effect of Γ on drop deformation can be seen in Table 3. The same trends for the average dimensionless extra-pressure drop at both arms of the parallel channel, with respect to λ

and Γ, were found for viscosity ratio $\sigma = 0.40$. Figure 5 shows the dependence of ΔP_1^+ and ΔP_2^+ on σ for $\Gamma = 0.016$. We can see that both ΔP_1^+ and ΔP_2^+ increase with increasing σ. Obviously, an increase in ΔP_2^+ corresponding to an increase in σ represents an increase in the deviated fraction of Q_1 to Test Section 2 (through the bypass tube) as a consequence of an increase of the obstructing effect of the drop at Test Section 1. Similar trends were found when Γ showed the dependence of ΔP_1^+ and ΔP_2^+ on σ for $\lambda = 0.0167$. We can see that both ΔP_1^+ and ΔP_2^+ increase with increasing σ. The same trend was found at $\Gamma = 0.031$ for the average dimensionless extra-pressure drop at both arms with respect to σ.

3.2 Large Γ-Systems

Systems 1 (with $\sigma = 0.0014$) 4, 5 and 6 were tested at two different total flow rates which yielded $\Gamma = 0.18$ and 0.34 for system 1, and $\Gamma = 0.50$ and 0.93 for systems 4, 5 and 6.

(a) Drop Shape and Drop Deformation

As expected, these large-Γ systems undergo greater deformation than those with small value for Γ. Drops for which $0.72 \leq \sigma \leq 14.6$ deform following the deformation pattern found in (V) for a constant pressure-gradient flow, i.e. more viscous drops deform more than less viscous drops. Table 4 shows the deformation parameter d as a function of the viscosity ratio and capillary number. We can see in these that d increases as σ increases for both capillary numbers.

(b) Drop Mobility

Figure 6 shows $\bar{u}/\bar{v}_{AV1}$ vs. λ for large-Γ systems and for the three viscosity ratios. We can see that $\bar{u}/\bar{v}_{AV1}$ is nearly independent of λ (fixed values of σ and Γ). Drop mobility shows the characteristic increase in magnitude with increasing values

of viscosity ratio found in (V) for flows under constant pressure-gradient conditions, as well as its familiar behavior, found earlier for both constant-flow rate and constant pressure-gradient experiments, with respect to capillary number.

(c) Average Dimensionless Extra-Pressure Drop Measured at Both Arms of the Parallel Channel

Figure 7(a) shows ΔP_1^+ vs. λ and ΔP_2^+ vs. λ for System 6 (σ = 14.6) at both Γ = 0.93 and 0.50. ΔP_1^+ and ΔP_2^+ are increasing functions of λ. We can see that they decrease as Γ increases because of the larger deformation. Figure 7(b) shows corresponding results for System 5 (σ = 7.5) where a similar trend can be seen, unlike those shown in Fig. 7(a). Comparison of Figs. 7(a) and 7(b) shows how ΔP_1^+ and ΔP_2^+ vary with respect to the viscosity ratio. A greater viscosity ratio corresponds to a greater value for ΔP_1^+ and ΔP_2^+, and from this it is certain that a greater fraction of Q_1 is being deviated through the bypass tube (proportional to ΔP_2^+).

The consequences of having a ratio of viscosity less than one (System 3) in an experiment performed in the parallel-channel apparatus at a constant pressure gradient begins to be noticeable, for the range of our variables, for System 3 (σ = 0.72). When a large drop ($\lambda \geq 1.04$) with viscosity ratio σ = 0.72 passes through Test Section 1 (both Γ = 0.93 and 0.50), it decreases the total flow resistance and the actual flow rate increases in Section 1 as is confirmed by the fact that a negative ΔP_2^+ is registered at Test Section 2, as shown in Fig. 7(c). An even more accentuated version of this behavior is observed for System 1, and will be discussed at the end of this section. Again, the same correspondence $(\Delta P_2^+/\Delta P_1^+) \sim (Q_2/Q_1)$ was also observed for these large-Γ systems.

System 1 (σ = 0.0014) gives a clear example of the effect caused by a drop with a very low viscosity ratio in the behavior of the flow through the parallel channel. We can see in Fig. 8 that a negative ΔP_1^+ measured at Test Section 1 is obtained, indicating an actual decrease in the total flow resistance. On the other hand, a negative ΔP_2^+ measured at Test Section 2 is also obtained, indicating a decrease in the volumetric flow rate through it. Figure 9 shows the actual time-dependent pressure signal from the stripchart recorder for System 1. The defect in volumetric flow rate through Test Section 2 is manifest by the fact that the outcome of the pressure indicator plotted in the striptchart recorder falls under the "zero" differential-pressure line, as compared with Fig. 2.

Conclusions

An experimental study of the two-phase flow of a suspended liquid drop in a suspending liquid moving through a wavy-wall tube was performed. For this study, a parallel channel was built and used to monitor not only the change in total flow resistance directly due to the presence of the drop, but also the pressure change at the bypass tube due to the variation in the deviated flow through it which is also due, indirectly, to the presence of the drop.

The ratio of the average dimensionless-pressure drop in the bypass tube to the average dimensionless-pressure drop in the wavy-wall arm was found to be constant. This constant was approximately equal to the ratio of deviated flow through the bypass tube to the flow rate through the wavy-wall arm for the suspending fluid alone. The same ratio was preserved regardless of the different values of flow rate, viscosity ratio or drop size that were used in our experiments.

Presumably, the qualitative aspects of the flow through a parallel channel discussed here will be preserved for any geometrically similar arrangement provided that the flow under study is a constant pressure-gradient, driven flow. But the quantitative influence of the drop is expected to change according to the particular geometrical characteristics of each parallel-channel apparatus. The parallel-channel flow, itself a constant pressure-gradient driven flow, showed the same general properties found in (V) to be inherent in such a flow-driving mechanism.

Table 1. Properties of Systems.

System	Suspension Fluid	Drop Fluid	γ	σ	Γ (Q = 2.46 cc/min)	Γ (Q = 4.6 cc/min)
1	Ucon Oil LB 1715	Distilled Water	3.5	0.0014	0.18	0.34
2	95.2 Glycerol	DC 200 + CCl_4	22	0.40	0.0167	0.031
3	95.2 Glycerol	DC 200 + CCl_4	22	0.60	0.0167	0.031
4	Ucon Oil LB 1715	DC 510	1.3	0.75	0.50	0.93
5	Ucon Oil LB 1715	DC 510	1.3	7.52	0.50	0.93
6	Ucon Oil LB 1715	DC 510	1.3	14.6	0.50	0.93

Table 2. Drop Volumes and Corresponding λ.

Volume CC	λ
0.03	0.61
0.06	0.77
0.10	0.92
0.15	1.04
0.20	1.15

Table 3. Small-Γ systems. Deformation parameter d (see text).

Total Flow Rate Q_T = 2.46 cc/min, Γ = 0.0167					
λ →	0.62	0.77	0.92	1.04	1.15
σ = 0.40	0.26	0.35	0.49	0.62	0.75
σ = 0.60	0.28	0.36	0.49	0.62	0.76
Total Flow Rate Q_T = 4.6 cc/min, Γ = 0.031					
σ = 0.40	0.28	0.38	0.49	0.66	0.77
σ = 0.60	0.28	0.38	0.50	0.66	0.78

Table 4. Large-Γ systems. Deformation parameter d (see text).

Total Flow Rate Q_T = 2.46 cc/min, Γ = 0.50					
$\lambda \rightarrow$	0.62	0.77	0.92	1.04	1.15
σ = 0.72	0.23	0.51	0.65	0.88	1.04
σ = 7.58	0.36	0.52	0.80	1.00	1.20
σ = 14.6	0.39	0.56	0.82	1.05	1.30
Total Flow Rate Q_T = 4.6 cc/min, Γ = 0.93					
σ = 0.72	0.39	0.60	0.82	1.00	1.34
σ = 7.58	0.48	0.70	0.88	1.05	1.72
σ = 14.6	0.50	0.81	0.99	1.16	1.82

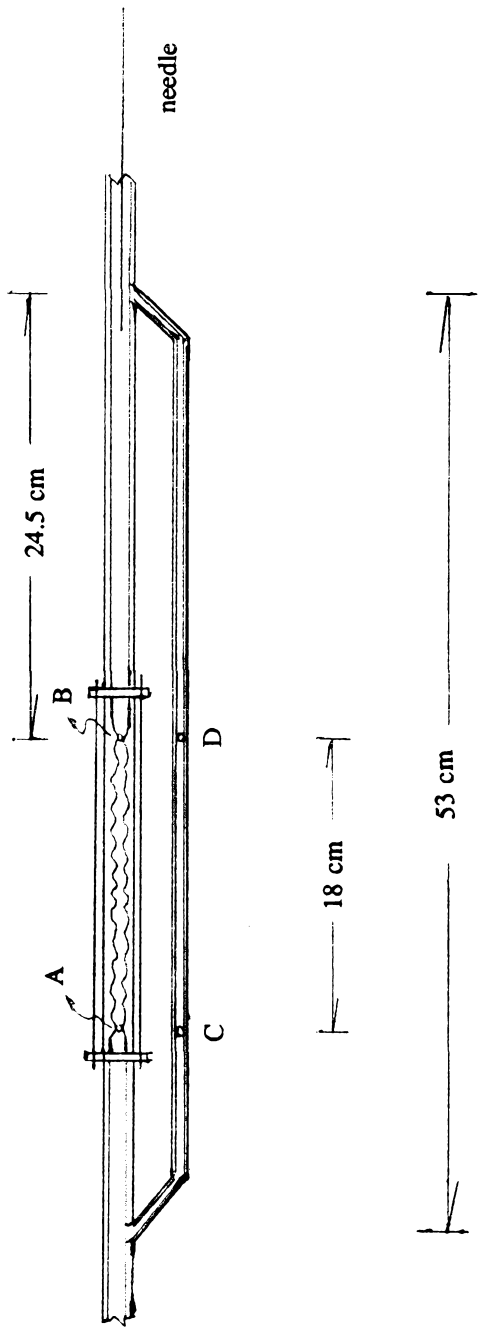

Figure 1. Schematic representation of parallel channel.

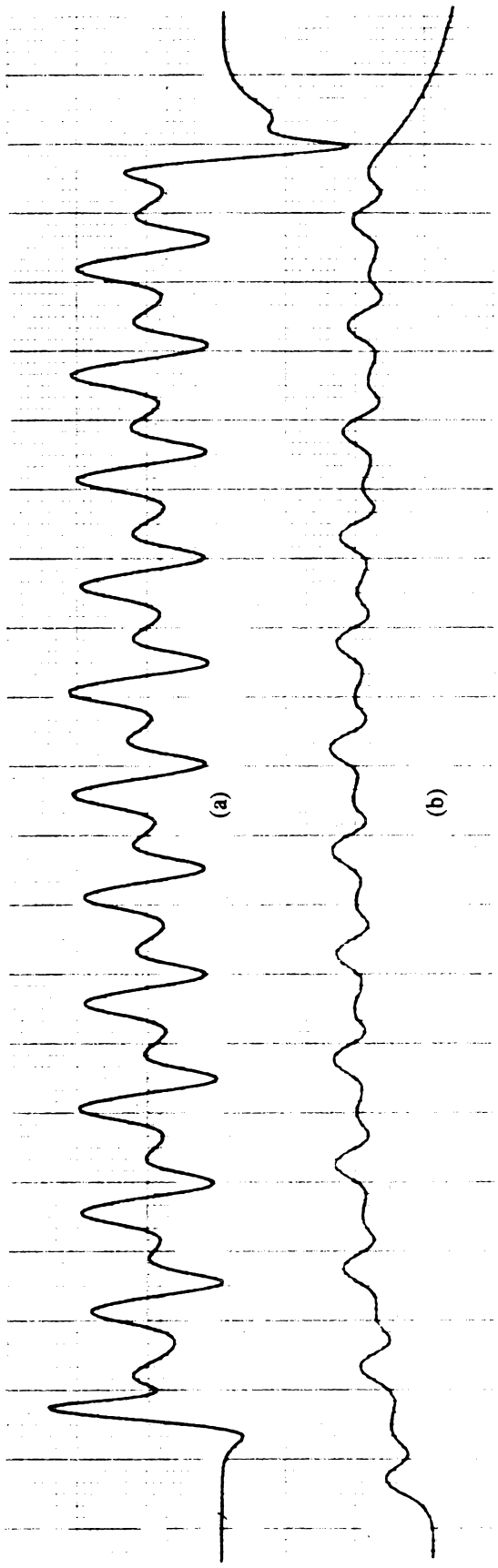

Figure 2. (a) Pressure signal caused by the drop in the test section 1. (b) Pressure signal caused by the increase in flow rate (of suspending liquid only) in test section 2. In this example Γ=0.0167, σ=0.60, λ=1.04.

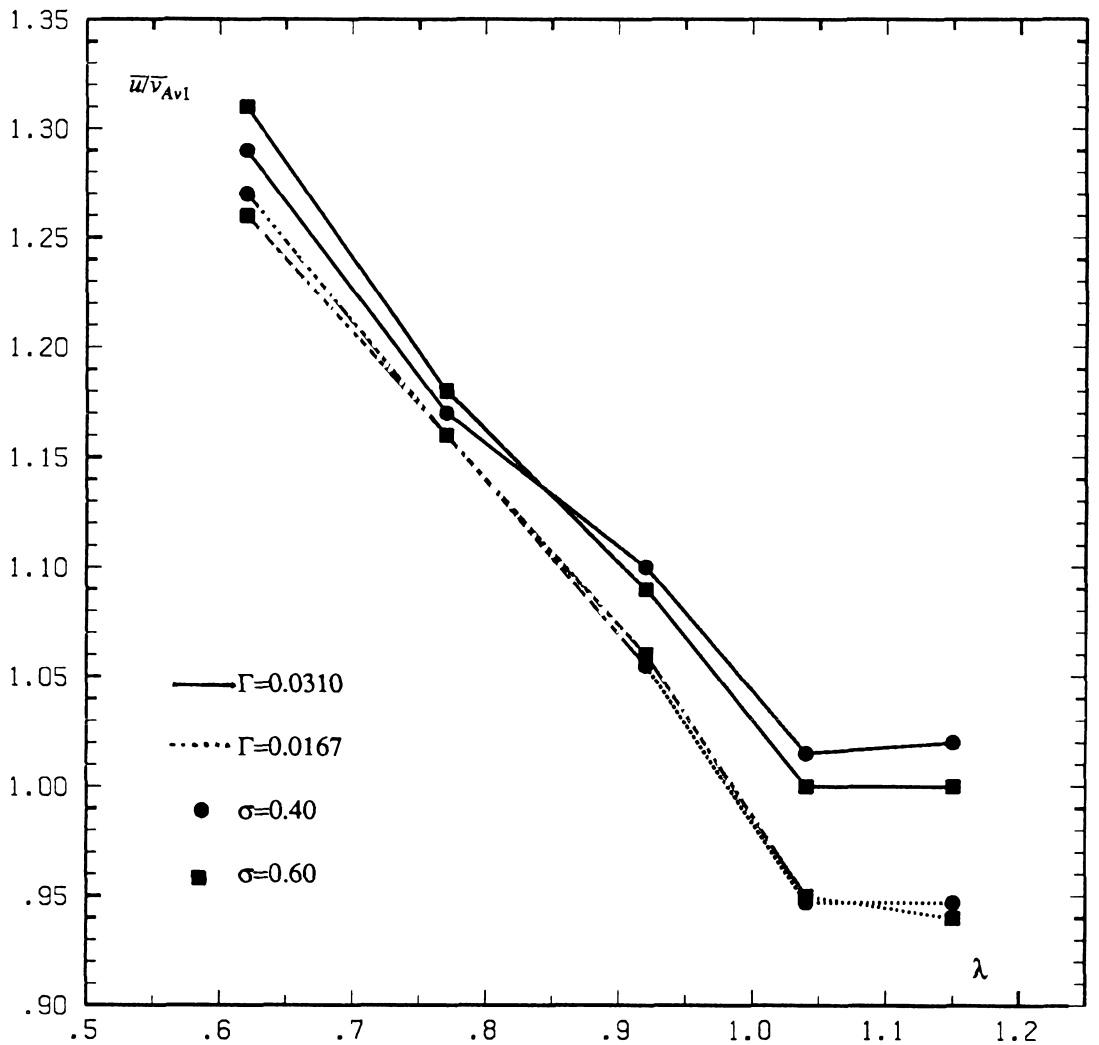

Figure 3. Drop mobility as a function of dimensionless drop size. Small-Γ systems (see text).

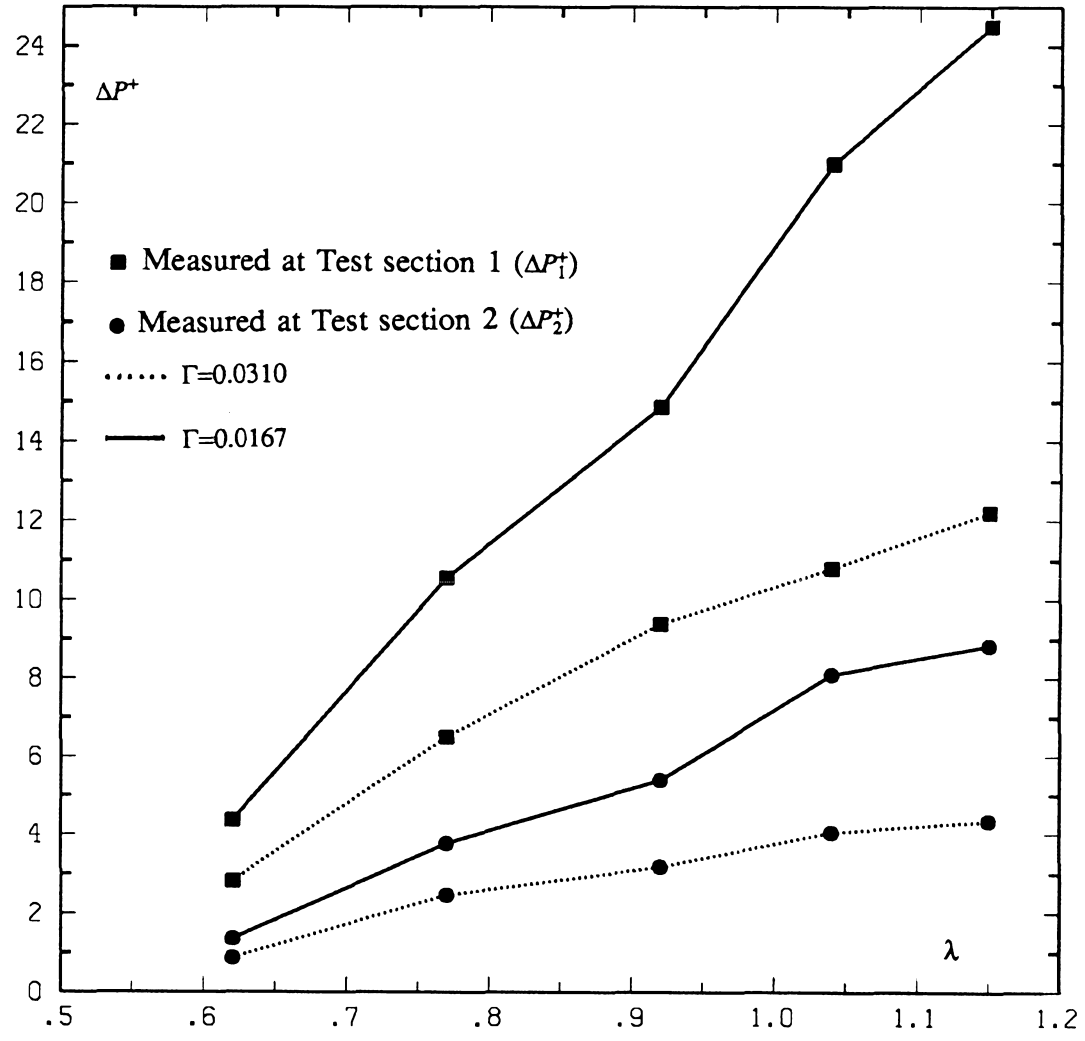

Figure 4. Dimensionless average of the extra pressure drop at both test sections 1 and 2 as a function of the dimensionless drop size. Small-Γ systems. The viscosity ratio in this case σ=0.60.

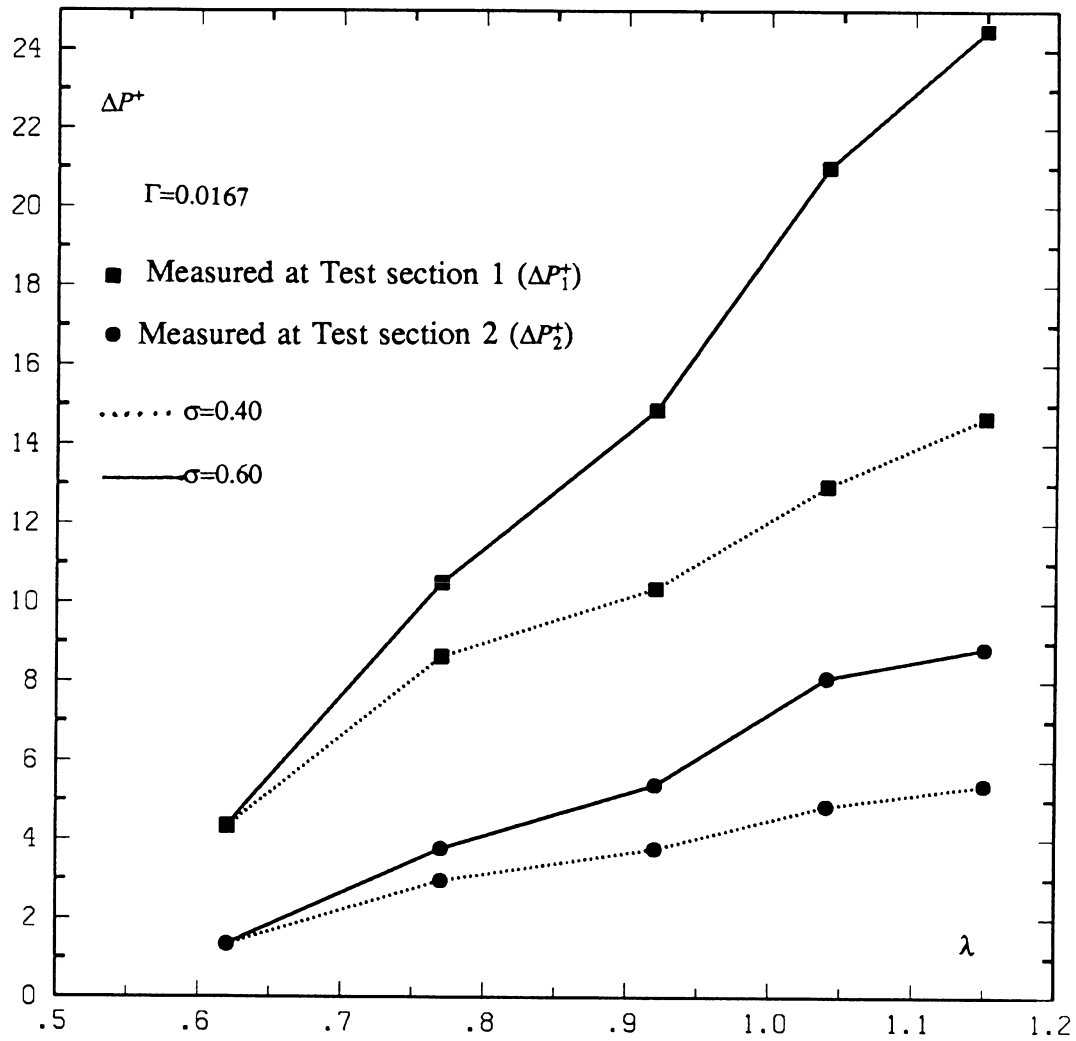

Figure 5. Dependence of the dimensionless average of the extra pressure drop on σ . Small-Γ systems. Similar results are found for Γ=0.031.

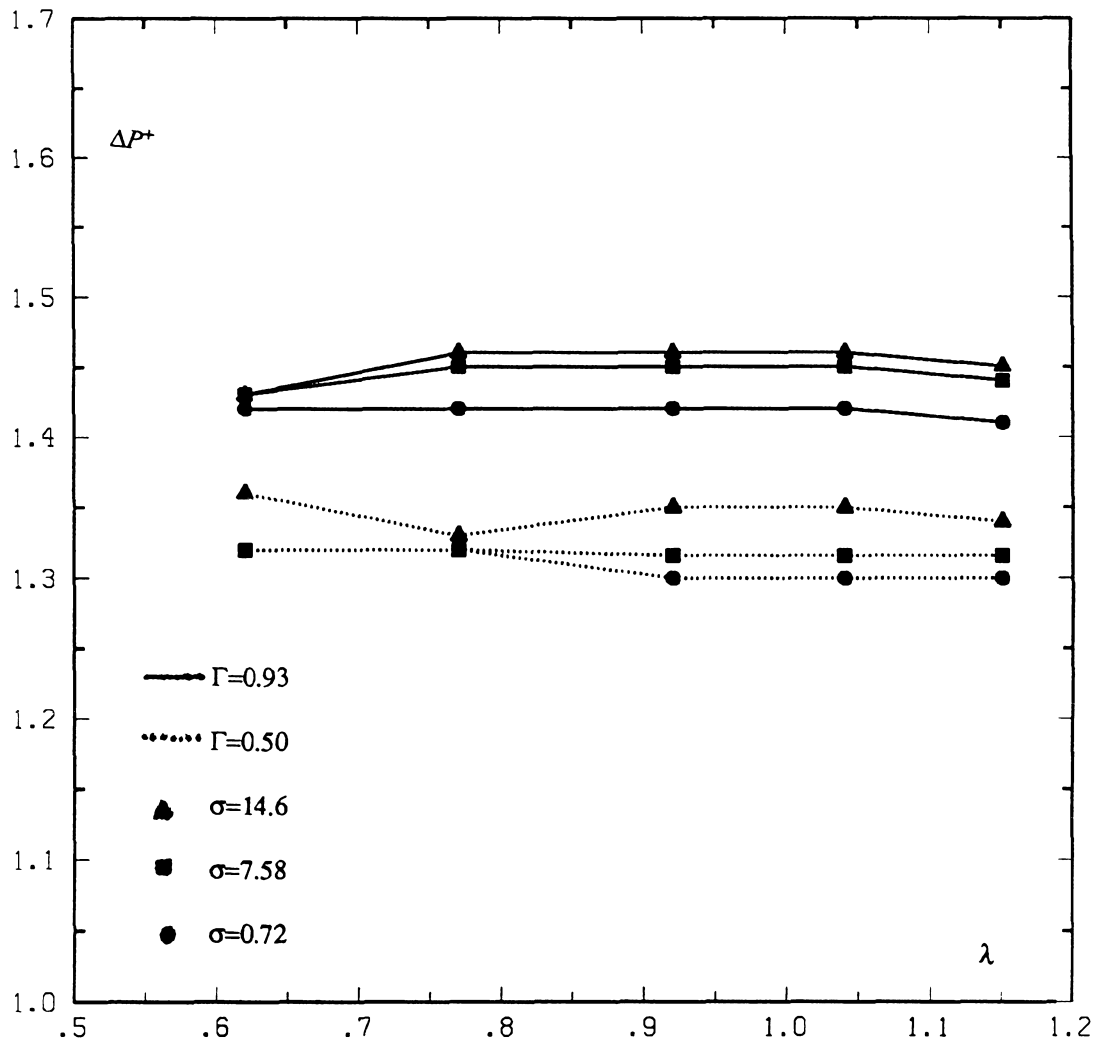

Figure 6. Drop mobility as a function of dimensionless drop size for large-Γ systems. The data is given for two capillary numbers and for three different viscosity ratios. Drop mobility increases with both Γ and σ.

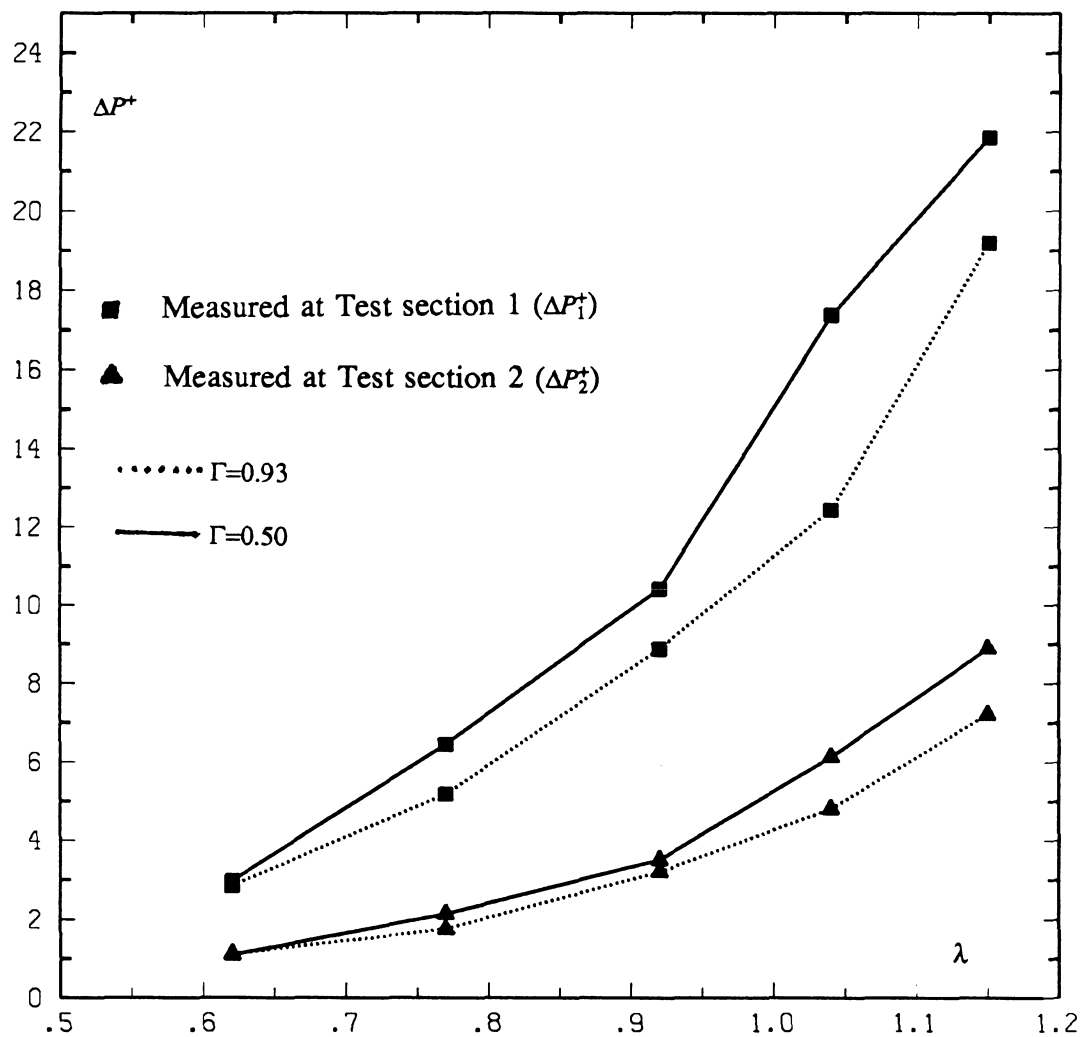

Figure 7(a). Dimensionless average extra presssure drop for large-Γ systems. The data shown is for system 6. Comparison with Fig. 7(b) shows the effect of viscosity ratio on $\Delta P+$.

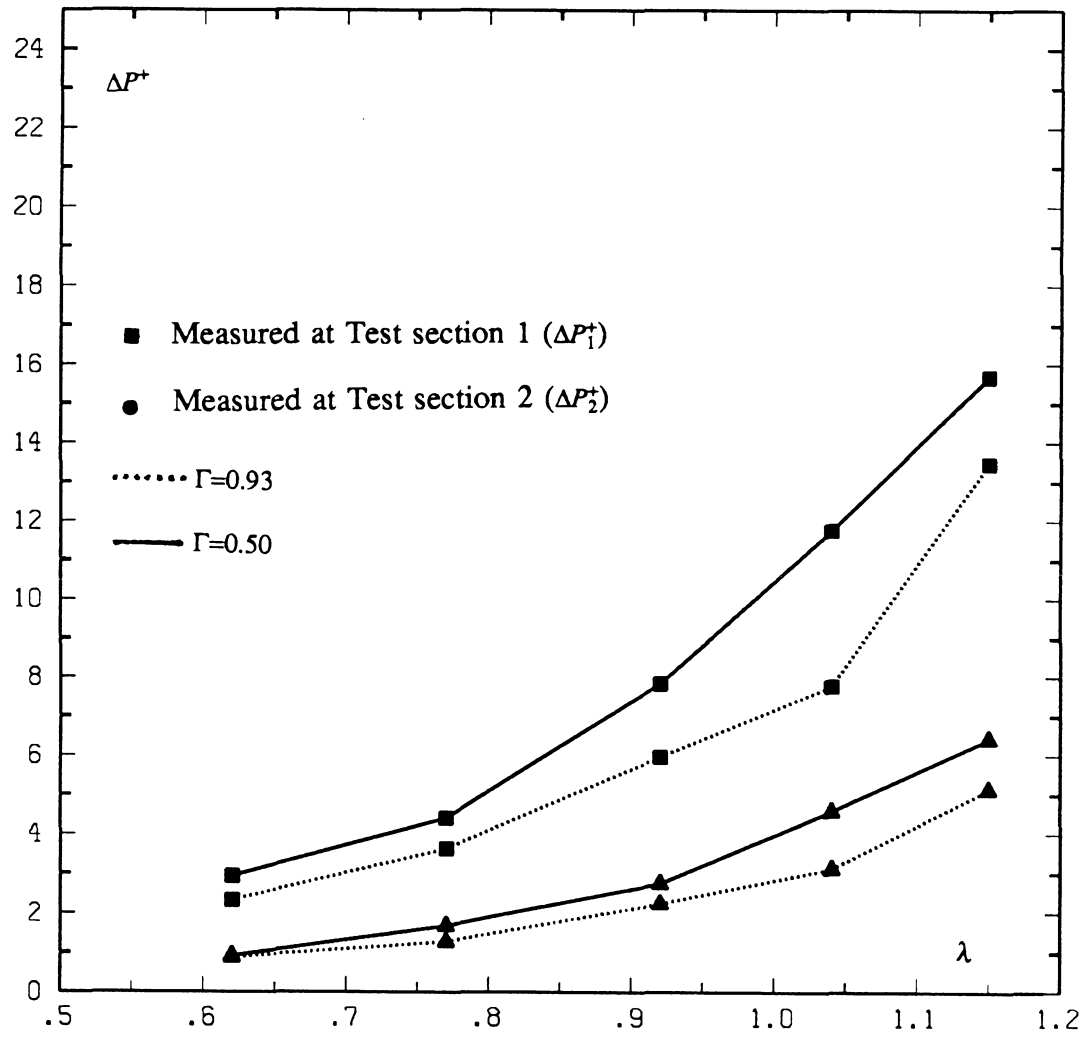

Figure 7(b). Dimensionless average extra pressure drop as a function of dimensionless drop size for large-Γ systems. The data shown is for system 5 at both capillary numbers.

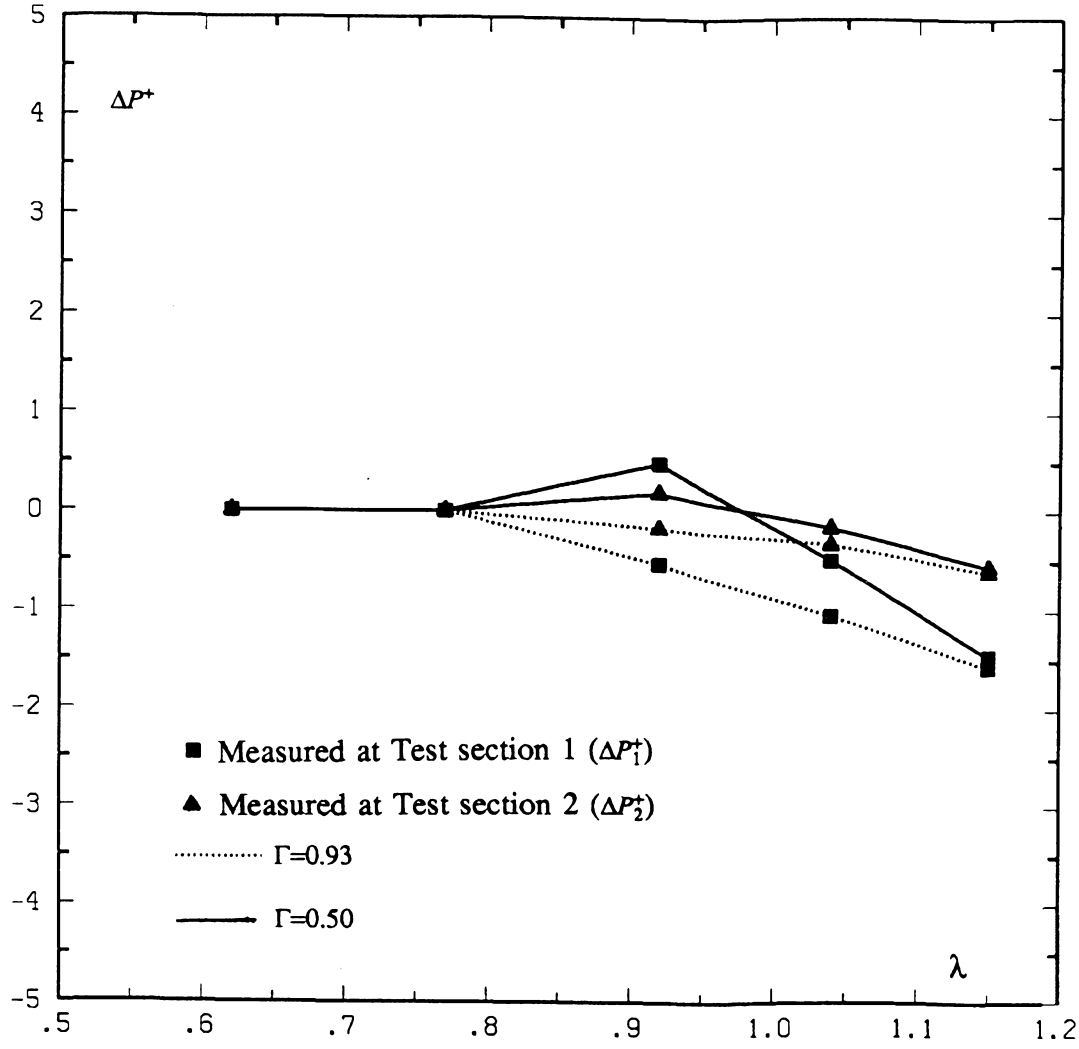

Figure 7(c). Large-Γ systems. This figure shows the incipient effect on ΔP_1^+ and ΔP_2^+ of $\sigma<1$. For the larger flow rate (dotted line) both ΔP_1^+ and ΔP_2^+ are negative quantities, this meaning a decrease in the flow resistance in test section 1 and a defect of volumetric flow rate in the bypass tube respectively. For the smallest flow rate there is still a small increase in flow resistance at $\lambda=0.92$ and hence the pressure losses of both test sections are positive quantities. When $\lambda\leq 0.77$, for both flow rates, there is no appreciable response in either one of the arms of the parallel channel.

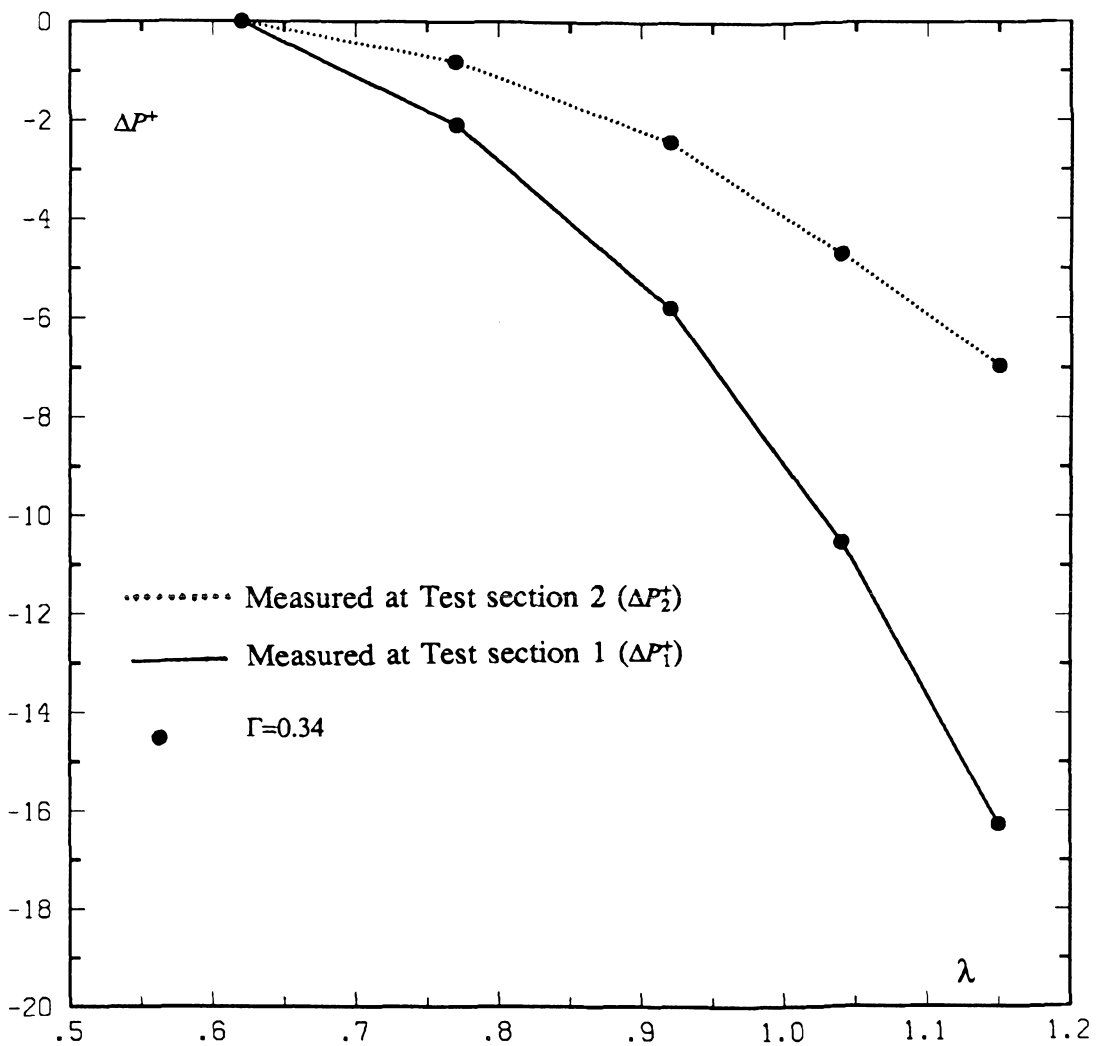

Figure 8. Dimensionless average extra pressure drop in both of the test sections as a function of dimensionless drop size for system 1 (σ=0.0014). The negative sign in both quantities indicates for ΔP_1^+ a decrease in the total flow resistance through test section 1, and for ΔP_2^+ indicates an actual defect in volumetric flow rate through the bypass tube (test section 2). See text.

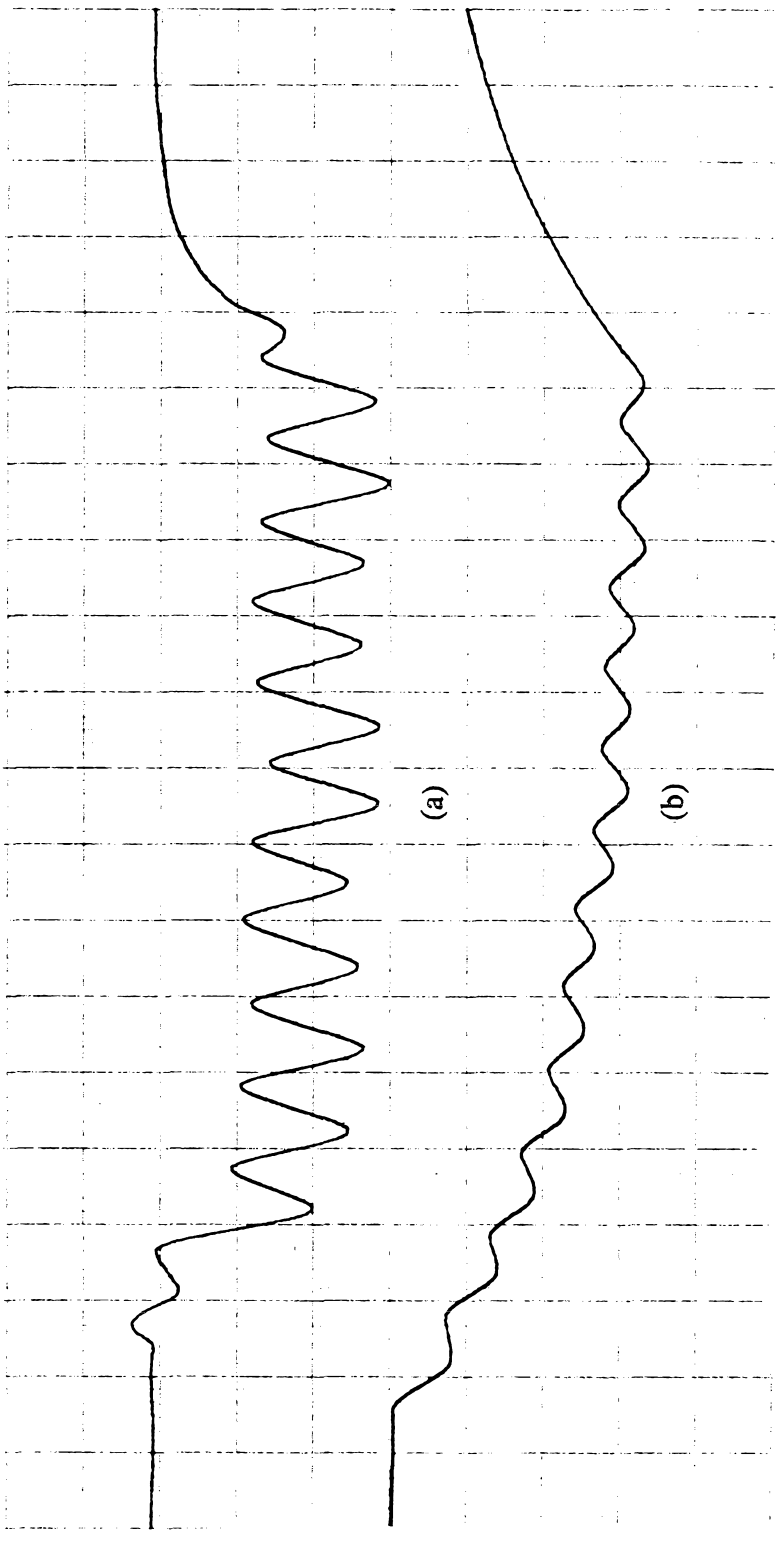

Figure 9. Pressure signal for a system with very low viscosity ratio, σ=0.0014. (a) Pressure signal in test section 1. (b) Pressure signal in test section 2. See text.

References

Chin, H. B. & Han, C.D. 1979. Studies on droplet deformation and breakup. I. Droplet deformation in extensional flow. *J. Rheol.* **23**, 557.

Chin, H. B. & Han, C.D. 1980. Studies on droplet deformation and breakup. II. Breakup of a droplet in non-uniform shear flow. *J. Rheol.* **24**, 39.

Gauglitz, P. A. & Radke, C. J. 1986. The role of wettability in the breakup of liquid films inside constricted capillaries. *Symp. Series* **82**, 50.

Gauglitz, P. A. & Radke, C. J. 1986. The dynamics of liquid film breakup in constricted cylindrical capillaries. *Submitted to J. Coll. Int. Sci., Sept. 1986.*

Gauglitz, P. A. & Radke, C. J. 1986. The dynamics of Haines jumps for compres -sible bubbles in constricted capillaries. *Submitted to AIChE J., Sept. 1986.*

Gauglitz, P. A. & Radke, C. J. 1986. Experimental determination of gas-bubble breakup in a constricted cylindrical capillary. *Submitted to Ind. Engng. Chem. Fund. J., Sept. 1986.*

Gauglitz, P. A. & Radke, C. J. 1986. An extended evolution equation for liquid film breakup in cylindrical capillaries. *Submitted to Chem. Engng.*

Sci. J., Sept. 1986.

Gauglitz, P. A. & Radke, C. J. 1986. The instability of a wetting film deposited by a long bubble as it moves through a constricted capillary. *Submitted to J. Fluid Mech., Sept. 1986.*

Gauglitz, P. A., St. Laurent, C. M. & Radke, C. J. 1987. An experimental investigation of gas-bubble breakup in constricted square capillaries. *SPE 16371*, presented at the California Regional SPE meeting, Ventura, April 8-10, 1987.

Han, C.D. & Funatsu, K 1978. An experimental study of droplet deformation and breakup in pressure-driven flow through convergent and uniform channels. *J. Rheol.* **22**, 113.

Ho, B.P. & Leal, L. G. 1975. The creeeping motion of liquid drops through a circular tube of comparable diameter. *J. Fluid Mech.* **71**, 361.

Leal, L.G., Skoog, J. & Acrivos, A. 1971. On the motion of gas bubbles in a viscoelastic fluid. *Can. J. Chem. Engng.* **71**, 569.

Marshall, R.J. & Metzner, A.B. 1967. Flow of viscoelastic fluids through porous media. *Ind. Engng. Chem. Fund.* **8**, 393.

Olbright, W. L. 1980. The motion of macromolecules and immiscible drops in creeping flow, Ph. D. thesis, California Institute of Technology,1981.

Olbright, W. L. & Leal, L. G. 1982. The creeping motion of liquid drops through a circular tube of comparable diameter: the effect of density differencies between the fluids. *J. Fluid Mech.* **115**, 187.

Olbright, W. L. & Leal, L. G. 1983. The creeping motion of immiscible drops a converging/diverging tube. *J. Fluid Mech.* **134**, 329.

Pickell, J. J., Swanson, B. F. & Hickman, W. B. 1966 Application of air-mercury capillary pressure data in the study of pore structure and fluid distribution. *J. Soc. Pet. Engng., March 1966*, 55.

Ransohoff, T. C., Gauglitz, P. A. & Radke, C. J. 1987. Snap-off of gas bubbles in smoothly constricted noncircular capillaries. *J. AIChE* **133**, 753.

Roof, J. G. 1970. Snap-off of oil droplets in water-wet pores. *J. Soc. Pet. Engng.* **10**, 125.

Taylor, G.I. 1934. The formation of emulsions in definnable fields of flow. *Proc. R. Soc. Lond.* **A146**, 501.